Spring 5-31-2021

Numerical Study On Oscillating Flow Over A Flat Plate Using Pseudo-Compressibility in Intermittent Turbulent Regime

Shivank Srivastava Mr.
University of New Orleans, ssrivast@uno.edu

Numerical Study On Oscillating Flow Over A Flat Plate Using Pseudo-Compressibility in Intermittent Turbulent Regime

A Dissertation

Submitted to the Graduate Faculty of the
University of New Orleans
in partial fulfillment of the
requirements for the degree of

Doctor of Philosophy
in
Engineering And Applied Science
Naval Architecture and Marine Engineering

by

Shivank Srivastava

M.S. University Of New Orleans, 2018

May, 2021

Dedicated to my wife

Dr. Manika Bhondeley

and my mother

Mrs. Kshipra Bharti

Acknowledgments

I would like to express my deepest gratitude to my advisors Kazim M. Akyuzlu and Brandon M. Taravella for believing in me and providing with an opportunity to work under them and carry out this research. Their teachings have always been an encouragement for me in overcoming roadblocks that have come up during the course of this research. Dr. Akyuzlu's guidance through providing new perspective in approaching a problem, constructive criticism, asking the right scientific questions, and providing avenues for publishing and presenting this work has always been a driving force in making of a scientist. Dr. Brandon has always been a strong pillar of support through tough times. His technical and editorial advice was essential in completion of this thesis and has taught me innumerable lessons on workings of academic research.

Each of my committee member, Lothar Birk, Martin Guillot, and Jairo Santanilla also deserves a thanks for agreeing to participate in my thesis committee. They have always been helpful with their insightful advice through out my dissertation. The Office of Naval Research is thanked for providing funding and support.

I would also like to thank the two most important member without their support this work would not have been completed. George Morrissey and Ryan Thiel who have been a very helpful in setting up the equipment for the research and have been interested in the work throughout. George, has always been there to overcome the obstacles faced with equipment and has never rested till its solved. Ryan has always helped me thinking about an issue with a different perspective. I am grateful for their help.

I would also like to thank my dear friends, colleagues and fellow PhD students, Jonathan Eastridge and David Bonneval with whom I have collaborated to work on this project. They have been there in tough and good times and have helped me beyond the scope of their obligations. Their suggestions and comments have been very valuable in this dissertation.

I would also like to thank my lovely wife Dr. Manika Bhondeley, we are together since I

started my PhD and got married. I am grateful for your support, patience and scientific insights. She has always been a source of motivation and without her persuasion this work wouldn't have been complete. Here is to our new chapter. Last but not the least I would like to thank my family for their constant support and strength that they have provided during tough times. Hey Maa I did it !

Table of Contents

List of Figures

List of Tables

Abstract

A Computational Fluid Dynamic (CFD) in-house code is developed to study unsteady characteristics of incompressible oscillating boundary layer flow over a flat plate under laminar and intermittently turbulent condition using pseudo-compressible unsteady Reynolds Averaged Navier-Stokes (RANS) model. In the in-house code, the two-dimensional, unsteady conservation of mass and momentum equations are discretized using finite difference techniques which employs second order accurate (based on Taylor series) central differencing for spatial derivatives and second order Runge-Kutta accurate differencing for temporal derivatives. The in-house code employs Fully Explicit-Finite Difference technique (FEFD) to solve the governing differential equations of the mathematical model. In the study two different closure models are adopted, Chien's (k–ϵ) and Jones and Launder (k–ϵ) turbulence model. For the purpose of validation and verification of the proposed pseudo-compressibility method, flow over a flat plate is chosen as benchmark case. The numerically predicted velocities are compared to experimentally observed velocity fields using Particle Image Velocimetry (PIV) in laminar regime. The verification of the proposed model is performed using Grid Convergence Index (GCI) method. The discretization errors observed are less than 5% which are within the acceptable range.

Once verified and validated, the technique of pseudo-compressibility is use to simulate oscillating flow problem. The velocity fields predicted by the in-house code in laminar regime are compared to the one given by the analytical solution to Stokes' second problem of oscillating flow. An intermittency equation (γ) is proposed which couples with Jones and Launder (k–ϵ) along with unsteady RANS equations to simulate intermittently turbulent oscillating boundary flows. Using the proposed unsteady pseudo-compressible NS and RANS models, numerical experiments were conducted for unsteady cases for Reynolds number (based on Stokes' thickness) corresponding to laminar and intermittently turbulent flows, respectively. Predicted time dependent velocity profiles and shear stress distributions are compared to LES results and experimental

data. Turbulence properties during acceleration and deceleration phases are also predicted. The sudden rise in shear stress during the acceleration phase of the oscillation, indicating the onset of intermittence, is observed and discussed. Comparison of the results show that the observed deviations between the velocity magnitudes predicted by the in-house code and experimental data are within acceptable range for laminar and intermittently turbulent flow conditions. Based on the results of the present study, one can conclude that the proposed unsteady pseudo-compressible intermittent RANS model is capable of predicting the characteristics of oscillating external flows successfully.

Keywords: CFD; Intermittent Turbulence; Pseudo-Compressible; Oscillating Boundary layer; Finite-Difference; Wall Shear-Stress; Kinetic Energy; RANS

Introduction

It is very common to encounter the phenomenon of incompressible flow in nature. Many engineers working in disciplines of hydrodynamics, aerodynamics, coastal and offshore engineering have to model fluid flows that are commonly incompressible in nature. Even the incompressible form of equations, developed by Sir George Stokes and Claude Louis Navier, which governs the fluid flow motions have a million-dollar prize on them for their existence and uniqueness yet to be proved. These partial differential equations called Navier-Stokes (NS) equations are simply too complicated to solve analytically; however, with powerful numerical techniques they give approximate solutions to many real world fluid flow problems. The study of such fluid flow problems numerically is called Computational Fluid Dynamics (CFD) and is used in many engineering applications.

Many commercially available CFD packages solve incompressible form of NS equations using pressure correction based approach such as SIMPLE (Semi-Implicit Method for Pressure Linked Equations) or PISO (Pressure Implicit Splitting of Operators), as explained by Tannehill et al. (1997). Even in the realm of numerical techniques, incompressible form of conservation are delicate to solve. The sole reason for this is the absence of temporal derivative in mass the conservation equation. To study incompressible flows using accurate and efficient numerical methods, one requires a time derivative term in the continuity equation to make the pressure waves generated of finite speed, which otherwise would be of infinite speed in incompressible flows.

Aim 1: One such goal of this present study is to develop a computer code to investigate the boundary layers in incompressible flows. Such is accomplished by using a method called Pseudo-Compressibility, which introduces a time derivate term of density to the continuity equations. Such computer code will be validated for accuracy with benchmark cases and

experimental data and also verified with the established methods available for testing the accuracy and robustness of such numerical methods (Celik et al. (2008)).

One very common application of incompressible flows that can be found in nature are oscillatory boundary layer flows. Understanding such flows is of importance due to their application in wide variety of physical phenomenon such as coastal and geophysical flows, damping of waves, biomedical applications for studying hemodynamics and also in many engineering applications such as internal combustion engines for examining pulsating flows in turbocharger. Such oscillating flow have received quite attention since the early 1800's. Stokes (1850) defined a formation of boundary layer (Stokes layer) for an oscillating flow over a flat plate. This Stokes solution has become a prototype for such unsteady boundary layer flows.

Aim 2: The next objective of this study thus becomes, to use the method of pseudo-compressibility in developing a numerical solver to study oscillating boundary layer flows over a stationary flat plate to determine shear stress profiles and boundary layer thickness.

Hsu et al. (2000) explained that to understand the shallow water sediment transportation, one must first understand the interactions between surface gravity waves and sea bottom. As the waves propagate from deep water to the coast there exits a phenomenon where flow on the bottom bed becomes oscillatory in nature, and transition (intermittent turbulent) starts to occur within the boundary layer from laminar to turbulent. There exists a need to understand these oscillatory boundary layers for their velocities, turbulent properties and shear stresses.

This phenomenon is important; therefore, many studies (discussed in details in section 1) have been conducted experimentally, using Large-Eddy Simulations (LES) and Direct Numerical Simulations (DNS). LES and DNS have given much more insight on such flows with accuracy. However, these techniques require a lot of computational power and time. Such may not be available to many researchers, students or even industries. High-Performance Computing is still in its developmental phase, on which the above mentioned numerical techniques rely on. On the other hand, Reynolds-Averaged Navier-Stokes equations (RANS) along with linear eddy viscosity turbulence close model is still the preferred method of modeling turbulence in a lot of industrial applications. This is because RANS is faster, robust, easy to implement and foremost

computationally inexpensive and give good results. By far, only three studies have been found in open literature that study oscillating flow over a flat plate in intermittent turbulent regime (discussed in section 1).

Aim 3: Thus the main objective of this study is, to investigate the oscillating boundary layer flow over a stationary flat plate using method of pseudo-compressibility to solve RANS equations along with a proposed intermittency k–ϵ–γ turbulence closure model.

One such phenomenon of the oscillating boundary layer flow, can be found in an undulatory motion of a biological form used to propel themselves underwater. Such kind of motions have been of interest to engineers and scientists in developing autonomous underwater vehicles or biomimetic robots. One such study has been conducted at the University Of New Orleans (UNO) under grant N00014-17-1-2099 titled, "Investigation into the Boundary Layer of an Anguilliform-like Propulsor." The study involves understanding the fluid dynamics of an underwater robot that mimics the motion of an anguilliform and is designed for wakeless swimming. To study such 3D, unsteady flow problems accurately using LES or DNS can be challenging and computationally expensive. Another challenge arises when the flow is intermittently turbulent for such complex problems. To study this particular problem within realistic time frame, with available resources and without compromising the accuracy, a RANS method would be a way to go. Therefore, the motivation is to develop a simple intermittency turbulence closure model that can be used along with a RANS equation to simulate and study such complex problems of an undualtory anguilliform-like propulsor under water.

1 Literature Survey

1.1 History Of Pseudo-Compressibility

A.J Chorin (1967) is the researcher who first proposed the method of pseudo-compressibility . In his proposed formulation, a time derivative term of artificial density was introduced in the continuity equation for incompressible flows. This term relates to pressure by an artificial compressibility using an artificial equation of state. Chorin used explicit finite difference-techniques, which employed the Dufort-Frankel scheme to solve for the governing differential equations for steady state laminar flows only. He applied his technique to simulate flow inside a rectangular channel and thermal convection inside a closed cavity. He successfully demonstrated the independence of the solution from an artificial compressibility factor.

Chang and Kwak (1984) presented an extensive explanation of the pseudo-compressibility factor. The nature of pseudo-compressibility , physically and numerically, was well clarified by these authors. They used implicit finite difference techniques to simulate laminar flow inside an annular duct and over a cylinder. Their work was initiated to develop a computer code to analyze the complex flow field observed in the hot gas manifold of Space Shuttle Main Engine (Chang, Kwak, et al. (1985)). Their paper demonstrated the pivotal role played by the pseudo-compressibility factor in convergence of the numerical solution and also identifies the criteria for selecting the lower and upper-bounds of the same.

A three-dimensional application of the proposed pseudo-compressibility concept was demonstrated first by Kwak and Chakarvarthy (1986). They used implicit finite difference techniques to study laminar and turbulent flows over a cylinder and inside a channel. They adopted Baldwin & Lomax model for their turbulent study. They also explained upper and lower bounds of the pseudo-compressibility factor which was used in their code to predict laminar flow characteristics; however, higher order smoothing was required near the walls to make algorithm stable.

The accuracy of the pseudo-compressibility model was tested by S. Rogers et al. (1989) using the code (INS3D) which was developed by Chang and Kwak (1984) & used by Chang, Kwak, et al. (1985). The code simulated flow over a backward facing step and impulsively started circular cylinder for unsteady laminar flows. Authors provided a detailed explanation of the effects on numerical dissipation by addition of second-order accurate smoothing terms. The accuracy and stability of the algorithm depends upon the proper selection of smoothing methods. Authors presented accurate steady state solutions of the above mentioned simulations.

The model of pseudo-compressibility was used by S. Rogers et al. (1987) to simulate unsteady flows. The authors developed a computer code to solve the governing differential equations which adopted an upwind differencing scheme along with implicit solution algorithm to simulate a steady state laminar flow inside a channel and unsteady flow inside an artificial heart with a moving boundary. The authors claimed that the unsteady conservation of mass and momentum equations, which are hyperbolic in pseudo-time, can be solved, using their code, by achieving a steady state solution at each time step.

Soh and Goodrich (1988) used a finite difference scheme to solve unsteady incompressible NS equation using pseudo-compressibility method. The authors used Crank-Nicolson implicit scheme to solve the governing differential equations. They presented time accurate solutions for two-dimensional fluid flows in square cavity with an impulsively starting lid and oscillating lid. The authors claimed with their method they can extract the singularity in the drag on the lid for an impulsively started cavity flow and also obtain a crisp periodicity in the solution of oscillatory flows.

Chen and Pletcher (1993) solved the governing differential equations, which used the pseudo-compressibility model, using Coupled Modified Strongly Implicit Procedure to simulate three-dimensional free surface unsteady incompressible flows. Their study was on sloshing motion in a spherical container undergoing motion characteristics of that experienced aboard a spin-stabilized satellite. The authors successfully demonstrated tracking of free surface particles for laminar flows using two different fluids (Glycerin & Kerosene). The authors were convinced that their numerical simulations exhibit similar behavior as expected in the physical world, but there was no experimental data available at that time to verify their results.

Rahman and Sükonen (2001) developed pseudo-compressibility method which is characterized by the pressure-based algorithm on non-orthogonal collocated grids for incompressible fluid flow problems, using cell-centered finite volume approximation. The authors used a non-traditional way of provoking the density perturbations, assisting the transformation between primitive and conservative variables. They validate the proposed method by simulating forced- and natural-convection inside some selected geometries. Their results indicate that the primitive formulation, utilizing either the momentum-based dissipation scheme or the dual dissipation scheme at the cell face to prevent nonphysical oscillations, has competency in producing satisfactory stabilization for the iteration process.

ZhanSen et al. (2010) used implicit Lower Upper Symmetric Gauss-Siedel algorithm to solve governing differential equations, which uses pseudo-compressibility model. The proposed preconditioning of pseudo-compressibility method for time marching in solving incompressible NS equations, which are stiff hyperbolic in nature. The authors presented the eigenvalues and eigenvectors for Jacobian preconditioned pseudo-compressibility NS equations and claim that a self adaptive pseudo-compressibility factor can increase the convergence rate significantly and Roe's upwind scheme is superior to the second order central scheme for discretization.

Madsen and Schäffer (2006) used the method of pseudo-compressibility to a obtain linear wave solution for progressive and standing waves. They used Euler equations excluding convective and viscous terms.

Later Srivastava et al. (2019) verified and validated the pseudo-compressibility model for incompressible RANS and NS equations in laminar and intermittent turbulent regime respectively for a flow over flat plate. They used the method of Grid Convergence Index, proposed by Celik et al. (2008), for verification and used experimental data obtained using a Particle Image Velocimetry technique for a flow over flat plate to validate of their computer code.

This study provides more details of the author's work on developing a finite-difference fully explicit solver to solve NS and RANS equations, along with turbulence closure model, for steady and unsteady oscillating incompressible flows over a flat plate.

1.2 Intermittent Turbulent Oscillating Flow

In fluid dynamics there exists a closed form solution for an oscillating boundary layer in determining the flow created by an oscillating solid surface. This problem is famously known as Stokes second problem and named after Sir George Stokes. The flow is characterized by oscillating part defined within layer of thickness $\delta_s = (2\nu/\omega)^{1/2}$, where ν is kinematic viscosity of fluid & ω is frequency of oscillation. Then the Stokes Reynolds number $Re_\delta = \delta_s A\omega/\nu$, where A is amplitude of oscillation. Stokes (1850) also presented a closed form analytical solution for oscillating flow over a stationary infinite long plate. The solution of this problem forms the benchmark case for many oscillating flow problems.

The past experimental studies conducted by Hino et al. (1983), Jensen et al. (1989), Akhavan et al. (1991a) and Sarpkaya (1993) on oscillatory boundary layer flows observed the beginning of turbulence as streaks or bursts toward the end of the acceleration phase and sustains in deceleration part of the oscillation cycle. These experimental studies revealed that four distinct flow regimes exist for oscillatory flow over a flat plate. These regimes are (a) Laminar regime which is $Re_\delta < 100$. (b) Disturbed laminar regime that exits for $100 < Re_\delta \leq 550$, here small perturbation occurs, which indicates onset of turbulence.(c) Intermittently turbulent regime, where bursts or streaks of turbulent occurs during the end of acceleration phase and sustains in deceleration phase of cycle for $550 < Re_\delta \leq 3000$.(d) Fully developed turbulent regime for $Re_\delta > 3000$ throughout the cycle.

In 1989, Spalart and Baldwin (1989) used the method of DNS to simulate turbulent boundary layer under free stream velocity that varies sinusoidally in time around zero mean. The results of the authors' study suggested that the oscillating boundary layer is believed to be linearly stable, it exhibits transition stages; pre-transition and well developed turbulence in the different parts of cycle. they also presented an algebraic turbulence model, designed and calibrated for the oscillating flow. It yielded satisfactory results in agreement with DNS results.

Akhavan et al. (1991b) also studied transition to turbulence in bounded oscillatory stokes flow using DNS. The authors' results suggested that transition to turbulence in oscillatory Stokes layers can be explained by secondary instability mechanism of two-dimensional finite amplitude

waves to three-dimensional infinitesimal disturbances. The author claimed that value of the transitional Reynolds number and the statistics of turbulent flow were well predicted by secondary instability mechanism.

In 1998, Vittori and Verizzco (1998) studied intermittent turbulent oscillating flow over a flat plate but imperfect wall, using DNS. The compared their results to experimental studies conducted by Akhavan et al. (1991a) and Hino et al. (1983). The authors presented that in intermittently turbulent regime, the vertically integrated specific kinetic energy is independent of amplitude of wall imperfection and weakly dependent on Reynolds number based on Stokes thickness. The authors concluded that while accelerating part of the cycle is characterized by turbulence production, dissipation starts to be effective during the decelerating phase.

Hsu et al. (2000) studied oscillatory flow over a flat plate using LES and RANS methods. The authors employed dynamic Subgrid scale (SGS) model, while Saffman's turbulence model in RANS. The authors compared RANS results with experimental data reported by Hino et al. (1983). They reported the decrease in phase angle shift between wall shear stress and free stream oscillations in intermittent turbulent regime when predicted by RANS and LES. The authors concluded that because of an excellent agreement between their LES and RANS results in oscillating flow structures as well as the wall shear stress, Saffman's turbulence model is applicable for unsteady flows.

Costamagna et al. (2003) simulated oscillating flow over a flat plate using DNS. The study was performed for values of Reynolds number, based of Stokes boundary layer thickness, within disturbed boundary layer and intermittent turbulent regime. They also suggested that small imperfections in the wall played a fundamental role in triggering transition to turbulence. The authors concluded that low speed streaks starts to appear during the end of the oscillating phase and grows, oscillate and eventually break and dissipates because viscous effects near to the wall. This streak instability mechanism is the dominant mechanism generating and maintaining turbulence in oscillatory boundary layer flows.

In 2007 Salon et al. (2007) investigated intermittent oscillatory flow using LES that incorporated dynamic SGS model for $Re_\delta = 1790$. They compared their results to experimental results obtained by Jensen et al. (1989). The authors' results of dynamic LES model asymptotically

converged towards their DNS with increased grid resolution. The authors successfully predict and simulate the evolution of turbulence over the alternation of acceleration and deceleration phases of cycle of oscillations.

LES simulations for oscillating boundary layer flows over smooth and rough walls was carried by Radhakrishnan and Piomelli (2008) in fully turbulent flows. They compared several methods for unresolved SGS stresses where none of the momentum transport eddies are resolved. The authors claimed that the dynamic SGS eddy viscosity model predicted more accurate results and they validated the LES model with experimental results by Jensen et al. (1989) in the fully turbulent regime. The authors concluded that consistent application of boundary conditions together with use of more advanced SGS model results in accurate flow prediction.

Shome (2013) numerically studied oscillating boundary layer flow over a flat plate using RANS equations with a three equation ($k - k_L - \omega$) phenomenological eddy viscosity turbulence model, developed by Walter and Cokljat (2008). Based on past studies, the author as well identified the distinct flow regimes occurring in oscillatory boundary layer flow. The author simulated oscillating flow over a flat plate using commercial CFD package (ANSYS). The Re_δ ranged from fully laminar to fully turbulent flows. They compared the predicted results for velocity profile and wall shear stress to LES data by Salon et al. (2007) and experimental data by Jensen et al. (1989) for intermittent turbulent regime. The author was able to predict pre-transitional fluctuations which is believed to lead to onset of turbulence with sudden change in shear stress profile. The profiles for laminar and turbulent kinetic energy near to the wall along with Reynolds shear stress at profile at different phase angles were presented for low intermittently turbulent Reynolds number ($Re_\delta = 990$). The author claimed that model did well in the fully turbulent region as well.

All the studies mentioned above using LES and DNS successfully predicts the mean and higher order turbulent statistics for the transitional and fully developed flow regimes and give a successful understanding of oscillatory flow behavior. This however, comes at great computational expense. It can be observed from the above literature that the Re_δ is limited to ≤ 1790 (Salon et al. (2007); Vittori and Verizzco (1998)). Radhakrishnan and Piomelli (2008) also pointed out that application to DNS for fully and near to fully turbulent regime would require

significant amount of computational time and resource. Such resources and computational power may not be available to many researchers and students.

On the other hand the linear eddy viscosity based turbulence model along with RANS equations provides a computational cheaper and robust alternative for industrial applications. These models are widely used in engineering application. Even though these models provide a cheaper alternative, there aren't much studies available on the application of these models on oscillatory boundary layer flows over a flat plate. The studies that can be found in open literature are Blondeaux (1987), Hsu et al. (2000) & Shome (2013). Hence the objective of this thesis is to study the oscillatory boundary layer flow over a flat plate using simpler, robust and accurate two equation k-ϵ turbulence model, modified for the wall, along with RANS equations in intermittently turbulent regime. The author expects to study the kinetic energy and dissipation function during the phase where onset of transition occurs and the phase where the production of turbulent kinetic energy reaches its peak value bridging the viscous and logarithmic layer in wall bounded flows. Due to the nature of this eddy viscosity model, which assumes the turbulence to be isotropic, there may be required a physics based calibration to the model to induce an instability mechanism which creates onset of turbulence in intermittent flow regimes as indicated by the above mentioned studies.

1.3 Undulatory Self-Propulsor

In biological systems, aquatic movements are a result of years of evolution which have been perfected to achieve high efficiency. Amongst such movements, anguilliform locomotion is a form of movement in which the swimmer propels itself forward by propagating a backward traveling wave towards its posterior whose amplitude is increasing over the entire body length. Due to its ability to achieve high propulsive efficiency, arguably, anguilliform swimming has attracted attention of researchers and engineers from various areas in the field of marine propulsion (Lamas and Rodriguez 2020). Anguilliform locomotion is a characteristic of long bodied forms such as eels and lampreys.

One of the earliest theories on anguilliform locomotion and how it produces thrust was developed by Gray who studied eels extensively (Gray 1933). Later, one of the studies (M. S.

Triantafyllou and G. S. Triantafyllou 1995) proved Gray's calculations wrong and found the drag to be lower for an undulating body corresponding to a rigid body. Lighthill (1960) developed a slender body theory to study hydrodynamics on lampreys using ideal flow theory with vortex shedding along with skin friction corrections to account for viscosity. Similar waving-strip idealization of swimming fishes were also studies by Lighthill (1970), Lighthill (1971) and Wu (1961). Vorus (2005) developed a new theoretical model of steady self-propulsion of the waving strip that predicted the production of thrust with no shed vortical wake and high Froude efficiency using ideal flow theory.

Vorus and Taravella (2011) extended the same mathematical theory to be applied in three dimensions and argued that anguilliform undulation with specific motion can generate reactive swimming thrust through fluid inertial reaction without generating circulation, in context of thin boundary layer flows. The lift and vortex shedding does not occur in high Reynolds number anguilliform swimming in achieving the highest propulsive efficiency possible. The above two studies form the theoretical groundwork for the present study. Such ideal flow theories for self-propulsion with no shed vortical wake have been studied in past as well by Saffman (1967) and Miloh and Galper (1993).

Many studies have been conducted on live eels using Particle Image Velocimetry (PIV). Müller et al. (2001) visualized the wake field of live eels using PIV and concluded that they generally undulate either for maximum swimming efficiency or maximum maneuverability. Their findings also suggested that anguilliform swimmers shed two vortices per half tail-beat cycle, which organizes itself into two distinct rows of vortices (Müller et al. 2001). Tytell and Lauder (2004) found a similar wake structure of double row of wake vortex ring aligned in swimming direction for *Anguilla rostrata*. They also used a PIV technique to study wake structures and calculate the swimming efficiency of anguilliform using Lighthill's elongated body theory.

Carling et al. (1998) investigated 2D self-propelled numerical simulations of the eel; however, the predicted wake structure did not agree well with the experiments. Kern and Koumoutsakos (2006) simulated self-propelled eel swimming in 3D and clarified the difference of Carling et al. (1998) by pointing out that 2D simulations do not capture the actual 3D effects which are important. The swimming motion was not specified *a priori* but was obtained through an

evolutionary algorithm used to optimize swimming efficiency and burst efficiency. They observed that for optimized swimming efficiency wake pattern did not result with reverse Kàrmàn vortex sheet. This was consistent with postulation by Müller et al. (2001). They also observed that for burst swimming the tail is responsible for the majority of the thrust, while in efficient swimming the forward part is responsible for thrust generation.

Borazjani and Sotiropoulos (2009) performed numerical simulations to investigate hydrodynamic performance of anguilliform swimmers and compared to that of carangiform swimmers as a function of Reynolds number and Strouhal number. Their virtual swimmer is a 3D lamprey-like flexible body undulating with prescribed kinematics same as experimental anguilliform type (Gray 1933). They found that the net mean force is dependent on Strouhal number and the critical Strouhal number at which the force is zero is a decreasing function of Reynolds number and approaches to the range of Strouhal numbers at which live anguilliform swimmers actually swim. They also found that anguilliform swimmers generate thrust more smoothly than carangiform swimmers and Froude efficiency peak in transitional regimes. The 3D wake structure is primarily dependent on the Strouhal number.

Potts (2015) performed experimental studies on an in-house developed robotic eel and was primarily interested in determining whether a circulation free wake field is achievable as proposed by Vorus and Taravella (2011). Measurements of thrust, drag and lift were collected using a load cell on the robot. The viscous drag on the robot was estimated by analytically computing the thrust component thereby decoupling the robot's drag from it predicted produced thrust. These results were compared with the quasi-static empirical approach that was initially used to predict the viscous drag (Vorus and Taravella 2011), and it is shown that the quasi-static approach significantly under-predicts the viscous drag. The same eel robot is simulated for hydrodynamic analysis in this study. The wake pattern was also investigated using PIV. Potts concluded that with exact motion replication and constant swimming at design speed, the anguilliform robot could achieve vortex free wake. Eastridge (2020) investigated the boundary layer on the same anguilliform robot using PIV. Eastridge observed no turbulent structures or indication of separation of boundary layer at design speed. Skin friction coefficients were estimated and correlated with measurements made for an oscillating rigid cylinder and stationary rigid cylinder.

The preliminary semi-empirical, quasi-static attempts to estimate frictional drag were shown to under-predict the actual drag determined using the net force measurements taken while towing the robot at its design speed which was undulating for that expected swimming speed. This is in agreement with findings of Potts.

As pointed out by Borazjani and Sotiropoulos (2009) and many other studies, it is difficult to perform experiments with live swimmers due to lack of control over the test subject. Perhaps, this was tackled well by Potts (2015) by creating a robotic swimmer. It is still challenging to estimate the complete hydrodynamic characteristics since obtaining 3D flow measurements specially inside the boundary layer, to compute drag and thrust, are extremely difficult even with state-of-the-art 3D PIV techniques that are currently available. Furthermore, pressure field is an important parameter in defining the hydrodynamic forces (Dabri 2005). Therefore, a carefully designed numerical experiment with fully controllable virtual swimmers can be used to investigate hydrodynamics of swimmers over a wide range of flow regimes and body kinematics (Borazjani and Sotiropoulos 2009).

Taravella and C. T. Rogers (2017) numerically investigated the theory proposed by Vorus and Taravella (2011) using a model similar to the robot designed by Potts (2015). They found good agreement with the theory for near body velocity. They concluded that it is plausible for an undulating body to produce purely inertial thrust via body acceleration acting through hydrodynamic added mass. The eel model simulated by Taravella and C. T. Rogers (2017) did not have the ability to rotate the head and tail hemispherical caps, and body segments normal to the anguilliform's center-plane during the dynamic meshing process. The investigation is also limited to inviscid flow simulation and computations of thrust and drag force were yet to be discussed. Therefore, the present investigation concerns the development of a fundamental understanding of fluid dynamics associated with particular autonomous underwater vehicle or the anguilliform robot which could eventually meet some special naval and maritime objectives such as intelligence, surveillance and reconnaissance missions; oceanographic observation; pipeline inspection; etc. Furthermore, this idea of undulatory propulsion can be applied to improve the mobility, efficiency and affordability of low-speed ships and submarines. In this present investigation, the anguilliform robot is simulated with prescribed kinematics as proposed by

Vorus and Taravella (2011) to investigate hydrodynamic characteristics and compute efficiency in viscous and inviscid flow regimes. The rotational motion of head, tail hemispheres and body segments are considered for in this study. The simulations are performed using structured hex-mesh rather than unstructured tetra-mesh. The method of overset mesh is used to circumvent the problem of decreasing quality of the mesh during re-meshing which is experienced in conventional dynamic meshing method.

2 Physical Model

To understand the oscillatory boundary layer flow over a flat plate using numerical techniques, it fist advised to test the proposed numerical solver which uses methos of pseudo-compressibility on a benchmark case. In such flow conditions, flow over a stationary flat plate serves as a good benchmark case study.

2.1 Flat Plate

Flow over a stationary flat plate is adopted as the benchmark model to test the robustness and accuracy of method of pseudo-compressibility . In numerical study mesh resolution plays an extremely important role in achieving a correct converged solution. Especially in boundary layer studies, the mesh near the wall has to be resolved to predict correct time and space evolution of boundary layer and shear stresses. For this purpose, flow over a flat plate serves as a good base model, and it also verifies and validates the accuracy of the numerical solver. Figure 2.1 shows the model of flat plate used in this study.

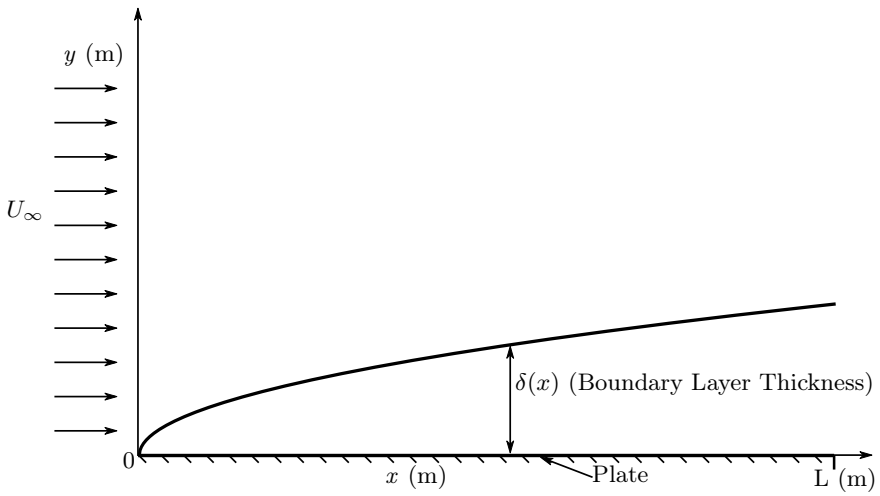

Figure 2.1: Model for Flat Plate

2.2 Oscillating Flow

The objective of this study is to investigate boundary layer in oscillating free stream over a flat plate. Figure 2.2 represents the physical model which will be used to solve for the unknowns in the time dependent oscillating boundary layer flows. The plate is infinitely long and the flow driven by zero mean harmonic pressure gradient (Salon et al. 2007, Radhakrishnan and Piomelli 2008 & Shome 2013) The harmonic pressure gradient in stream wise direction can be given:

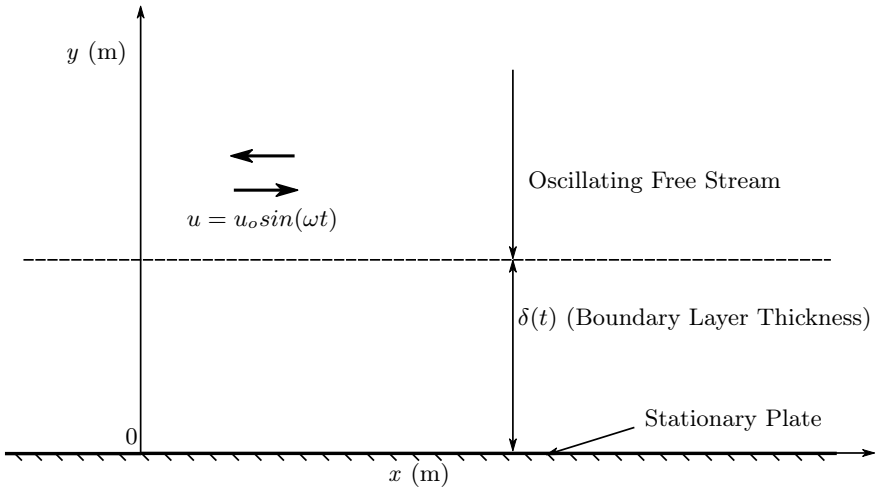

Figure 2.2: Model for Oscillating Free Stream

$$\frac{\mathrm{d}P(t)}{\mathrm{d}x} = -\rho U_{\mathrm{ref}} \omega \cos(\omega t)$$

where P is kinematic pressure and this gives the following free stream velocity:

$$u(t) = \rho U_{\mathrm{ref}} \sin(\omega t)$$

3 Mathematical Model

3.1 Governing Differential Equations

The conservation equation for mass and momentum for two dimensional, unsteady, viscous, incompressible, sub-sonic and turbulent flow can be written as follows.

The continuity equation:

$$\frac{\partial \tilde{u}_j}{\partial x_j} = 0 \tag{3.1}$$

The RANS momentum equation :

$$\rho \left[\frac{\partial \tilde{u}_i}{\partial t} + \frac{\partial (\tilde{u}_j \tilde{u}_i)}{\partial x_j} \right] = -\frac{\partial \tilde{p}}{\partial x_i} + \frac{\partial}{\partial x_j} \left(\mu \frac{\partial \tilde{u}_i}{\partial x_j} \right) + \frac{\partial \tau_{ij}}{\partial x_j} \tag{3.2}$$

where convective term in Equation 3.2 is expressed in conservative form, and:

$$\tau_{ij} = -\rho \overline{u_i' u_j'} \tag{3.3}$$

is *Reynolds-stress term* that incorporates the effect of turbulence on the mean stresses. The Reynolds stress-tensor is symmetric, which includes diagonal components as normal stresses and off-diagonal components as shear stresses. The system of Equations 3.1 and 3.2 is not closed yet, as the Reynolds-stress tensor contains six independent unknowns.

3.2 Turbulence Model

3.2.1 Boussinesq Assumption

The problem of closure of RANS equation requires the Reynolds-stresses in Equation 3.2 to be modeled in terms of mean viscous stress tensor. A common method employs a constitutive relation called "Boussinesq Assumption" which relates Reynolds-stresses to mean velocity gradients

through artificial viscosity called "eddy viscosity" or "turbulent viscosity" and is given as:

$$-\rho\overline{u_i' u_j'} = 2\mu_t \tilde{S}_{ij} - \frac{2}{3}k\rho\delta_{ij} \tag{3.4}$$

where **turbulence kinetic energy** is defined as:

$$k \equiv \overline{ke'} = \frac{1}{2}\overline{u_i' u_i'} \tag{3.5}$$

where μ_t is **kinetic eddy viscosity** and $\tilde{S}_{ij}$ is mean strain rate tensor:

$$\tilde{S}_{ij} = \frac{1}{2}\left(\frac{\partial \tilde{u}_i}{\partial x_j} + \frac{\partial \tilde{u}_j}{\partial x_i}\right) \tag{3.6}$$

The assumption is appropriate as it assumes that the eddy viscosity is an isotropic scalar quantity-which according to Alfonsi (2009) is not. The turbulent viscosity is considered to be uniform in all directions within the computational cell. The turbulent kinetic energy is determined from an energy balance equation of the form:

$$\frac{\partial k}{\partial t} + \frac{\partial(\tilde{u}_j k)}{\partial x_j} = -\frac{\partial D_j'}{\partial x_j} + \mathcal{P}' - \epsilon' \tag{3.7}$$

Here D_j' is Turbulent diffusion, $\mathcal{P}'$ is turbulent energy production, and ϵ' is turbulent dissipation terms.

3.2.2 Chien's Low Reynolds k–ϵ model

The closure models for RANS equation are modeled to represent higher order moments of velocity fluctuations in terms of lower order moments. This is possible directly in turbulent viscosity (also called "First order" models) models. Due to success of these models in study of basic physical fluid flows phenomenon coupled by their advantage of less dependency on computational power. To simulate the problem of flow over flat plate this study adopts the use of Standard k–ϵ model modified near to the wall as per Chien (1982) modification.

The Turbulent Kinetic energy defined by Low Reynolds k–ϵ closure model (Chien's model)

adopted in this study is defined by:

$$\frac{\partial k}{\partial t} + \frac{\partial(\tilde{u}_j k)}{\partial x_j} = \frac{1}{\rho}\frac{\partial}{\partial x_j}\left[\left(\mu + \frac{\mu_t}{Pr_k}\right)\frac{\partial k}{\partial x_j}\right] - \tau_{ij}\frac{\partial \tilde{u}_i}{\partial x_j} - \epsilon - \frac{2\mu k}{\rho y^2} \tag{3.8}$$

The Turbulent dissipation function is defined as:

$$\begin{aligned}\frac{\partial \epsilon}{\partial t} + \frac{\partial(\tilde{u}_j \epsilon)}{\partial x_j} =& \frac{1}{\rho}\frac{\partial}{\partial x_j}\left[\left(\mu + \frac{\mu_t}{Pr_\epsilon}\right)\frac{\partial \epsilon}{\partial x_j}\right] - C_{\epsilon_1} f_1 \frac{\epsilon}{k}\tau_{ij}\frac{\partial \tilde{u}_i}{\partial x_j} - \frac{C_{\epsilon_2} f_2 \epsilon^2}{k} \\ & - \frac{2\mu\epsilon e^{-y^+/2}}{\rho y^2}\end{aligned} \tag{3.9}$$

The constants and kinetic eddy viscosity are defined as:

$$\begin{aligned} \mu_t &= \frac{C_\mu f_\mu \rho k^2}{\epsilon} & C_\mu &= 0.09 & f_\mu &= 1 - e^{-0.0115 y^+} \\ Pr &= 1.0 & Pr_e &= 1.3 & C_{\epsilon_1} &= 1.35 \\ C_{\epsilon_2} &= 1.80 & f_1 &= 1 \end{aligned} \tag{3.10}$$

The f_2 in Equation 3.9 is defined as:

$$f_2 = 1 - 0.22 e^{-\left(\frac{Re_t}{6}\right)^2}, \qquad Re_t = \frac{\rho k^2}{\mu\epsilon} \tag{3.11}$$

The effective viscosity that occurs in Equation 3.2 after substitution of Reynolds-stresses from Equations 3.3 and 3.4 is defined as:

$$\mu_{\text{eff}} = \mu + \mu_t \tag{3.12}$$

3.2.3 Jone and Launder k–ϵ model

Justesen and Spalart (1990) showed that Chien's k–ϵ model was calibrated using only experimental channel-flow data and flat plate boundary layer data. There were evidence from DNS that this data were not very accurate near the wall. Also for the case of the time dependent oscillating flow problem the model does not do well near the wall due to wall functions. Therefor to study the intermittent turbulent oscillating flow, the base model chosen is by Jones and Launder (1972) due to its simplicity and absence of wall functions. The eddy viscosity is modeled

using turbulent Reynolds number and is free from functions based on distance from the wall. The turbulent kinetic energy is defined as:

$$\frac{\partial k}{\partial t} + \frac{\partial(\tilde{u}_j k)}{\partial x_j} = \frac{1}{\rho}\frac{\partial}{\partial x_j}\left[\left(\mu + \frac{\mu_t}{Pr_k}\right)\frac{\partial k}{\partial x_j}\right] + \tau_{ij}\frac{\partial \tilde{u}_i}{\partial x_j} - \epsilon - 2\nu\left(\frac{\partial \sqrt{k}}{\partial x_j}\right)^2 \tag{3.13}$$

The Turbulent dissipation function is defined as:

$$\begin{aligned}\frac{\partial \epsilon}{\partial t} + \frac{\partial(\tilde{u}_j \epsilon)}{\partial x_j} =& \frac{1}{\rho}\frac{\partial}{\partial x_j}\left[\left(\mu + \frac{\mu_t}{Pr_\epsilon}\right)\frac{\partial \epsilon}{\partial x_j}\right] + C_{\epsilon_1} f_1 \frac{\epsilon}{k}\tau_{ij}\frac{\partial \tilde{u}_i}{\partial x_j} - \frac{C_{\epsilon_2} f_2 \epsilon^2}{k} \\ &+ 2\nu\nu_t\left(\frac{\partial^2 \tilde{u}_j}{\partial x_j^2}\right)^2\end{aligned} \tag{3.14}$$

The constants and kinetic eddy viscosity are defined as:

$$\begin{aligned}&\mu_t = \frac{C_\mu f_\mu \rho k^2}{\epsilon} && C_\mu = 0.09 && f_\mu = \exp\left(\frac{-2.5}{(1 + R_t/50)^2}\right) \\ &Pr = 1.0 && Pr_e = 1.3 && C_{\epsilon_1} = 1.44 \\ &C_{\epsilon_2} = 1.92 && f_1 = 1\end{aligned} \tag{3.15}$$

The f_2 in Equation 3.14 is defined as:

$$f_2 = 1 - 0.3\exp\left(-Re_t^2\right), \qquad Re_t = \frac{\rho k^2}{\mu\epsilon} \tag{3.16}$$

The effective viscosity that occurs in Equation 3.2 after substitution of Reynolds-stresses from Equations 3.3 and 3.4 is defined as:

$$\mu_{\text{eff}} = \mu + \mu_t \tag{3.17}$$

3.3 Non-Dimensional form

The non-dimensionalization of the independent and primitive variables can be done using:

$$\bar{x} = \frac{x}{L_{ref}} \qquad \bar{y} = \frac{y}{L_{ref}} \qquad \bar{u} = \frac{u}{U_{ref}}$$
$$\bar{v} = \frac{v}{U_{ref}} \qquad \bar{t} = \frac{tU_{ref}}{L_{ref}} \qquad \bar{p} = \frac{p}{\rho U_{ref}^2}$$

3.4 Pseudo-Compressibility

The difficulty in numerically solving laminar incompressible Navier-Stokes flow equations is the absence of the temporal term for pressure(or density), which arises due to absence of the equation of state, in the continuity equation. This void/absence decouples the continuity and momentum equations. As mentioned by Chen (1990), numerical methods developed for compressible flows are not appropriate for solving low Mach (<0.3) flows. Issa (1983) found that when density is used as primitive variable for incompressible flows, the pressure gradients in momentum equations become very sensitive to variation in density. The sensitivity causes round-off error to sometimes grow and dramatically slow down the convergence rate of calculation. Chorin (1967) is the first to propose an idea to circumvent the difficulty of pressure decoupling by introducing a method called *Pseudo-Compressibility* or *Artificial-Compressibility*. The idea is to introduce a time derivative term of artificial density in continuity equation which relates to the actual thermodynamic pressure in the momentum equation. This solves the problem of decoupling. Hence the continuity and momentum equations for turbulent flows become:

$$\frac{\partial \bar{\rho}}{\partial \bar{t}} + \frac{\partial \bar{u}_j}{\partial \bar{x}_j} = 0 \tag{3.18}$$

$$\frac{\partial \bar{u}_i}{\partial \bar{t}} + \frac{\partial (\bar{u}_j \bar{u}_i)}{\partial \bar{x}_j} = -\frac{\partial \bar{p}}{\partial \bar{x}_i} + \frac{1}{Re}\frac{\partial}{\partial \bar{x}_j}\left[\left(1 + \frac{\mu_t}{\mu}\right)\frac{\partial \bar{u}_i}{\partial \bar{x}_j}\right] \tag{3.19}$$

where $\bar{\rho}$ is the artificial density and is related to non-dimensional thermodynamic pressure by:

$$\bar{\rho} = \frac{\bar{p}}{\beta}, \quad \text{where } \beta \text{ is } \textbf{artifical compressibility} \tag{3.20}$$

For steady-state flow case $\bar{t} \equiv \tau$, an iteration time, analogous to real time in compressible flows. The system of equation for incompressible flows are of elliptic type. However, after the modification as per Pseudo-Compressibility the system of Equations 3.18 and 3.19 becomes hyperbolic-parabolic which are often less computationally expensive to be solved than elliptic equations. As per Chang and Kwak (1984), the pressure waves propagate with infinite speed in elliptic type formulation but in hyperbolic-parabolic, these pressure waves have finite speeds. The magnitude of the pressure waves depends upon the parameter β. This is a disposable parameter, analogous to relaxation parameter. This enables the system of equation to converge until divergence free velocity is obtained to satisfy incompressible condition and doing so, the effect of pseudo-compressibility decreases as the solution is reached to steady state. Hence Chorin (1967) found that solution does not depend on β but the speed at which the solution converges does. The above formulation is analogous to low speed compressible flows. In fact one can define an artificial speed of sound, $\bar{c}$, for above formulation as:

$$\bar{c} = \frac{1}{\sqrt{\beta}} \tag{3.21}$$

Where artificial Mach number M can be defined as

$$M = \frac{Re}{\bar{c}} max\sqrt{\bar{u}^2 + \bar{v}^2} \tag{3.22}$$

In this study, M <1 for flow simulated using pseudo-compressibility. The method of pseudo-compressibility can be extended to unsteady flows like oscillating flows by modifying Eqs 3.18 and 3.19 as:

$$\frac{\partial \bar{\rho}}{\partial \bar{\tau}} + \frac{\partial \bar{u}_j}{\partial \bar{x}_j} = 0 \tag{3.23}$$

$$\frac{\partial \bar{u}_i}{\partial \bar{\tau}} = -\frac{\partial \bar{u}_i}{\partial \bar{t}} - \frac{\partial (\bar{u}_j \bar{u}_i)}{\partial \bar{x}_j} - \frac{\partial \bar{p}}{\partial \bar{x}_i} + \frac{1}{Re} \frac{\partial}{\partial \bar{x}_j} \left[\left(1 + \frac{\mu_t}{\mu} \right) \frac{\partial \bar{u}_i}{\partial \bar{x}_j} \right] \tag{3.24}$$

The above system is iterated in pseudo-time τ at a particular time step till divergence free field is satisfied i.e, $\frac{\partial p}{\partial \tau} = 0$ and $\frac{\partial u_i}{\partial \tau} = 0$.

4 Numerical solution method

A Fully Explicit Finite Difference (FEFD) method is adopted to solve the governing differential equations presented in Chapter 3 along with the boundary condition. The discretization scheme adapted for solution method along with grid generation scheme and solution algorithm used for determining the primitive variables for the various cases under study are presented below (for laminar and intermittently turbulent regimes).

4.1 Computational Domain

A numerical study was conducted to validate and verify the accuracy of pseudo-compressibility model. Specifically to study the convergence of RANS equations with NS equations in intermittent turbulent regime for unsteady flows. For this purpose the first or base model is chosen as flow over a flat plate. To accomplish this study of primitive variables within the boundary layer, the computational domain size is chosen to be 0.0254×0.0254 m (stream wise × wall normal). The wall normal domain is sufficiently large enough to ensure no obstruction in the boundary layer growth for highest Reynolds number used in this study. The stream wise extent is large enough to keep the aspect ratio of mesh below 5 for all computational studies. The working fluid is taken as water (ρ=998.2 kg/m^3). Figure 4.1 shows a typical finite difference grid (similar grid

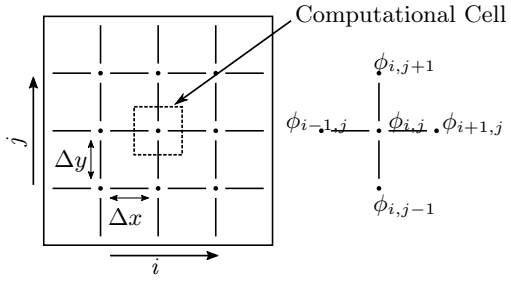

Figure 4.1: Typical Finite Difference Grid & Computational Cell

is adopted by this study) along with graphical representation of computational cell. The grid or

meshes generated for this study on which governing differential equations along with boundary conditions are discretized and solved are presented below. The meshes are stretched and cells are collapsed near the wall to achieve finer spatial resolution for study of boundary layer flows.

4.2 Grid Generation Scheme

In cases of wall bounded flows, the gradients of primitive variables are high near the wall which actually forms the boundary layer. Hence to study the distribution of unknown variables (velocity, pressure, kinetic energy and dissipation function) inside the boundary, the mesh near the wall needs to be finer. Another need for finer mesh near the boundary is to satisfy the criteria of $y^+<5$ to catch the viscous sublayer in intermittently turbulent flows, which needs the mesh to be extremely fine near the wall. However, making too fine mesh outside the boundary layer will only increase the computation time as the free stream flow does not change. Hence we adopt the technique of stretching the mesh near the wall in transverse direction of the flow. The mesh in stream-wise direction is equal/uniform. Mesh clustering is achieved near boundaries using transformation adopted from Özişik (1994):

$$\xi = x; \quad \eta = 1 - \frac{\ln(A(y))}{\ln(B)}; \quad A(y) = \frac{\bar{\beta} + (1 - y/h)}{\bar{\beta} + (1 + y/h)}; \quad \text{where} \quad B = \frac{\bar{\beta} + 1}{\bar{\beta} - 1} \tag{4.1}$$

Here $\bar{\beta}$ is the stretching factor ranging between $1<\bar{\beta}<\infty$. As the values approaches 1, more grids are clustered near boundary. The back transformation to x and y domain is achieved through:

$$x = \xi; \quad y = \left[\frac{(\bar{\beta} + 1) - (\bar{\beta} - 1)(B^{1-\eta})}{1 + B^{1-\eta}} \right] h \tag{4.2}$$

The governing differential equations are solved in ξ and η domain and then back transformed to x and y coordinates. Figures 4.2 & 4.4 shows meshes adopted for Laminar and Intermittent turbulent flow studies. 81×81 & 81×400 (stream wise × wall normal) for laminar and intermittent turbulent cases respectively. Figures 4.3 & 4.5 shows the magnified version of two meshes near the wall.

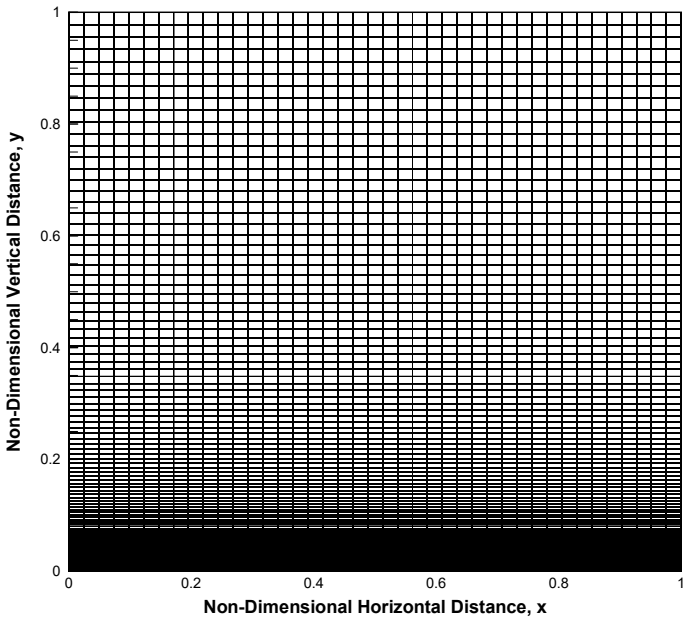

Figure 4.2: Computational Mesh for flow in Laminar regime (81×81)

4.3 Discretization Method

The thrust of this study is to investigate intermittently turbulent oscillating flow over a flat plate in incompressible flow using pseudo-compressibility. The governing differential equations used in the in-house computer code to predict the unknowns are discretized using explicit finite difference techniques. The terms in the governing differential equations are grouped as temporal, convective, pressure and viscous terms.

4.3.1 Temporal Term

Considering ϕ be a general independent variable. The temporal term are discretized using second order Runge-Kutta central differencing:

$$\frac{\partial \phi^{n+1}}{\partial t} = \frac{3\phi^{n+1} - 4\phi^{n} + \phi^{n}}{2\Delta t} \tag{4.3}$$

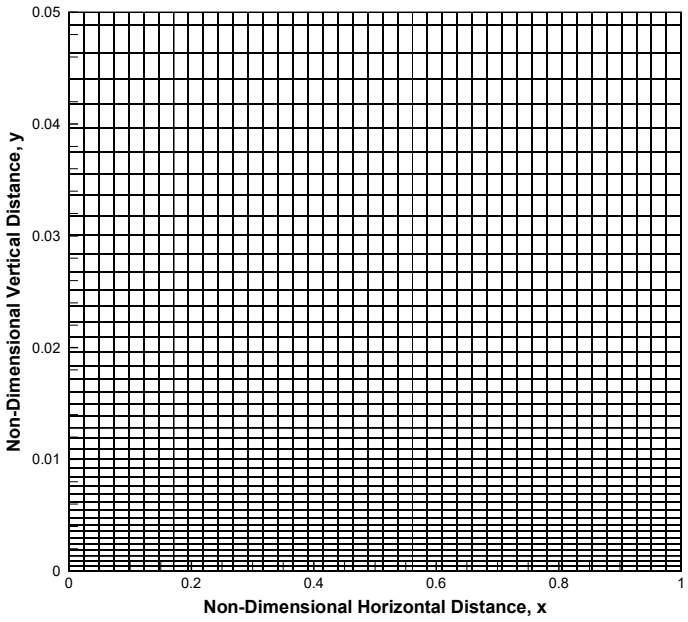

Figure 4.3: Mesh near the wall for flow in Laminar regime

4.3.2 Pseudo-Temporal Term

The temporal pseudo-term in Eq 3.24 is discretized using first order backward differencing:

$$\frac{\partial \phi^{n+1}}{\partial t} = \frac{\phi^{n+1} - \phi^{n}}{\Delta t} \tag{4.4}$$

4.3.3 Convective Term

The convective term in RANS Eq 3.23, closure model 3.13 & 3.14 and NS Eq 3.24 (without Boussinesq Assumption) for intermittently turbulent and laminar flows respectively are discretized using second order central differencing:

$$\frac{\partial \phi^{n}_{i,j}}{\partial x} = \frac{\phi^{n}_{i+1,j} - \phi^{n}_{i-1,j}}{2\Delta x} \tag{4.5}$$

Except the convective term in stream-wise direction is discretized using upwind scheme as suggested by S. Rogers et al. (1989)

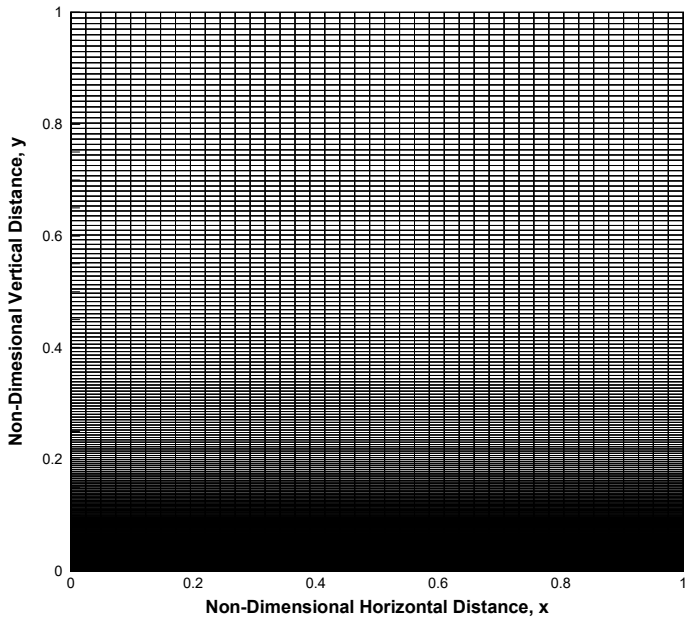

Figure 4.4: Computational Mesh for flow in Intermittent Turbulent regime (81×400)

4.3.4 Pressure Term

The pressure term is discretized using second order central differencing according to Equation 4.5.

4.3.5 Viscous Term

The viscous terms are also discretized using second order central differencing:

$$\frac{\partial^2 \phi_{i,j}^n}{\partial x^2} = \frac{\phi_{i+1,j}^n - 2\phi_{i,j}^n + \phi_{i-1,j}^n}{\Delta x^2} \tag{4.6}$$

The diffusion and generation term in the $k - \epsilon$ turbulence model Equations (3.8 & 3.9) are also discretized using second-order central differencing.

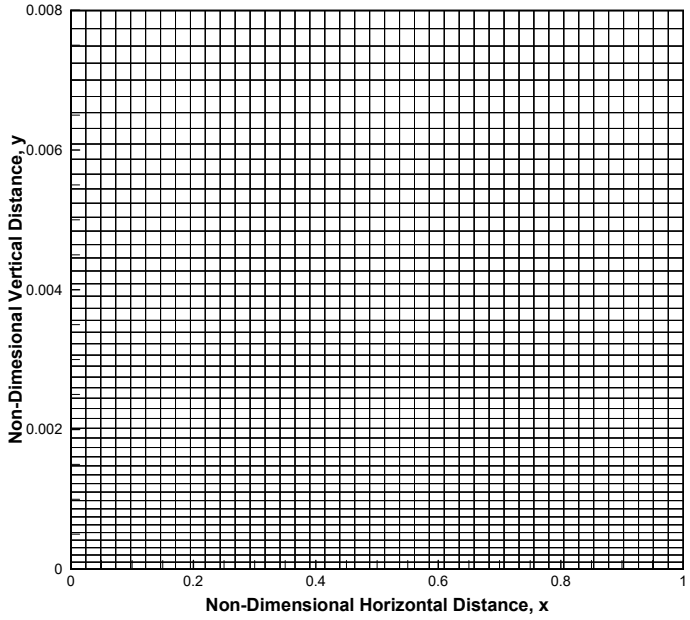

Figure 4.5: Mesh near the wall for flow in Intermittent Turbulent regime

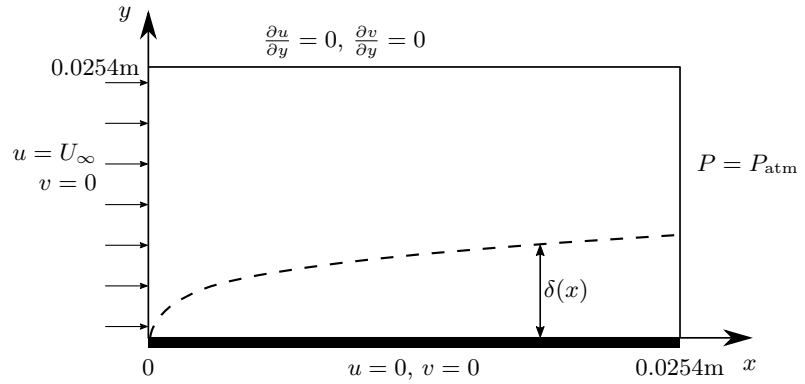

Figure 4.6: Computational Domain with Boundary Conditions

4.4 Boundary Conditions

4.4.1 Flat Plate

Figure 4.6 shows the computational domain of 0.0254×0.0254 m with boundary conditions for a flow over a flat plate. The boundary conditions are as follows. The bottom boundary plate, is treated as an impermeable wall with no slip condition. The vertical and horizontal velocity are

prescribed zero at the wall. Since it is nearly parallel flow, the derivative of horizontal velocity in y-direction at the top boundary can be prescribed as zero and the vertical velocity is prescribed as zero too. For the governing differential equations to be well posed, the horizontal and vertical velocities are interpolated at the exit boundary and pressure is prescribed as P_{atm}. At inlet, the free stream horizontal velocity U_{ref} is prescribed with vertical velocity as zero. The k-ϵ values at the bottom wall is prescribed as zero (Chien 1982) and derivatives of it at the top boundary in y-direction is prescribed zero. At the inlet, values to k-ϵ is prescribed as 10^{-6} and at exit they are extrapolated.

4.4.2 Oscillating Flow

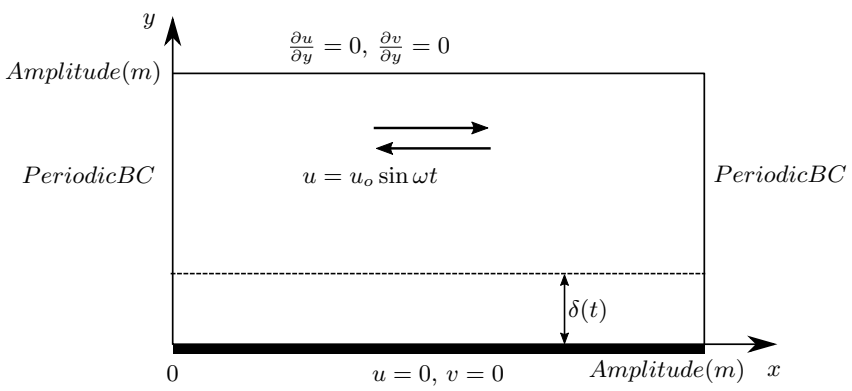

Figure 4.7: Computational Domain with Boundary Condition for Oscillating Flow

Figure 4.7 shows the computational domain for the oscillating flow over a flat plate problem. The size of computational domain depends on the amplitude which depends on the Reynolds number chosen. The boundary conditions are as follows. The bottom boundary plate, is treated as an impermeable wall with no slip condition. The vertical and horizontal velocity are prescribed zero at the wall. The kinetic energy and dissipation function is also applied zero at the wall. The derivatives of primitive variables in the y-direction are prescribed 0 at the top boundary. Periodic boundary conditions are prescribed at the inlet and outlet to simulate infinitely long plate. The flow is driven by harmonic pressure gradient as discussed in chapter 2. Since it is an unsteady problem, the initial conditions are, u and v as zero. Turbulent kinetic energy (k)

and dissipation function (ϵ), is calculated based on the turbulent intensity of 1.5% and turbulent viscosity ratio of 100.

4.5 Solution Procedure

The solution procedure adopted to solve laminar and intermittently turbulent flows require modified pseudo-compressibility Equation 3.18 to be solved for artificial density using velocities from previous iteration. The dynamic pressure is solved using Eq 3.20, where β is fixed for a particular time step and is calculated using pseudo-mach number, as per relations 3.21 and 3.22 and already converged velocities from previous time step. The horizontal and vertical velocities at the current iteration are calculated using discretized form Equation 3.19. Turbulent flows requires discretized form of Equations 3.8 and 3.9 to be solved for calculation kinetic energy and dissipation function which is needed to solve for effective (3.12) and eddy viscosity at each iteration. The boundary conditions remains fixed while the iterations proceeds in pseudo-time to achieve divergence free velocity field. This is checked using convergence criterion on each primitive variable as:

$$\left[\frac{\sum_{i,j=1}^{i_m,j_m}\left(\frac{\phi_n^{k+1}-\phi_n^k}{\phi_{n,rms}^{k+1}}\right)^2}{i_m \times j_m}\right]^{0.5} \leq 10^{-6} \tag{4.7}$$

Once the convergence is achieved, then the boundary conditions are updated and the solution moves to next time step and iterations begin all over again. The artificial compressibility β is calculated again at each time step, using relation 3.21 and 3.22 and velocities from previous time step, before the solution enters iteration loop at a particular time step. The pseudo-mach number remains fixed at every time step.

5 Flat Plate

5.1 Verification

The definition of Verification dictates the establishment of procedure for accuracy or validity of something. The objective of computational fluid dynamics is to model and predict results for physical events for which experimental data is not available. With rapid advancement in computing power and cost effective nature of numerical modeling has made CFD and important tool in designing and studying engineering problems. As per Feritas (1993), numerical simulation, just like physical experiments, are also needed to be evaluated for numerical errors and uncertainty and techniques for such processes are less well developed and accepted. The Fluids Engineering Division of ASME has worked on estimation and control of numerical uncertainty and error estimation in CFD studies. Celik et al. (2008) has established one such method called *Grid Convergence Index* (GCI) for evaluating numerical accuracy and uncertainty of a CFD simulation. This helps in verification of any computer code which is written for numerical study. This section elaborates more on use of GCI method to verify the accuracy and determine the numerical uncertainty for the Pseudo-Compressibility model as explained by Srivastava et al. (2019). In addition to GCI, mesh and time independent study is also conducted to determine the optimum mesh size and time step (for unsteady case) for laminar flows.

5.1.1 Mesh Independence Study

To verify grid independence for the pseudo-compressibility model, numerical simulations were repeated for three different meshes for Re=2099. Three meshes uniformly spaced grid were chosen, 41×41, 61×61 & 81×81. The general characteristic of the contour plot were changed to change very little, however, predicted velocities close to the wall at the trailing edge for flow over a flat plate, were better with 81×81 mesh size (also seen in Figure 5.2). As it can be observed

from Table 5.1, there is only 1.399% change in $\bar{u}_{max}$ from 41×41 to 81×81. To verify further, a finer grid of 121×121 was chosen however, no significant changes were observed in velocity profiles.

Table 5.1: Comparison of maximum $\bar{u}$ for three meshes at $\bar{y}$=0.11

Meshes	$\bar{u}_{max}$	% Deviation from 81×81 mesh results
41×41	1.0635	1.399
61×61	1.0721	0.4026
81×81	1.0733	0.0000

5.1.2 Time Independence Study

A time increment study was conducted for laminar flow regimes for Re=2099. It was observed due to the selection of pseudo-compressibility factor (δ) for fast convergence; FEFD method requires minimum of 10^{-4} $\bar{t}$. It can be observed from Table 5.2 that only 0.0093% change in $\bar{u}_{max}$ and any time increment smaller than this value did not result any significant changes in magnitude of predicted velocities. For the present study a $\Delta\bar{t}$ of 10^{-5} was chosen to attain a required stable convergence, even for turbulent flows.

Table 5.2: Comparison of maximum $\bar{u}$ for three $\Delta\bar{t}$ at $\bar{y}$=0.11

$\Delta\bar{t}$	$\bar{u}_{max}$	% Deviation from 10^{-6} time step results
10^{-4}	1.0729	+0.0373
10^{-5}	1.0734	-0.0093
10^{-6}	1.0733	0.0000

5.1.3 Grid Convergence Index

The methodology and equations used for calculation of uncertainty estimation and GCI index presented below are verbatim from Celik et al. (2008).

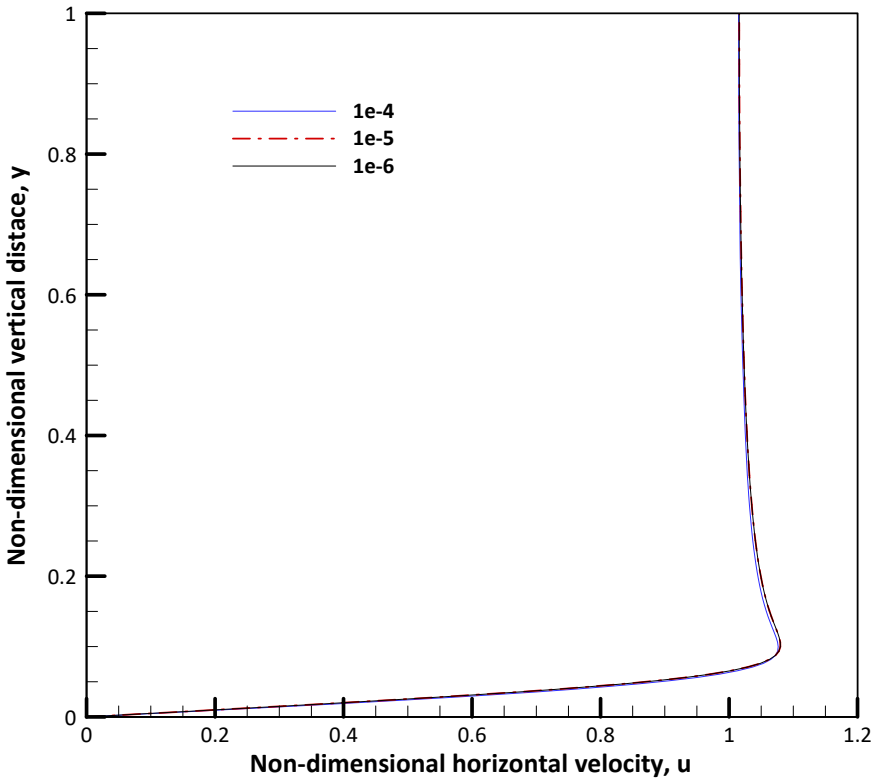

Figure 5.1: Horizontal Velocity Profiles at the outlet for three different time increments for Re 2099

1. Defining representative cell size h, for two dimension;

$$h = \sqrt{\frac{1}{N}\sum_{i=1}^{N}(\Delta A_i)} \tag{5.1}$$

ΔA_i is the area of i^{th} computational cell, and N is total number of cells used in computation.

2. Select three different grid sizes and run the simulation and determine the value of variable, example ϕ. The grid refinement factor $r = \frac{h_{coarse}}{h_{fine}}$ is recommended to be greater than 1.3.

3. Let $h_1 < h_2 < h_3$ and $r_{21} = h_1/h_2$, $r_{32} = h_3/h_1$, and calculate the apparent order p using

$$p = \frac{1}{\ln(r_{21})}|\ln(|\epsilon_{32} - \epsilon_{21}|) + q(p)| \tag{5.2}$$

$$\text{where} \quad q(p) = \ln\left(\frac{r_{21}^p - s}{r_{32}^p - s}\right) \tag{5.3}$$

$$s = 1.\text{sgn}(\epsilon_{32}/\epsilon_{21}) \tag{5.4}$$

where $\epsilon_{32} = \phi_3 - \phi_2$, $\epsilon_{21} = \phi_2 - \phi_1$ and above equations can be solved using fixed point iteration, with initial guess equal to the first term. Negative values of $\epsilon_{32}/\epsilon_{21}$ are an indication of oscillatory convergence.

4. Calculate the extrapolated values from

$$\phi_{ext}^{21} = \left(r_{21}^p \phi_1 - \phi_2\right) / \left(r_{21}^p - 1\right) \tag{5.5}$$

similarly, calculate ϕ_{ext}^{32}.

5. Calculate the following error estimates; Approximate relative error:

$$e_a^{21} = \left|\frac{\phi_1 - \phi_2}{\phi_1}\right| \tag{5.6}$$

Extrapolated relative error:

$$e_{ext}^{21} = \left|\frac{\phi_{ext}^{21} - \phi_1}{\phi_{ext}^{21}}\right| \tag{5.7}$$

Fine Grid Convergence Index (GCI):

$$\mathrm{GCI}^{21}_{fine} = \frac{1.25 e^{21}_a}{r^p_{21} - 1} \tag{5.8}$$

For the purpose of validation and verification of Pseudo-Compressibility model, flow over a flat plate is chosen as a benchmark case. The computational domain is 2D plane of 0.0245×0.0254 m, the free stream velocity was calculated from Reynolds number, based on characteristic length of 0.0254 m, to be 0.0941 m/sec. Three mesh configurations were considered (41×41, 61×61 and 81×81) for GCI calculation. 42 points along the outlet plane at trailing edge were chosen for calculation based on local parameter of non-dimensional horizontal velocity, ū.

Table 5.3: Sample Calculation for Discretization Error

Terms	ϕ
N_1, N_2, N_3	81×81,61×61,41×41
r_{12}	1.3278
r_{32}	1.4878
ϕ_1	1.0554
ϕ_2	1.0734
ϕ_3	1.0759
p	0.1074-8.6406
p_{avg}	2.1790
ϕ^{ext}_{21}	1.0780
e^{21}_a	1.714%
e^{21}_{ext}	4.801%
GCI^{21}_{ext}	5.726%

Table 5.3 illustrates the calculation of this procedure. GCI values were calculated with non-dimensional horizontal velocity as local parameter determining the numerical uncertainty. Figure 5.2 show outlet profiles for three different grids used (it is expanded to see the differences) and Figure 5.3 show same with extrapolated values calculated using global order of accuracy. The local order of accuracy ranged from 0.1074 to 8.6406 with global average of 2.179. Oscillatory convergence was observed in 2.439% of 42 points. Two separate GCI were calculated using local and global average of accuracy. The maximum GCI using local order of accuracy is 5.726%

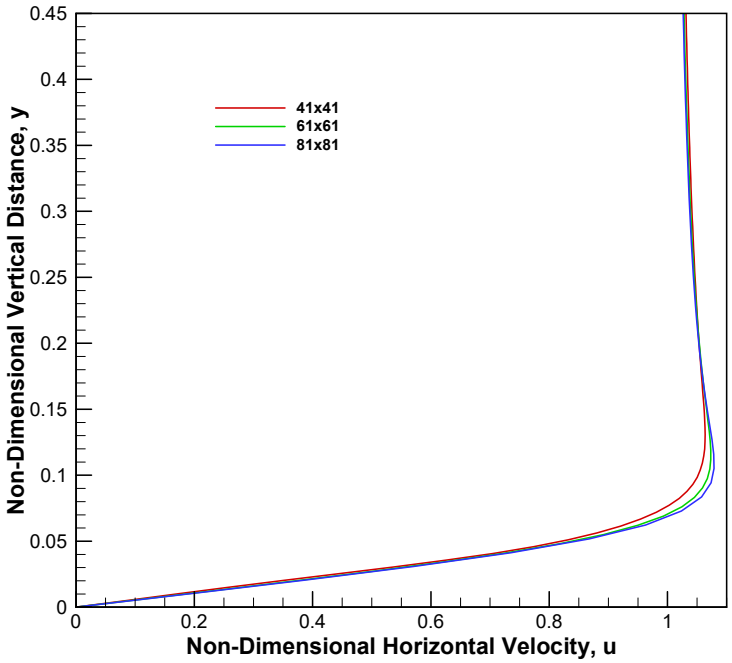

Figure 5.2: Horizontal Velocity Profiles at the outlet for three different meshes at x=0.0254 m and $\bar{u}_\infty = 0.0941$ m/sec

which corresponds to non-dimensional velocity of ± 0.00568. The maximum GCI using global average is 2.549% which corresponds to non-dimensional velocity of ± 0.000992. It is clear from these values that discretization error is small. The error bar plot show in Figure 5.4 indicates numerical uncertainty plotted with extrapolated values.

5.2 Validation

5.2.1 Experimental Setup

Experimental investigation is required to validate the accuracy of the numerical model. For this purpose a non-intrusive technique which measures the instantaneous velocity of fluid particles, called Particle Image Velocimetry (PIV) is adopted. PIV is also used to study the viscous effects on the hydrodynamic drag of an undulatory anguiliform like propulsors in broader scope of this project. In the initial stages of the same project this technique is employed to study uniform

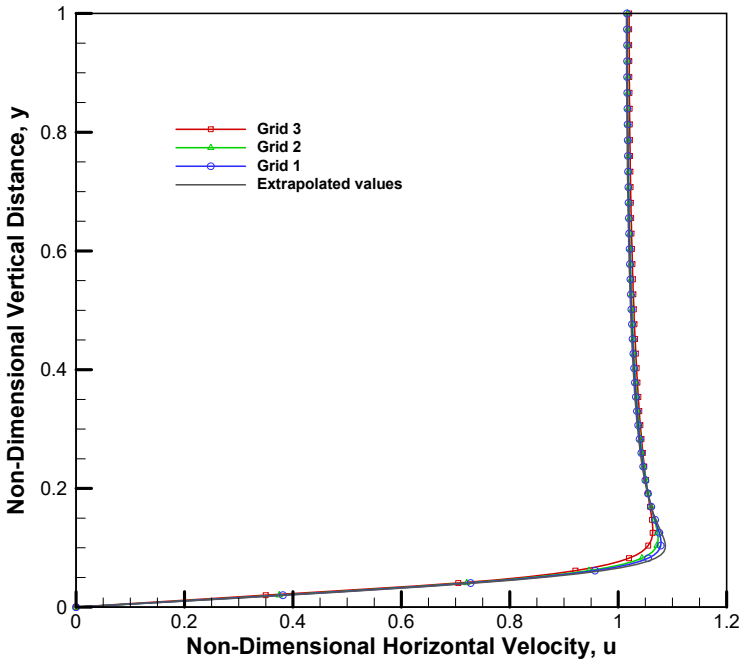

Figure 5.3: Horizontal Velocity Profiles at the outlet for three different meshes and extrapolated values at x=0.0254 m and $\bar{u}_\infty = 0.0941$ m/sec

laminar flow over a flat plate. For this purpose a hydraulic flume was developed at University Of New Orleans. The data collected was used to validate the numerical data predicted, for flow over a flat plate, by code which employs FDFE technique to solve Pseudo-Compressibility model equations. PIV technique is centered around optical tracking of tracer particles called seeding particles (added to the fluid), are neutrally buoyant, hollow, and silver-coated micro spheres. These seeding particles are illuminated in the region of interest by a dual cavity laser, twice within short known time interval. The light scattered by these particles is collected by high-speed cameras. The calibration of these cameras determines the displacement of the seeding particles in the real world coordinates from the image plane (pixels) captured. The in-built software process these images to provide velocity vector fields for the region of interest. Since the prime objective of this research is to study intermittent turbulence, viscous effects within boundary layer and wall shear stress near to the wall, there is a need to validate the global vector fields observed using optical flow visualization techniques (such as PIV) with another non-intrusive

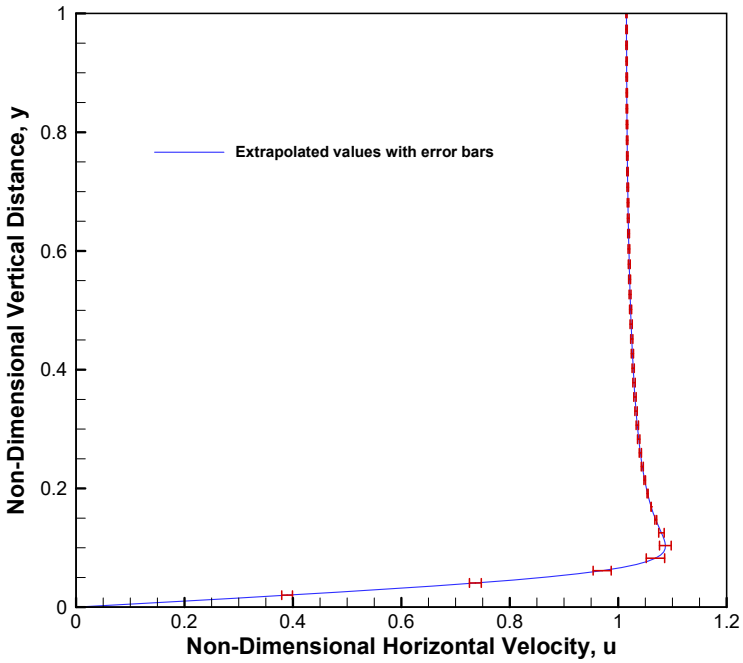

Figure 5.4: Fine Grid Solution with discretization error bars at x=0.0254 m and $\bar{u}_\infty = 0.0941$ m/sec

directional sensitive measurement technique which measure the velocity of the fluid particles locally and does not require calibration. Such technique used to validate PIV results is Laser Doppler Anemometry (LDA).

Another experimental setup built to study Lid-driven Flows (Akyuzlu (2017)) employs LDA technique to capture horizontal velocity magnitudes locally at spatial points situated close to the wall and to the center of the cavity. The same setup employs PIV as well which and its results are validated using LDA.

5.2.2 Hydraulic-Flume

A hydraulic flume is built to study flow over a flat plate using 2D PIV. A schematic diagram in Figure 5.5 shows two views of the flume arrangement. The channel walls and bottom are made of 25 mm thick transparent acrylic glass. This allows the high speed camera to see and capture images clearly. The laser sheet is situated beneath the flume's centerline and parallel to the flow.

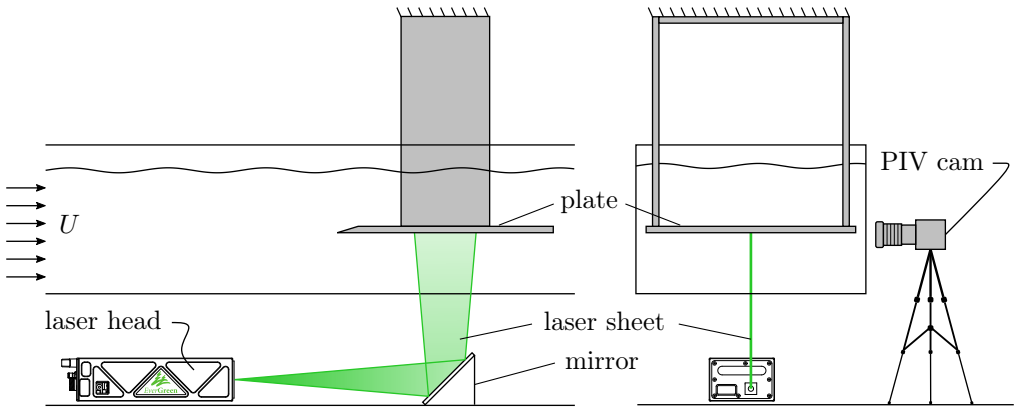

Figure 5.5: PIV configuration for flat plate investigations; side view (left) and cross-section (right)

The sheet is directed on the test article (plate) using an 45deg reflecting mirror. The test article is made up of 6 mm thick plexiglass, suspended in the flow from above, and the leading edge of the plate is clean cut to knife edge to reduce any sudden effects caused in the flow due to a blunt leading edge. The channel's hydraulic cross-section is constant 50×28 cm^2 and Figure 5.6

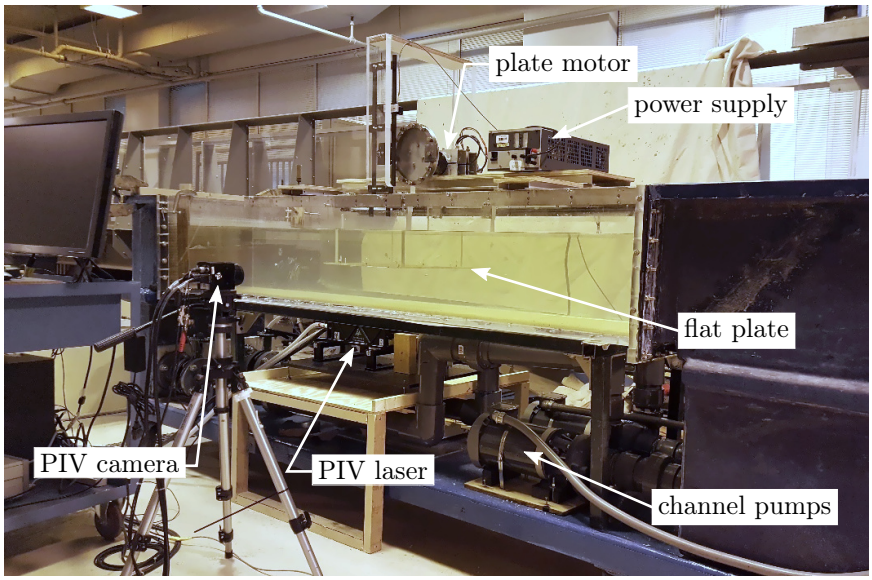

Figure 5.6: Experimental setup for flat plate experiments

is photographic description of experimental setup. The water is circulated through the flume via two 3 horsepower pumps to attain two uniform flow speeds of 0.0941 m/sec & 0.1865 m/sec. The laser pulses are synchronized with the PIV camera's frame rate to capture images of neutrally buoyant tracer particles suspended in the flow at known time increments Δt. Calibration of the

camera is accomplished to calculate the particle displacement which is converted to velocities by dividing known Δt. Spatial calibration yielded distance of 14.74 $\mu m/px$ (micro meter/pixel). Figure 5.7 shows a sample PIV image including plate edge and sufficient seeding representation.

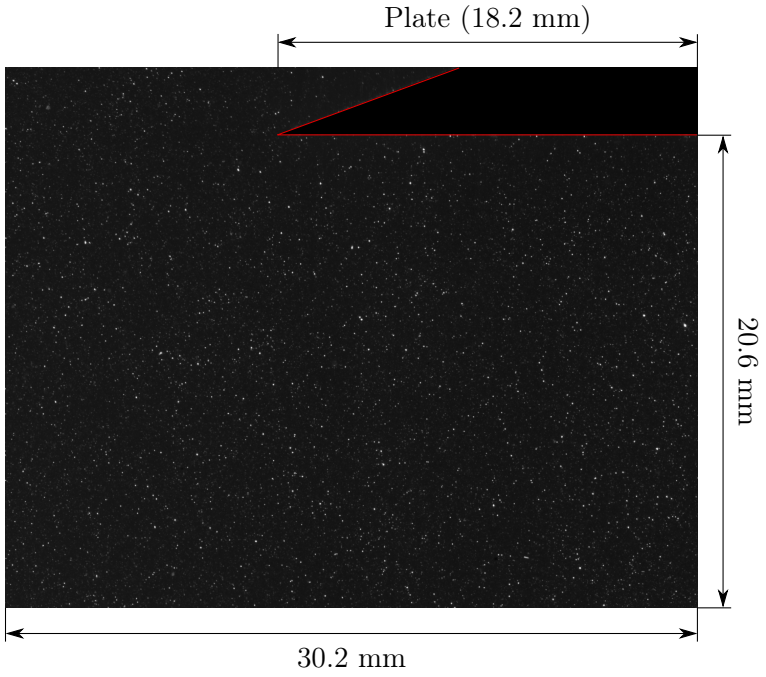

Figure 5.7: Sample PIV image with plate edge indicated and relevant dimensions annotated

It also shows the region of interest for PIV post processing. Two time increments Δt 2400μs & 1200μs for the two flow speeds of 0.0941 m/sec and 0.1865 m/sec.

Table 5.4: PIV processing settings for experimental flat plate data

Spatial calibration	14.74 µm/px	
Time interval, Δt	1200 µs	
Interrogation resolution	32 px/16 px (starting/final)	
Grid engine	Recursive Nyquist	
Correlation engine	FFT Correlator	
Peak engine	Gaussian peak	
Vector conditioning	Recursive with	
	Neighborhood size	2
	Kernel radius	2
	Gaussian sigma	0.8

PIV relies on the confident detection of tracer particles in two camera images. Fast Fourier

Transform (FFT) correlation is employed for displacement calculation and Table 5.4 gives a summary of PIV processing settings. A more detailed explanation of the setup and equipment used can be found in Srivastava et al. 2019.

5.3 Numerical Study

To determine the accuracy and robustness of pseudo-compressibility model to study oscillating boundary layer flows over a flat plate in intermittent turbulent region, first step is to test the model along with RANS equation for a flow over a steady flat plate. To demonstrate unsteady ability of the computer code/solver, the inlet velocity were varied in a fashion show in Figure 5.8. The code was allowed to run till steady state is achieved. To study oscillating flows in intermittent turbulent regime using RANS equation, an appropriate turbulence model is required to predict the unknowns well near to the wall. Chien's k-ϵ turbulence model (Low-Reynolds number turbulence model) is chosen for this study.

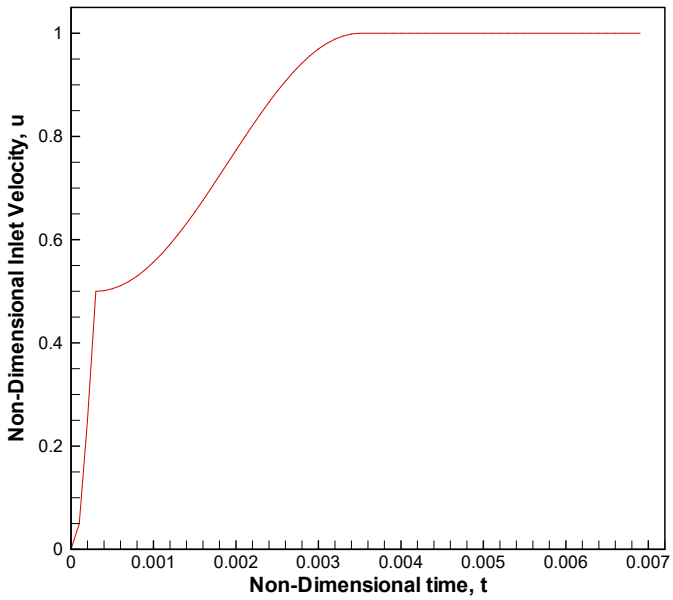

Figure 5.8: Inlet velocity function with respect to time

5.3.1 Code Validation

Numerical simulations were conducted for Re=2099 for verification of computed code. The Reynolds number was chosen on the basis of inflow velocity obtained in experimentation using PIV to study boundary layer on flow over a flat plate (as discussed in section 5.2). This Reynolds number corresponded to inflow velocity of 0.0941 m/sec. The experiments were conducted with identical flow parameters and the velocity profiles observed at the trailing edge of the plate are compared with velocities predicted by FEFD and Commercial CFD package. The computational domain chosen was 0.0254×0.0254 m & the experimental data was also observed at the same distance in stream wise direction from the plate. The non-dimensional velocity profiles obtained by all the methods described above are presented in 5.4 section. A quantitative comparison of velocity vectors and contours as predicted by FEFD and observed in experiments are presented. The NS equations were also reduced to boundary layer equations for flow over flat plate as mentioned in Özişik 1994 & Tannehill et al. 1997. A separate computer solver was developed to solve these equations using Alternating-Direction Explicit (ADE) finite difference techniques. Comparisons of horizontal & vertical velocity profiles are made for Re=1000 for Boundary layer solution, analytical solution (Blasius), FEFD and commercial CFD package. While solving the boundary layer equations, it was observed that the expected vertical velocity profile for prescribed boundary conditions, as described in section 3, can be obtained with adopting an ADE technique.

5.3.2 Parametric Study

A parametric study is conducted to validate the robustness of pseudo-compressibility model along with Unsteady-RANS or URANS equation (Chien's k-ϵ as turbulence closure model) and to study the convergence of solution of URANS equation to ones predicted by Laminar NS equations in intermittent turbulent flow regime. This forms a basis of study of oscillating boundary layer flows over a flat plate which are unsteady in nature and have intermittent characteristics of turbulence while transitioning from laminar to turbulent flow regime. This study covers free stream velocity of 0.399 m/sec, 3.99 m/sec and 19.95 m/sec which corresponded to Reynolds number of 10000, 100000 & 500000 respectively for chosen characteristic length of 0.0254 m. The horizontal velocity profiles predicted by FEFD at the trailing edge of the plate are compared

to ones predicted by commercial CFD package which employed two turbulence model, Standard k-ϵ along with standard wall-functions and Transitional SST model. These comparison are presented in section 5.4. To verify the convergence of chosen turbulence model, the horizontal velocity profiles predicted by URANS equations are compared to the ones predicted by laminar unsteady NS equations for Reynolds number 10000, 100000 & 500000. All the comparison were made ones the solution reaches steady-state.

5.4 Results & Discussion

5.4.1 Results of Validation Study

A set of numerical simulations were carried out using FEFD pseudo-compressibility code with working fluid as water (ρ=998.2 kg/m^3).

For Re=1000, the velocity profiles predicted at the trailing edge of the plate by FEFD, Boundary layer equations, Commercial CGF package, and analytically obtained are presented in Figure 5.9. Quantitative comparison are made between FEFD, Commercial CFD package, Boundary layer equations (ADE) & Blasius solution. It can be observed from Table 5.5 that Blasius and

Table 5.5: Comparison of maximum $\bar{u}$ for different methods at Re=1000

Meshes	$\bar{u}_{max}$	% Deviation $\bar{u}$ from FEFD results
Blasius Solution	1.000	+8.680
Boundary Layer Equation (ADE)	1.000	+8.680
Commercial CFD Package	1.101	-0.244

boundary layer equations (ADE) under predicts maximum horizontal velocity by 8.68% while the commercial CFD package over predicts by only 0.244%. This over prediction seems within acceptable range. One can only speculate from this observation that boundary layer solutions or analytical solution would not serve as benchmark case for this study. It is in the nature of the assumptions made to arrive at the boundary layer equations which perhaps makes it not suitable for the comparison in this study. Hence, there arises a need to define a criteria for boundary layer thickness for real world problems for flow over a flat plate (such as in this study), which

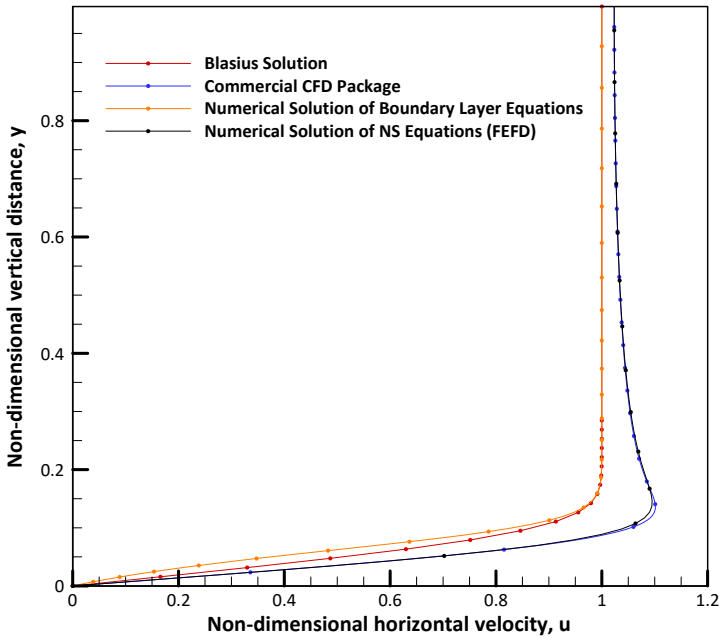

Figure 5.9: Comparison of $\bar{u}$ at $\bar{x}$=1 for Analytical solution, Boundary Layer Code, FEFD and Commercial CFD package for Re=1000

may include pressure drop as mentioned in boundary conditions. The accurate boundary layer thickness would define the correct shear at the solid wall which in turn defines drag and lift forces needed in practical engineering applications. Non-dimensional vertical velocity profiles obtained at the trailing edge of plate using the methods listed above for Re=1000 are presented in Figure 5.10. It was observed that the expected vertical velocity profile obtained using ADE technique while solving boundary layer equations, numerically, with prescribed boundary conditions.

5.4.2 Comparison with Experimental PIV results

The experimentally observed velocities at the trailing edge of the plate are compared with ones predicted by FEFD, Commercial CFD package and Analytical solution (Blasius solution) for Re=2099. It can be seen from Figure 5.11, that FEFD under predicts the maximum horizontal velocity only by 2.2% from experimental data and Commercial CFD package over predicts FEFD by 0.19%. These deviations are within the acceptable range. The non-dimensional horizontal

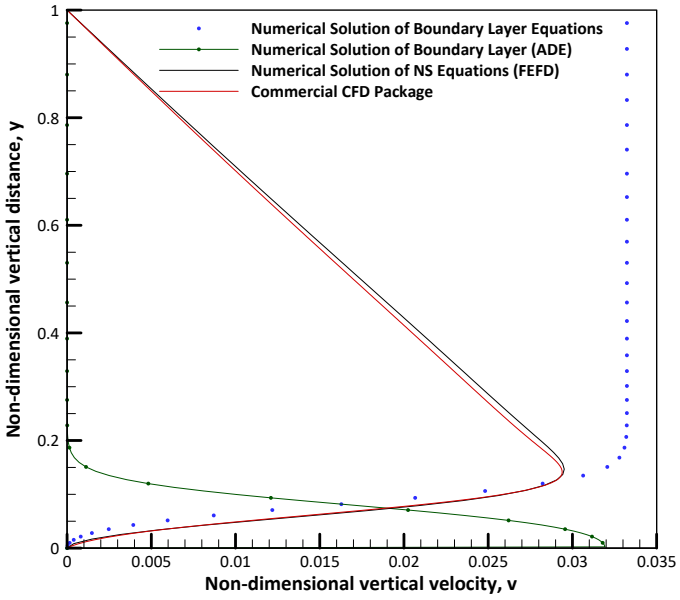

Figure 5.10: Comparison of $\bar{v}$ at $\bar{x}$=1 for Analytical solution, Boundary Layer Code, FEFD and Commercial CFD package for Re=1000

velocity field contour plots along with vector, as predicted by FEFD and observed by experiments for Re=2099 are presented in Figure 5.12. As it can be seen that the velocity fields predicted by FEFD pseudo-compressibility code compares well with experimentally observed velocity fields.

5.4.3 Results Of Parametric Study

The results of parametric study conducted to compare turbulence models,FEFD (Chien's k-ϵ) and CFD package (Standard k-ϵ with standard wall-functions and Transitional SST model) for Re=100000 (Intermittent turbulent regime) are presented in Figure 5.13. The mesh chosen for this study was 81×400, which corresponded to y^+ of 0.5 for FEFD, 1.2 for Standard Wall Functions and 2.1 for Transitional SST model, for free stream velocity of 0.399m/sec. The predictions of FEFD code and Commercial CFD package exhibits the same behavior in shape and fairs well in free stream. It can be observed that Chien's k-ϵ model & Transitional SST fairs well with each other near to the wall. The near wall effects one can expect in flow over flat plate with these prescribed boundary conditions is predicted well with Chien's k-ϵ model.

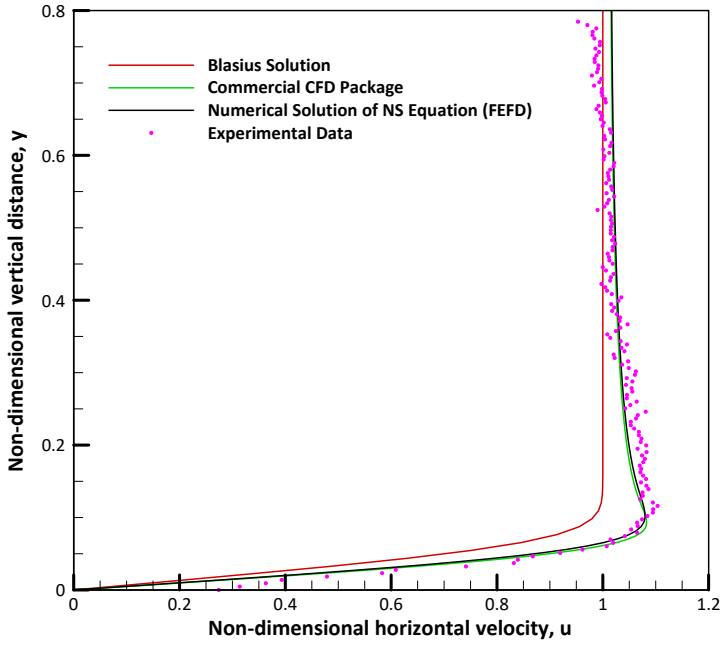

Figure 5.11: Comparison of $\bar{v}$ at $\bar{x}$=1 for Analytical solution, Experimental PIV data, FEFD and Commercial CFD package for Re=2099

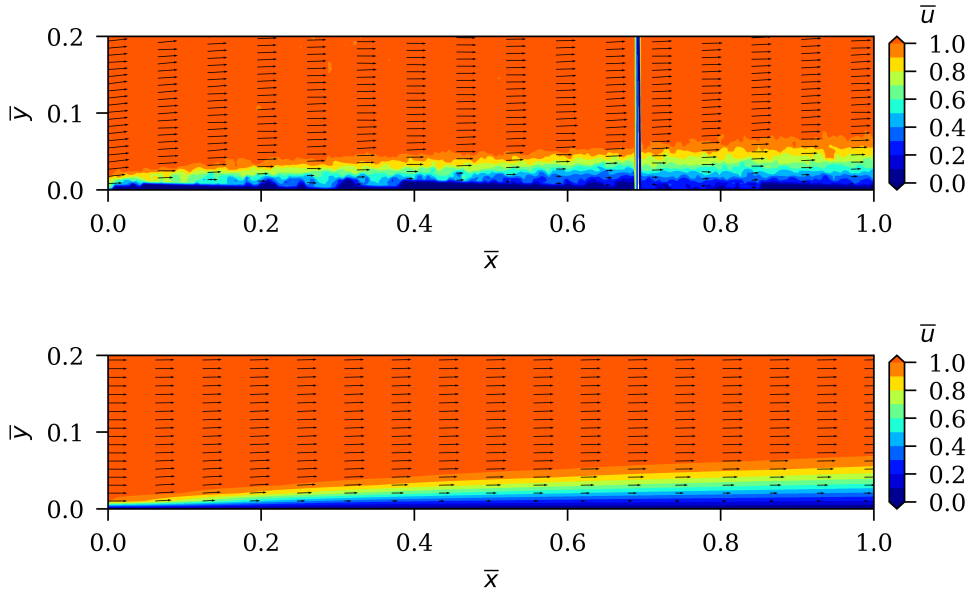

Figure 5.12: (Top): Fluid Horizontal Velocity Contour on the plate as observed by experiments and (Bottom): as predicted by FEFD for Re=2099

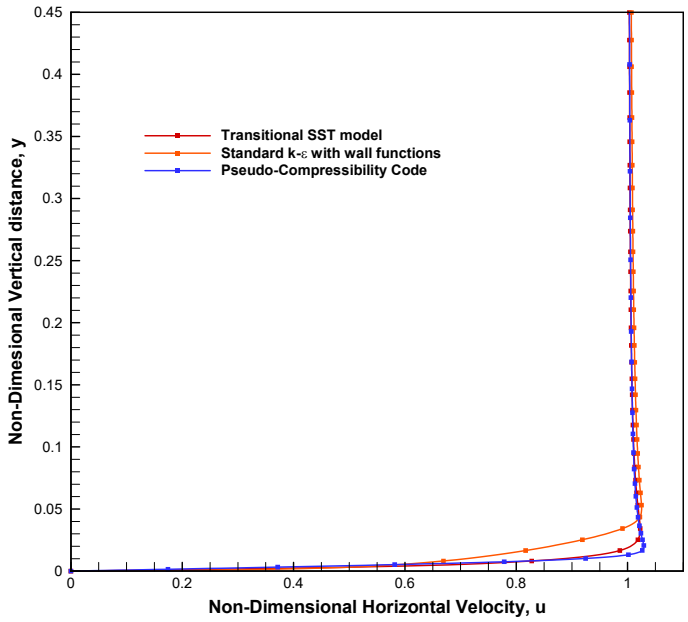

Figure 5.13: Comparison of $\bar{u}$ at $\bar{x}$=1 for Chien's k-ϵ, Standard k-ϵ with wall function (Fluent) & Transitional SST (Fluent) for Re=100000

This argument is supported by Figure 5.14, where FEFD for laminar case (NS-Equations) with Re=100000 is compared with FEFD for RANS equations for same Re number.

Same study is conducted for Re=10000 and 500000 in Figures 5.15 & 5.16 respectively, to validate the convergence of RANS equations (along with turbulence model) to Laminar NS equations at low (10000) and high (500000) Reynolds number range during transitioning from laminar to turbulence and vice verse. It can be observed that the chosen turbulence model predicts well in intermittent turbulent regime and fairs well with laminar case at low Reynolds number. The prediction of collapse in boundary layer as one expects can be observed in Figure 5.16.

In summary a CFD numerical solver based on pseudo-compressibility is developed to solve governing differential equations for laminar (NS) and intermittently turbulent flow (RANS) for flow over a flat plate. This code is successfully validated using analytical solution and commercial CFD predictions. It is also validated by comparing to experimentally measured velocities obtained by PIV techniques. The discretization accuracy is also verified by using GCI method.

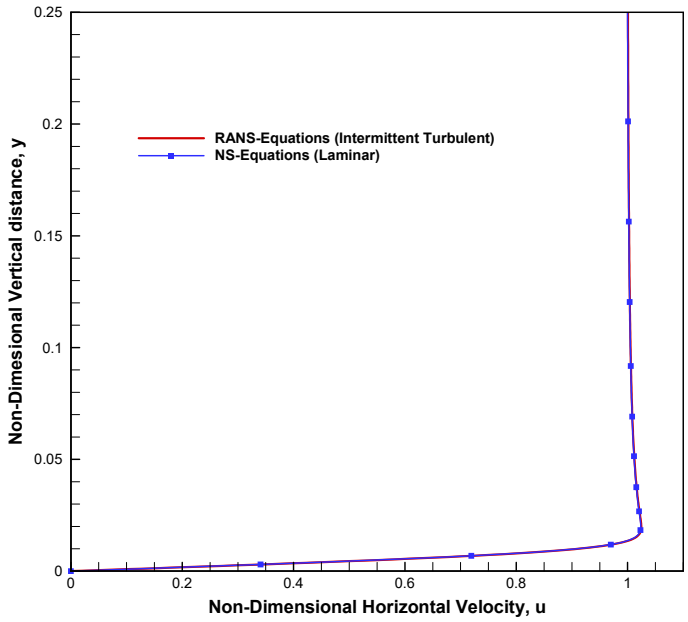

Figure 5.14: Comparison of $\bar{u}$ at $\bar{x}$=1 for RANS equations (Intermittent Turbulent) & NS equations (Laminar) at Re=100000

The velocity profiles predicted by RANS equations along with turbulence closure models are compared to ones predicted by NS equations in lower and higher band of intermittent turbulent regime. The preliminary results indicate that chosen k-ϵ model, modified for the wall (Chien (1982)) does predict well in intermittent turbulent regime for flow over flat plate.

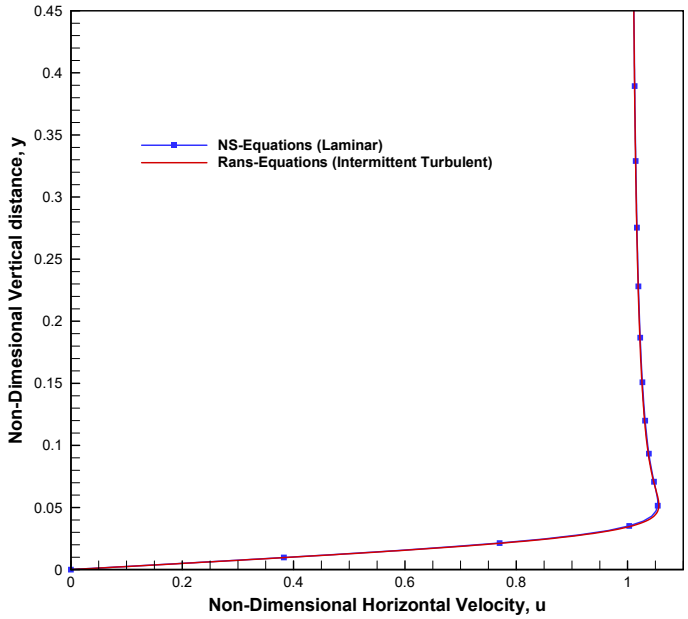

Figure 5.15: Comparison of $\bar{u}$ at $\bar{x}$=1 for RANS equations (Intermittent Turbulent) & NS equations (Laminar) at Re=10000

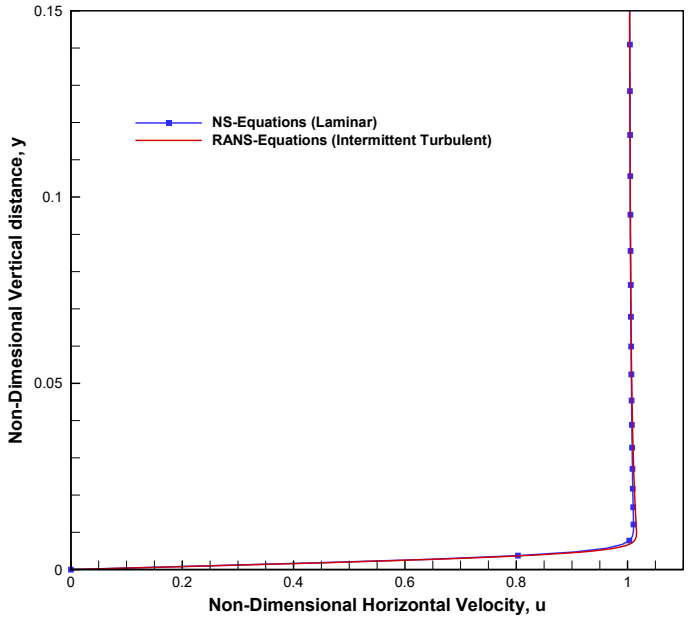

Figure 5.16: Comparison of $\bar{u}$ at $\bar{x}$=1 for RANS equations (Intermittent Turbulent) & NS equations (Laminar) at Re=500000

6 Oscillating Flow

To study oscillating flow over a stationary flat plate in intermittent turbulent regime, the base closure model chosen is k–ϵ by Jones and Launder (1972) and as described in chapter 3. Herein, a single γ equation is formulated in local variables with no reference to data correlation. The model proposed will be henceforth referred as k–ϵ–γ in this study. The proposed model only address bypass transition, which is the transitional phenomenon occurring in oscillatory boundary layer flows over a flat plate (Jensen et al. (1989),Hino et al. (1983) and Akhavan et al. (1991a)). In this chapter, the development of the model is discussed in detail. Before, mesh and time independent study is conducted along with validation of the model with analytical solution in laminar regime.

6.1 Mesh and Time Independent Study

To assess the grid independence of the results, three meshes were taken in consideration, 21×121, 41×321 and 81×421. The shear stresses obtained from these for $Re_\delta = 90$ were compared to analytical (Stokes' Analytical solution) shear stress. It was observed that there is only 0.24% deviation in maximum shear stress in 81×421 mesh and analytical shear stress. The maximum value of wall shear stress obtained for Re_δ=1790 for 81×421 mesh differed by 0.02% from 41×321. In addition reducing the time step size by factor of 10 from base Δt=$2\pi/360\omega$ did not result in much change in the general characteristics of velocity and shear stress profiles. To conserve the computational efforts and obtain the y^+ value of <5, base time step (Δt=$2\pi/360\omega$) was chosen along with 81×421 mesh.

6.2 Validation Study

To validate the proposed model, the problem was solved for laminar flow regime characterized by Re_δ of 90. The predicted stream wise velocity by model is compared to closed form analytical

solution (Schlichting and Gersten 2017) given by:

$$u = U_{inf}\left[\sin(\omega t) - \exp(-y/\delta)\sin(\omega t - y/\delta)\right] \tag{6.1}$$

where δ is the Stokes thickness. The comparison are shown in Figs 6.1 and 6.2 for acceleration and deceleration phases, respectively. As seen in the figure the proposed k–ϵ–γ results agree well with analytical solution. This demonstrates the capability of the proposed model to predict correctly in the limiting laminar case of fully laminar flow regime.

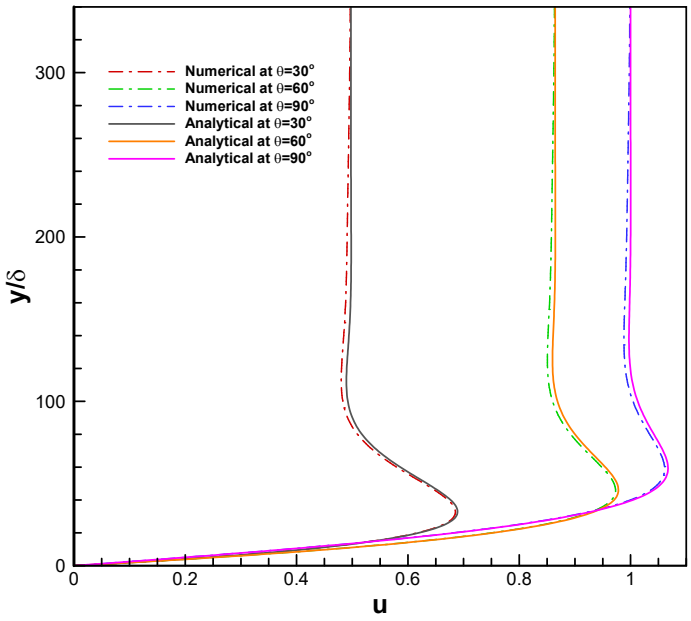

Figure 6.1: Comparison of predicted stream-wise non-dimensional velocity with analytical solution for accelerating laminar flow regime, Re_δ=90

6.3 Calibration/Development of Intermittency Model

The proposed k–ϵ–γ model is based on the Jones and Launder (1972) k–ϵ model. It is a two equation turbulence model (see Eqs 3.13 and 3.14). The intermittency function γ is placed in into the production term $\tau_{ij}\frac{\partial \tilde{u}_i}{\partial x_j}$ of kinetic energy equation. This is the only appearance of γ in

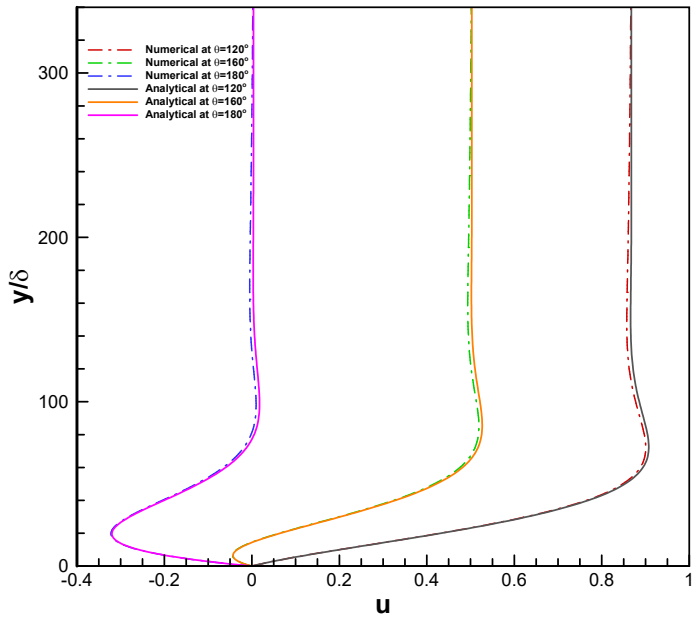

Figure 6.2: Comparison of predicted stream-wise non-dimensional velocity with analytical solution for decelerating laminar flow regime, Re_δ=90

the turbulence model, hence Eq 3.13 becomes:

$$\frac{\partial k}{\partial t} + \frac{\partial(\tilde{u}_j k)}{\partial x_j} = \frac{1}{\rho}\frac{\partial}{\partial x_j}\left[\left(\mu + \frac{\mu_t}{Pr_k}\right)\frac{\partial k}{\partial x_j}\right] + \gamma\tau_{ij}\frac{\partial \tilde{u}_i}{\partial x_j} - \epsilon - 2\nu\left(\frac{\partial\sqrt{k}}{\partial x_j}\right)^2 \tag{6.2}$$

and there is no change to the dissipation function Eq 3.14.

The intermittency function is used to suppress the production of turbulent kinetic energy and γ forestall the early prediction of transition. In laminar flow $k\approx 0$ and eddy viscosity is 0. When γ is small, Eq 6.2 will force k to be small. Assuming γ to be 0 inside the boundary layer and unity in the free-stream turbulent region, non-zero γ will diffuse into the boundary layer, enhancing the production of k, increasing eddy viscosity and hence initiating transition (Durbin 2012). Similar observations were reported by Jensen et al. (1989), Akhavan et al. (1991a) and Salon et al. (2007) for oscillating flow that the turbulence is diffused into the boundary layer from free stream causing the initiation or transition to turbulence from laminar regime. Consider

an intermittency equation of the form (Lodefier et al. 2004)

$$\frac{\partial \gamma}{\partial t} + \frac{\partial (\tilde{u}_j \gamma)}{\partial x_j} = \frac{1}{\rho} \frac{\partial}{\partial x_j} \left[\left(\frac{\mu}{\sigma_l} + \frac{\mu_t}{\sigma_t} \right) \frac{\partial \gamma}{\partial x_j} \right] + F_\gamma |\Omega| \left(\gamma_{max} - \gamma \right) \sqrt{\gamma} \tag{6.3}$$

$$where \quad \Omega = \frac{1}{2} \left(\frac{\partial u_i}{\partial x_j} - \frac{\partial u_j}{\partial x_i} \right)$$

Lodefier et al. (2004) and Durbin (2012) used the intermittency model on steady flow over flat plate with k–ω model. To be coupled with k–ϵ model and applied to oscillating unsteady flows, some calibration is required. The γ is 1 in free-stream and 0 at the wall. Fig 6.3 shows the

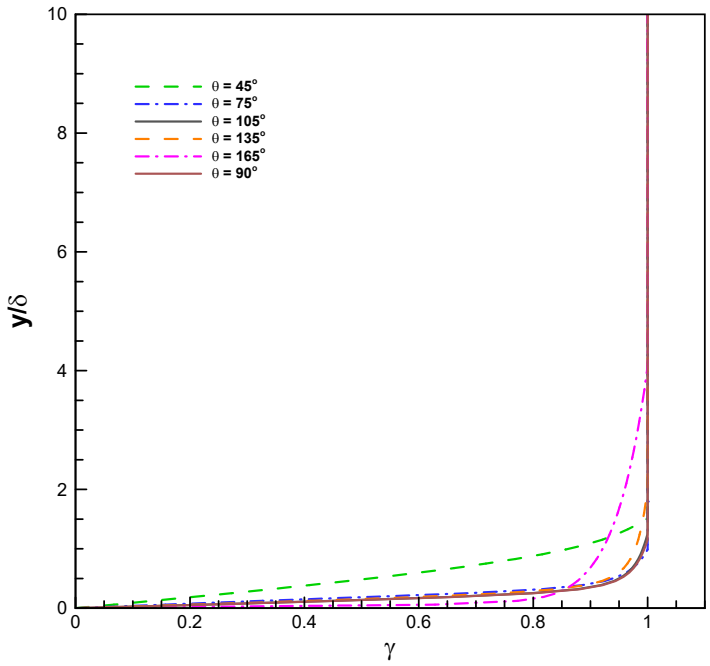

Figure 6.3: Profiles of intermittency function γ in acceleration and deceleration phase

characteristic profiles of function γ in acceleration and deceleration phases. It cab be observed that in the free stream γ is 1. Similar characteristic was observed by Durbin (2012).

6.3.1 Diffusion Term

The influence of two constants σ_l and σ_t in Eq 6.3 is discussed below. For the purpose of this study they are set to 7.5 and 0.35 respectively. From the diffusion term itself, we can predict

that increasing σ_t decreases turbulent diffusivity and delays transition, while decreasing it cause reverse effects on turbulent diffusivity.

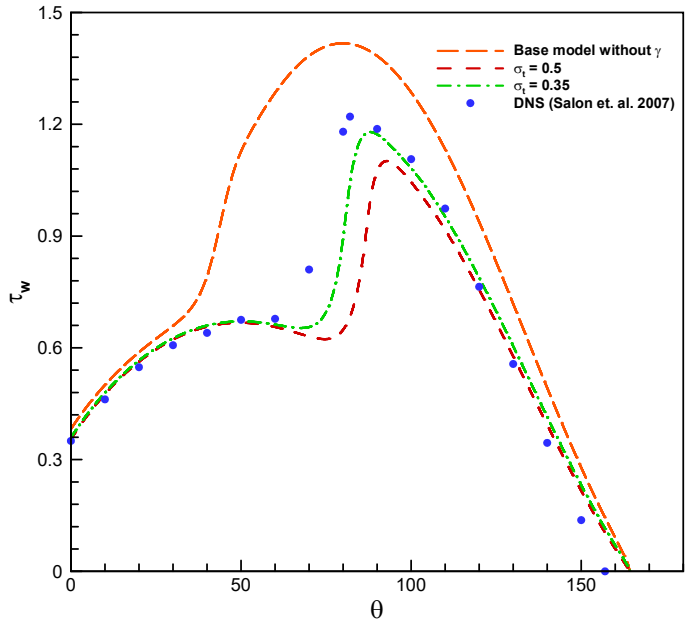

Figure 6.4: Sensitivity of σ_t on non-dimensional τ_w with fixed σ_l of 5 for Re_δ 990

Fig 6.4 shows the non-dimensional shear stress in a half cycle of oscillation for Re_δ of 990. The values are compared to ones predicted by Salon et al. (2007). It can be clearly observed that without the intermittency equation the base model predicts an early transition which also cause higher shear stress. By adding the intermittency transport equation the production of kinetic energy is clearly forestalled. It can be clearly observed that the decreasing σ_t (for a fixed value of σ_l=5) the diffusion is enhanced causing early transition. Not shown in this study but reducing the value of σ_t below 0.2 this particular parameter becomes less sensitive. For the purpose of this study 0.35 is chosen. However, the effect of σ_l is a bit subtle. As shown in Fig 6.5 when σ_l is doubled (for a fixed value of σ_t=0.35) the diffusivity is increased causing advanced transition. The effects of σ_l is opposite to σ_t. Hence decreasing σ_l delays transition. For the purpose of this study σ_l of 7.5 is chosen.

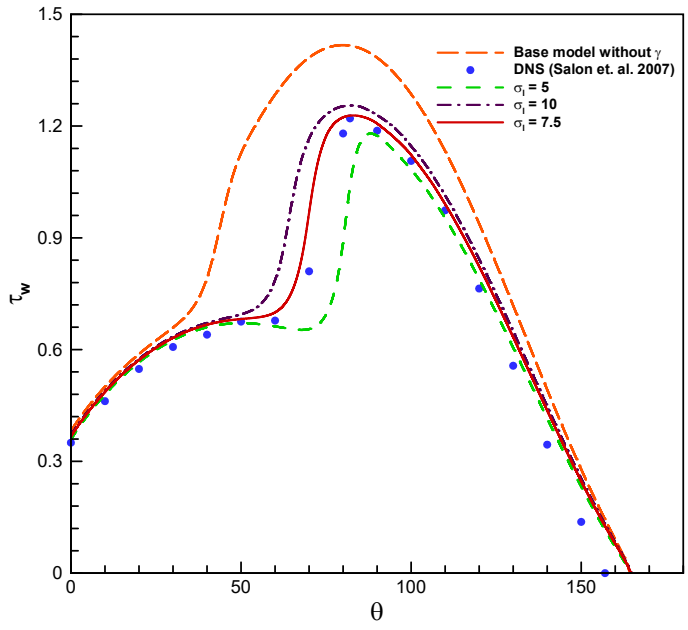

Figure 6.5: Sensitivity of σ_l on non-dimensional τ_w with fixed σ_t of 0.35 for Re_δ 990

6.3.2 Source Term

The source term is very familiar to one used by Durbin (2012). The γ_{max} placed in the source term is 1.1, in order to enhance the effects of source term to drive γ to unity. It may be possible for γ to exceed unity due to such source, which is not allowed. So after each step of the computation, γ is forced to the value of min(γ,1) to chop off the values greater than unity. This has a small effect, but it does force a full transition to turbulence. It was also observed that it was required for stability of the solver. The factor F_γ switches on as transition proceeds. Once it comes to play, γ will increase up to unity within the region F_γ affects. Therefore the turbulent kinetic energy k increases as well as the eddy viscosity.

F_γ has two parameters. The magnitude of mean rate of rotation or vorticity is represented by

$|\Omega|$, which vanishes in free stream. The three non-dimensional parameters involved,

$$\begin{aligned} R_t &= \frac{\nu_T}{\nu} \\ R_\nu &= \frac{d^2|\Omega|}{2.188\nu} \\ T_\epsilon &= R_t \frac{|\Omega|k}{\epsilon} \end{aligned} \tag{6.4}$$

where d is the distance to the wall. R_t is ratio of the eddy viscosity to molecular viscosity, namely the turbulent Reynolds number. R_ν is the vorticity Reynolds number, which depends only on local variables. The function F_γ is determined by two parameters R_ν and T_ϵ. T_ϵ is used to form a critical Reynolds number, R_c. It is a decreasing function of T_ϵ. If the turbulent intensity is low the T_ϵ will be low and R_c will be high. The value of R_c are chosen from Durbin (2012) as 400 and 40 as follows:

$$R_c = 400 - 360\min\left(\frac{T_\epsilon}{2}, 1\right) \tag{6.5}$$

As the local Reynolds R_ν crosses R_c, F_γ ramps up from 0. Meanwhile if the R_ν crosses R_c without the flow becoming turbulent, then to avoid this, another condition is imposed which checks the bounds of R_ν (100/0.7). This is done to suppress the F_γ namely the source term to switch on for low-free stream turbulence. The formula for F_γ thus becomes:

$$F_\gamma = 2\max\left[0, \min\left(100 - 0.7R_\nu, 1\right)\right] \times \min\left[\max\left(R_\nu - R_c, 0\right), 4\right] \tag{6.6}$$

As per Durbin (2012):

$$F_\gamma = \begin{cases} 0, & \text{if } R_\nu \leq R_c, \text{or if } R_\nu \geq 100/0.7 \\ 8, & \text{if } R_\nu > R_c + 4 \text{ and } R_\nu \leq 100/0.7 \end{cases}$$

6.4 Numerical Study

Numerical simulations are carried out for intermittently turbulent regimes characterized by Re_δ 990, 1790 and a fully turbulent regime characterized by Re_δ of 3464. Predicted velocity profiles and wall shear stress by k–ϵ–γ model for 990 are compared to LES and DNS results by Salon et al. (2007). This is simply due to fact that experimental results by Jensen et al. (1989) were not reported. Further the proposed model k–ϵ–γ was tested for Re_δ 1790 and predicted velocity profiles along with wall shear stress are compared to experimental data by Jensen et al. (1989).

A parametric study of k–ϵ–γ model in fully turbulent regime, Re_δ 3464, is performed. The predicted velocity profiles and wall shear stress are compared to experimental data by Jensen et al. (1989). A study is conducted for Re_δ ranging from 32 to 5000 and variation of friction coefficient (C_f, defined as $2 < \tau_w >_{max}/(\ \rho U_{inf}^2)$) with respect to Reynolds number Re (based on amplitude) is presented and discussed. The reduction of phase lag between max wall shear stress ($< \tau_w >_{max}$) and free stream velocity (U_{inf}) is also presented and discussed. The distributions of turbulent kinetic energy and dissipation function across the boundary layer as a function of phase is also presented and discussed for Re_δ of 990.

6.5 Results & Discussion

6.5.1 Results for $\mathrm{Re}_\delta = 990$

Fig 6.6 and Fig 6.7 shows the mean stream velocity profiles in acceleration phase for for 15^o, 45^o, 75^o and 90^o and for deceleration phase for 105^o, 135^o, 165^o and 180^o respectively. As compared to the laminar solution Fig 6.1 and Fig 6.2 the boundary layer is collapsed as one would expect in a turbulent flow. Figures 6.8, 6.9, 6.10 and 6.11 compare the velocity profiles in u^+ and y^+ coordinates with LES results by Salon et al. (2007) for 15^o, 75^o, 105^o and 135^o.

It can be observed that the predicted velocity profiles by k–ϵ–γ model fairly well with the LES results. The absence of the logarithmic profile is because of the non-equilibrium behavior, which is characteristic of the intermittently turbulent flow regime for Re_δ of 990. This is consistent with findings of Salon et al. (2007) and Shome (2013) who used k–k_L–ω model for prediction of oscillating boundary layer flows in intermittent turbulent regime. The variation of wall shear

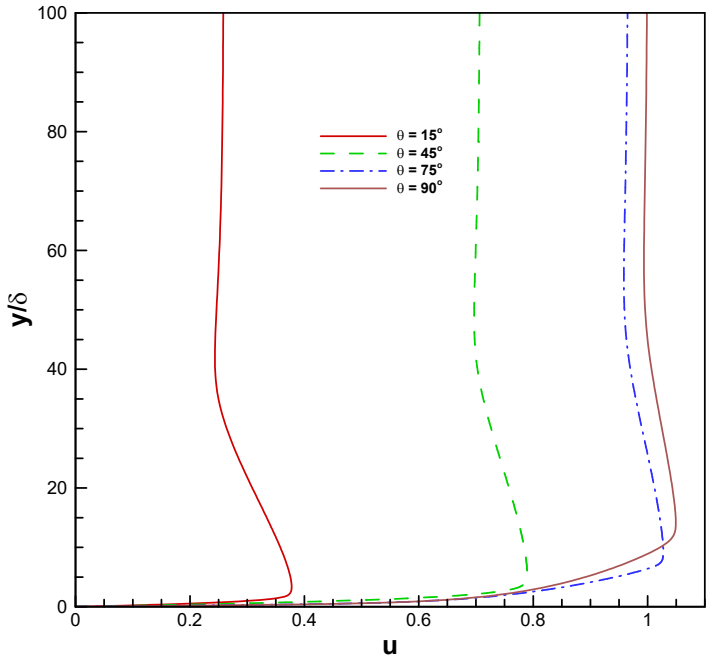

Figure 6.6: Non-dimensional u profiles in acceleration phase for Re_δ of 990

stress with phase angle is shown in Fig 6.12. The predicted profile is compared to DNS results Salon et al. (2007).

It can be observed that wall shear stress agrees well with the data. The wall shear stress rapidly increases at angle of 60^o which is consistent with DNS predictions. This sudden increase marks the onset of of transition to turbulence. The maximum value of shear stress differs by about 1% from the DNS data as compared to k–k_L–ω model which observes an under-prediction of 10% (Shome 2013). The triangular profile indicates the non-equilibrium turbulence effects that occur in intermittently turbulent regime as demonstrated by Jensen et al. (1989) and Costamagna et al. (2003). The shear stress profile also peak around 8^o earlier as compared to DNS results. Also the the flow reversal characterized by zero value of shear stress is at about 165^o as compared DNS data, which predicts at an angle of 158^o. These differences can be attributed to base model of k–ϵ which is based on the assumption of linear-eddy viscosity modeling approach. Even though the proposed model is improved in predicting maximum shear stress and time at which is occurs, some refinement are required to improve the accuracy. Figures 6.13 and 6.14 shows the kinetic

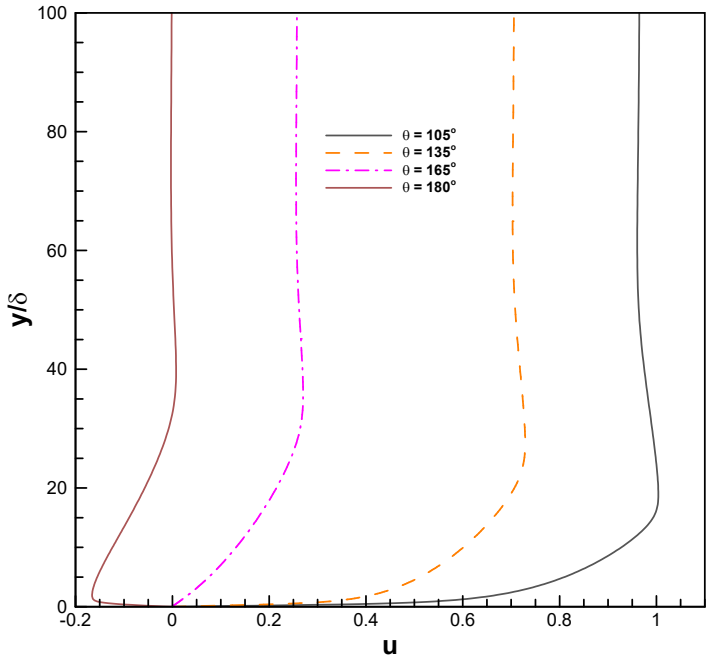

Figure 6.7: Non-dimensional u profiles in deceleration phase for Re_δ of 990

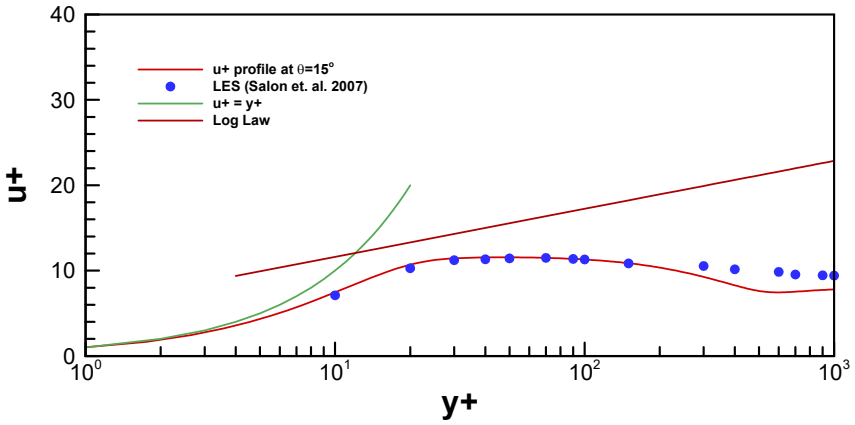

Figure 6.8: Comparison of predicted stream-wise velocity profile with LES results of Salon et al. (2007) for Re_δ of 990 at θ=15^o

energy profiles in acceleration and deceleration phase across the boundary layer for Re_δ 990.

It can be observed as the flow accelerates the magnitude of kinetic energy near the wall increases, as the turbulence is diffused into the boundary layer from free stream causing pre-

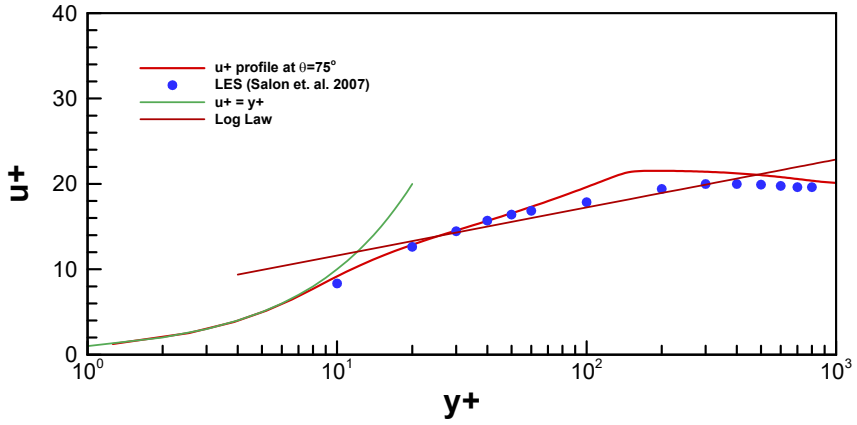

Figure 6.9: Comparison of predicted stream-wise velocity profile with LES results of Salon et al. (2007) for Re_δ of 990 at θ=75^o

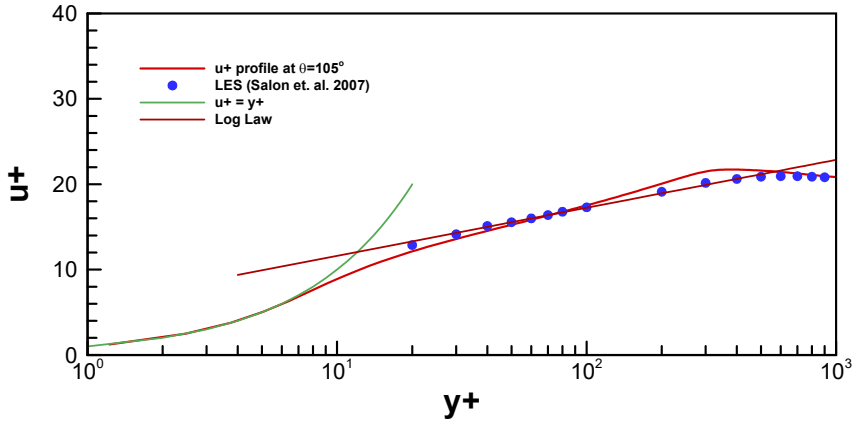

Figure 6.10: Comparison of predicted stream-wise velocity profile with LES results of Salon et al. (2007) for Re_δ of 990 at θ=105^o

transitional fluctuations. As the flow accelerates beyond 60^o, the near wall kinetic energy increases sharply. This is caused by pre-transitional fluctuations that leads to the onset of transition. This is consistent with the sudden increase in shear stress profile as seen in Fig 6.12 around the same phase angle. As the flow accelerates further, the kinetic energy increases and peaks at 90^o beyond which the flow decelerates and the energy starts to decrease due to diffusion through the boundary layer.

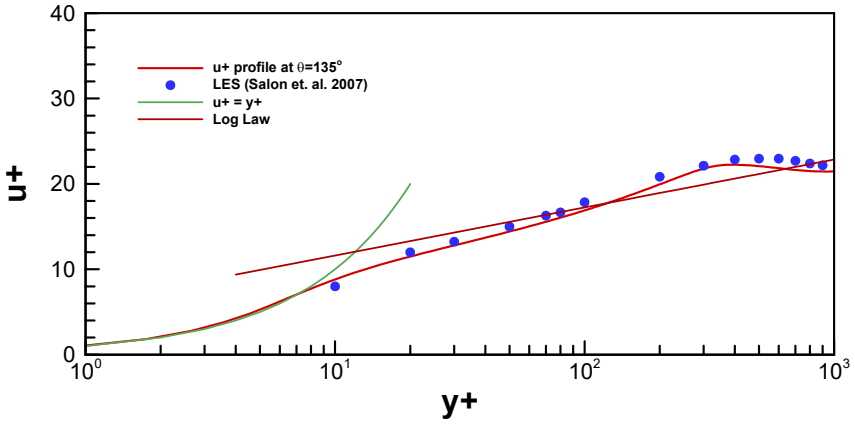

Figure 6.11: Comparison of predicted stream-wise velocity profile with LES results of Salon et al. (2007) for Re_δ of 990 at θ=135^o

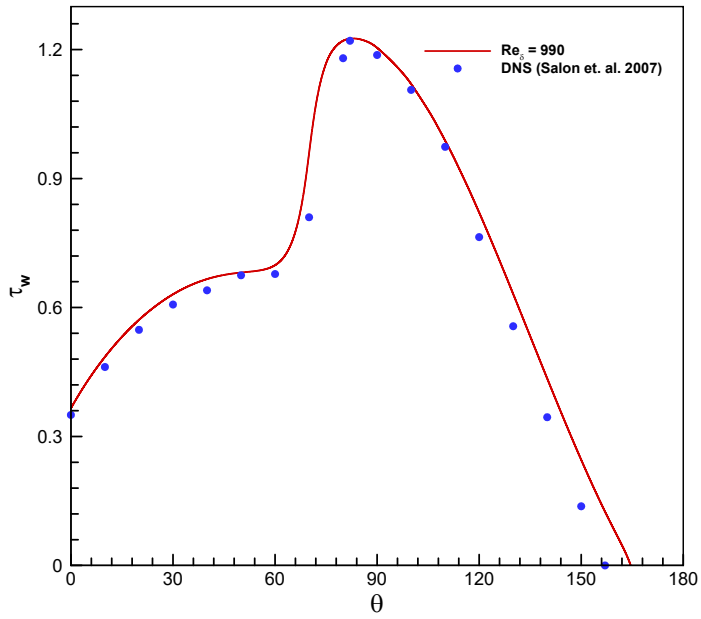

Figure 6.12: Comparison of predicted non-dimensional wall shear stress profile with DNS results of Salon et al. (2007) for Re_δ of 990

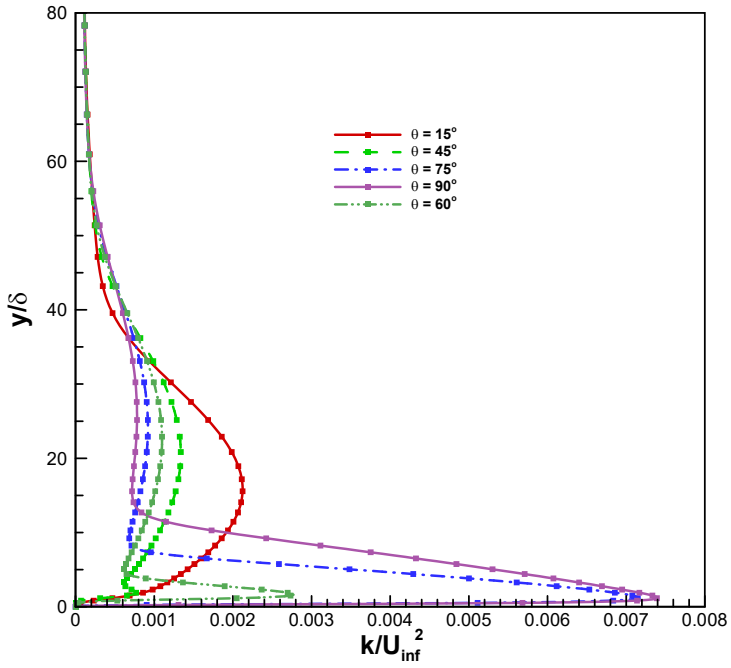

Figure 6.13: Predicted non-dimensional kinetic energy profiles in acceleration phase for Re_δ 990

6.5.2 Results for $\mathrm{Re}_\delta = 1790$

The k–ϵ–γ model is tested for higher range of intermittently turbulent regime characterized by Re_δ 1790. The stream wise velocity profiles are compared to experimental data by Jensen et al. (1989) in Figs 6.15 to 6.20 in u^+ and y^+ coordinates. A good agreement with experimental data can be observed except for phase angle of 165^o.The logarithmic profile plotted in the velocity profiles is given by $\mathrm{u}^+ = 2.44\ \ln(y^+) + \mathrm{A}$.

It can be observed that log region exits from a phase angle of 45^o to around 135^o. However the intercept is 6 for $\theta < 75^o$ and 4 for $\theta \geq 75^o$. Fig 6.21 shows the wall shear stress comparison with experimental data of Jensen et al. (1989). The predictions of k–ϵ–γ model agrees well with the experimental data. The peak value predicted by the proposed model is well within 1% range of experimental data. In addition the peak value occurs at phase angle of about 80^o which is 3^o more than experimental data but well within the range. The sharp increase of profile at a phase angle of about 30^o indicating the transition to turbulence is consistent with experimental findings. The flow reversal characterized by zero shear stress occurs at a phase angle of 168^o as compared

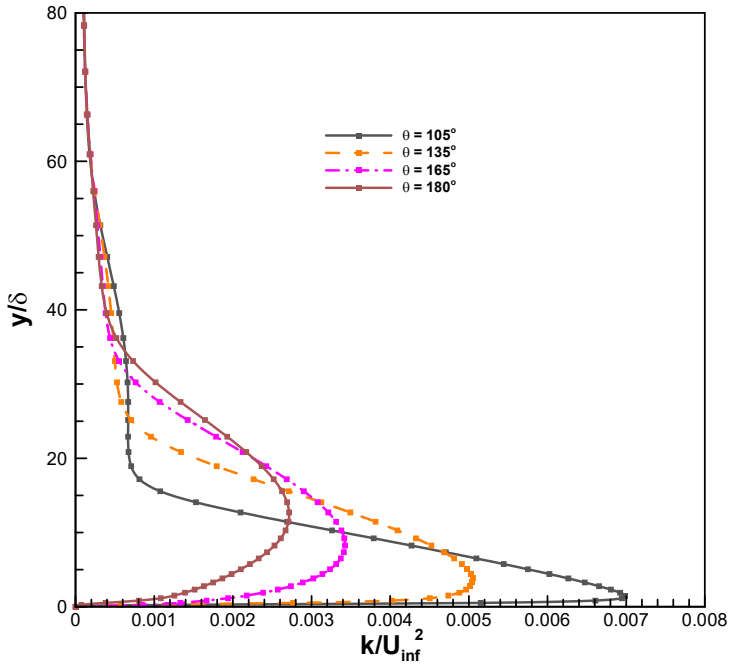

Figure 6.14: Predicted non-dimensional kinetic energy profiles in deceleration phase for Re_δ 990

to 161^o as observed by experimental data. However, this difference between predicted value and experimental value is consistent from the previous Re_δ study and affirms that calibration is required in order to achieve accuracy. The results have demonstrated that the k–ϵ–γ model is capable of predicting the transition to turbulence.

6.5.3 Results of Parametric Study for $Re_\delta = 3470$

A parametric study for fully turbulent regime of Re_δ 3464 is tested. Figs 6.22, 6.23 and Fig 6.24 show the velocity profile in u^+ and y^+ coordinates in acceleration and deceleration phase respectively. The predicted values are compared to experimentally observed values by Jensen et al. (1989) and are in good agreement. The log region is observed from phase angle of 15^o to about 150^o. Fig 6.25 shows shear stress profile as predicted by k–ϵ–γ model. As observed it fairs well with the experimental data. The predicted peak values of wall shear stress agrees within 8% as well the phase angle at which it peaks also agrees well with experimental data. The flow reversal as characterized by zero value of shear stress is predicted to be 166^o which is close

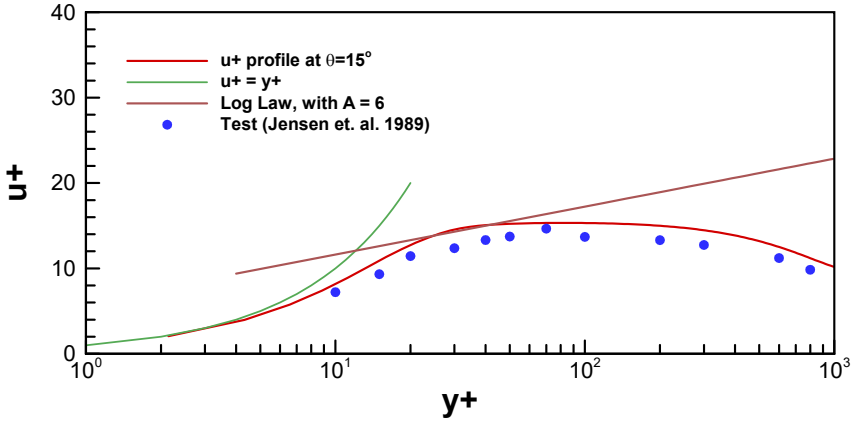

Figure 6.15: Comparison of predicted stream-wise velocity profile with experimental results of Jensen et al. (1989) for Re_δ of 1790 at θ=15^o

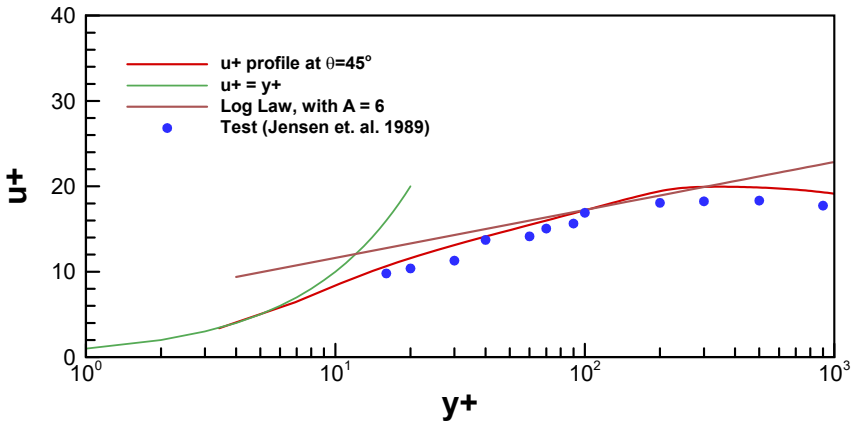

Figure 6.16: Comparison of predicted stream-wise velocity profile with experimental results of Jensen et al. (1989) for Re_δ of 1790 at θ=45^o

to experimentally observed value of 164^o. The change in slope of shear stress profile at about 20^o indicates the onset of turbulence. The reduction in phase angle is expected as in case of fully turbulent flow, the turbulence is initiated very early. Figs 6.26 and 6.27 shows the kinetic energy profiles in acceleration and deceleration as predicted by k–ϵ–γ model for fully turbulent regime. As expected and can be observed the onset of turbulence happens at an early phase angle as compared to intermittently turbulent regime. The turbulence has high value almost

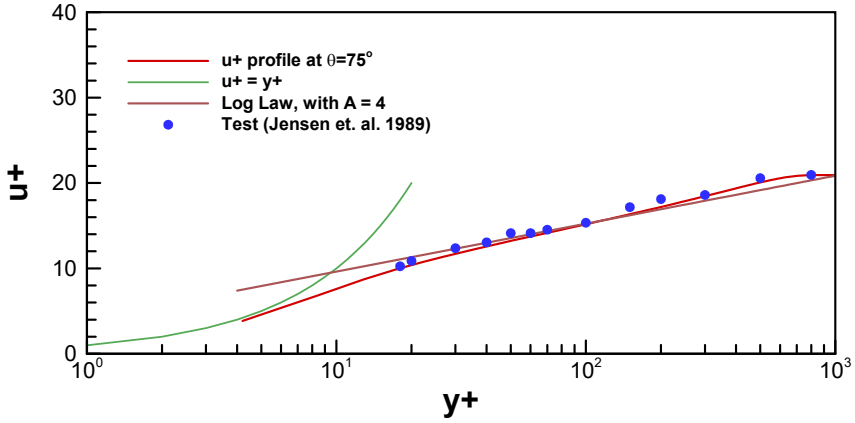

Figure 6.17: Comparison of predicted stream-wise velocity profile with experimental results of Jensen et al. (1989) for Re_δ of 1790 at θ=75^o

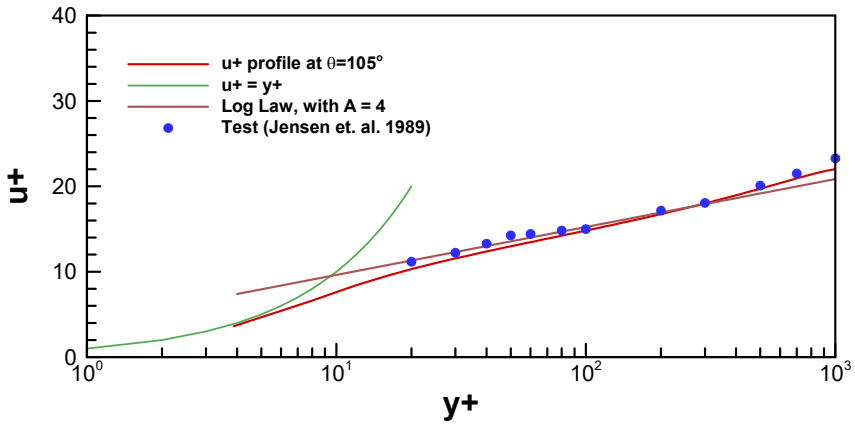

Figure 6.18: Comparison of predicted stream-wise velocity profile with experimental results of Jensen et al. (1989) for Re_δ of 1790 at θ=105^o

throughout the acceleration and some part of deceleration phase. The peak of turbulent kinetic energy is also moved closer to the wall indicating collapse in boundary layer. Fig 6.28 and 6.29 shows the eddy viscosity profiles through the boundary layer as a function of phase angle in acceleration and deceleration phase. The peak value observed is at 90^o which is in phase with the mean stream velocity. The value as expected, is about 200 times the value of molecular viscosity. The eddy viscosity in free stream remains constant throughout the cycle indicating

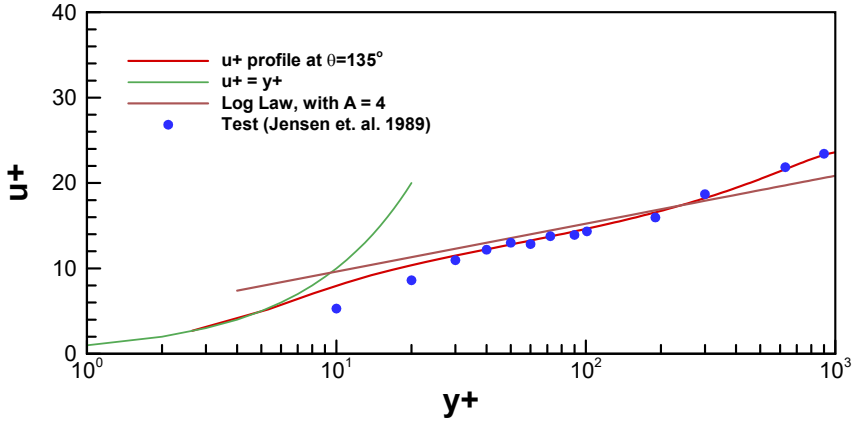

Figure 6.19: Comparison of predicted stream-wise velocity profile with experimental results of Jensen et al. (1989) for Re_δ of 1790 at θ=135^o

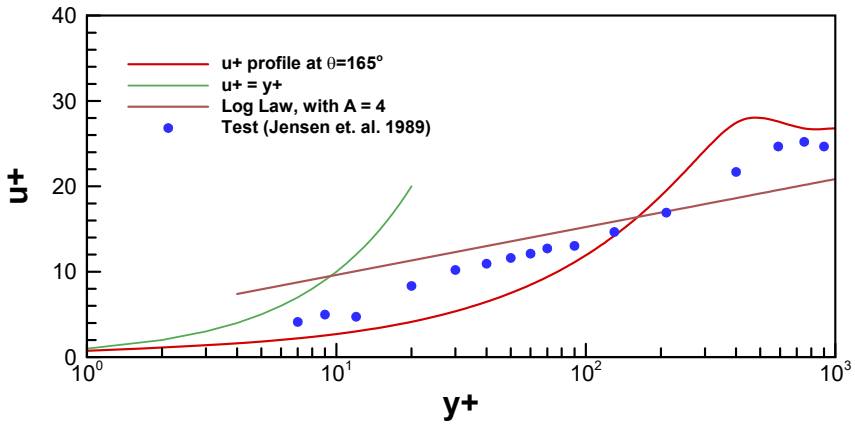

Figure 6.20: Comparison of predicted stream-wise velocity profile with experimental results of Jensen et al. (1989) for Re_δ of 1790 at θ=165^o

that turbulent flow regime. This is necessary to initiate turbulence.

After the parametric study the k–ϵ–γ model was tested for Reynolds number based on amplitude, ranging from 1000 to 8×10^6. Fig 6.30 shows variation of the friction coefficient (C_f) with Reynolds number. Experimental data reported by Jensen et al. (1989) is also reported in the Fig 7.4. It can be observed that the transition begins at Reynolds number of about 2×10^5 as indicated by deviation of friction coefficient from laminar value. Till the value of 6×10^5 the flow

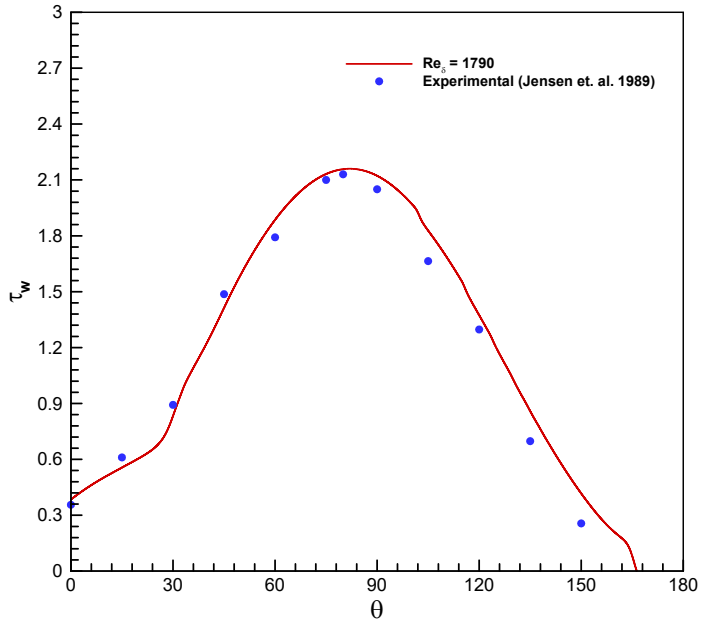

Figure 6.21: Comparison of predicted non-dimensional wall shear stress profile with experimental results of Jensen et al. (1989) for Re_δ of 1790

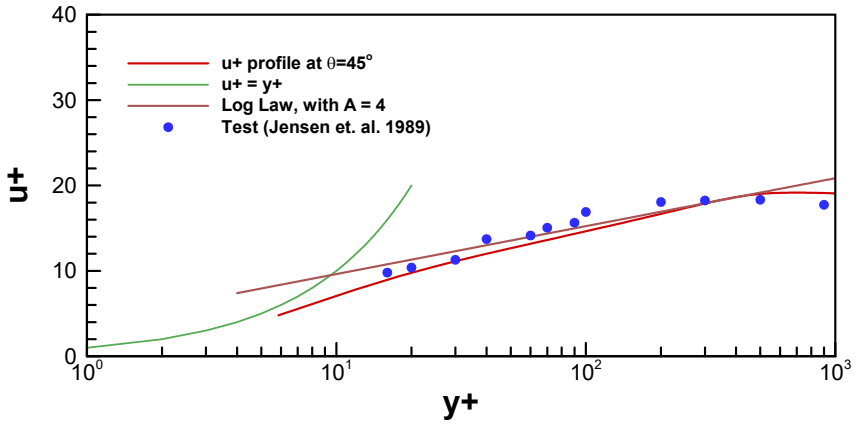

Figure 6.22: Comparison of predicted stream-wise velocity profile with experimental results of Jensen et al. (1989) for Re_δ of 3464 at θ=45^o

is in transitional phase or intermittently turbulent and beyond which it starts to become fully turbulent flow. The predicted values of friction coefficient are in well agreement with experimental

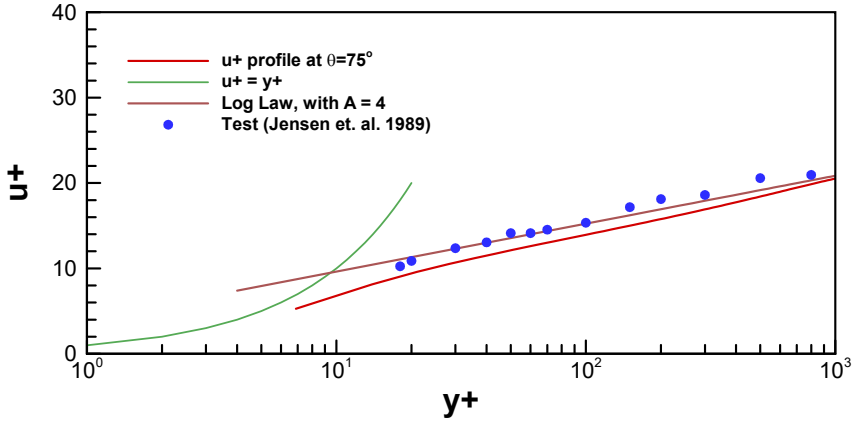

Figure 6.23: Comparison of predicted stream-wise velocity profile with experimental results of Jensen et al. (1989) for Re_δ of 3464 at θ=75^o

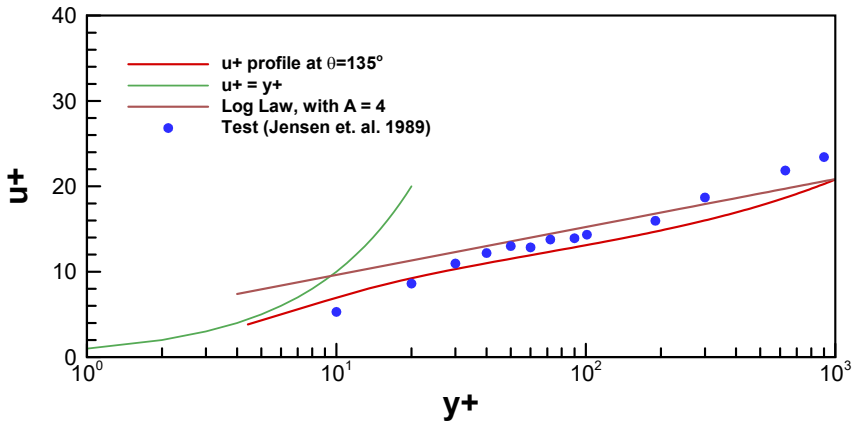

Figure 6.24: Comparison of predicted stream-wise velocity profile with experimental results of Jensen et al. (1989) for Re_δ of 3464 at θ=135^o

data. Fig 7.4 indicates that k–ϵ–γ model is capable of predicting onset of transition as well as friction coefficient accurately for fully laminar and fully turbulent flow regimes.

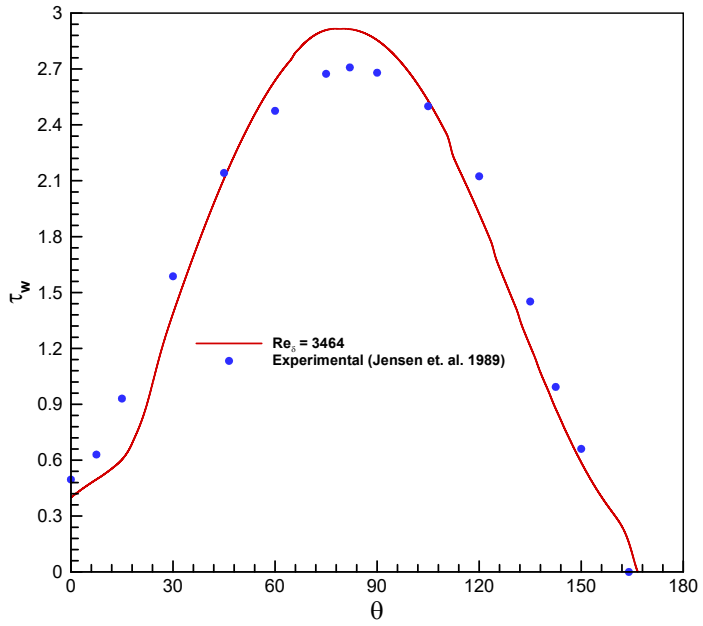

Figure 6.25: Comparison of predicted non-dimensional wall shear stress profile with experimental results of Jensen et al. (1989) for Re_δ of 3464

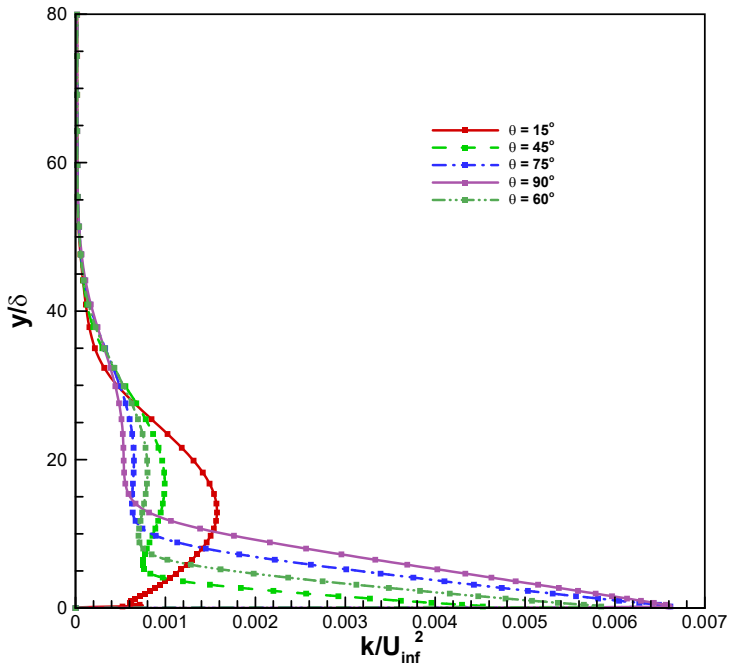

Figure 6.26: Predicted non-dimensional kinetic energy profiles in acceleration phase for Re_δ 3464

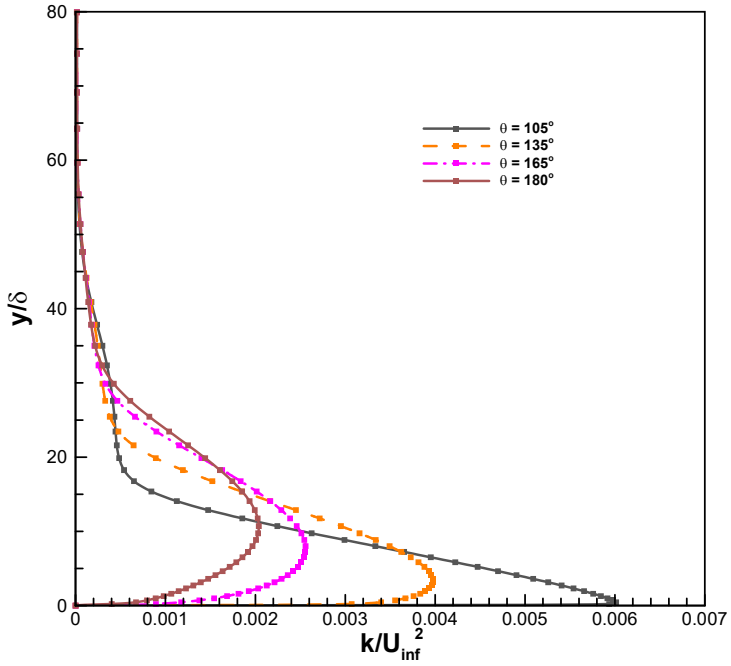

Figure 6.27: Predicted non-dimensional kinetic energy profiles in deceleration phase for Re_δ 3464

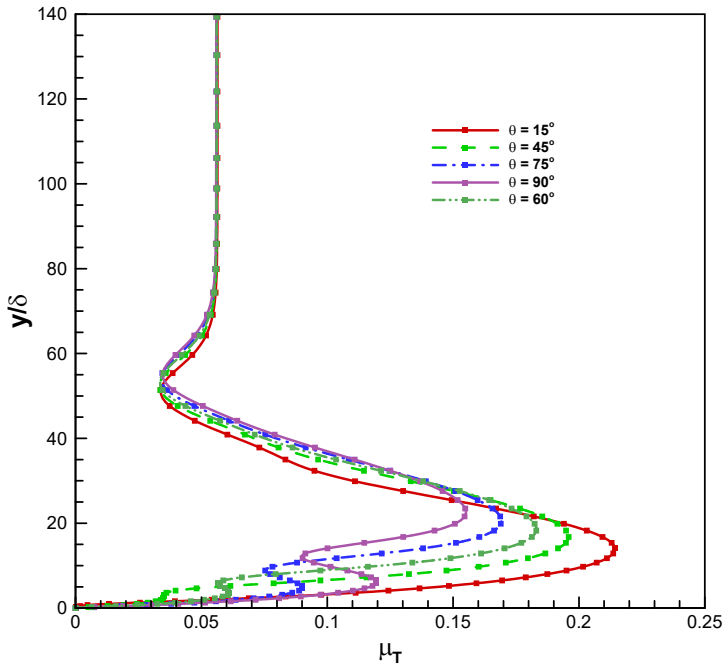

Figure 6.28: Predicted eddy viscosity profiles in acceleration phase for Re_δ 3464

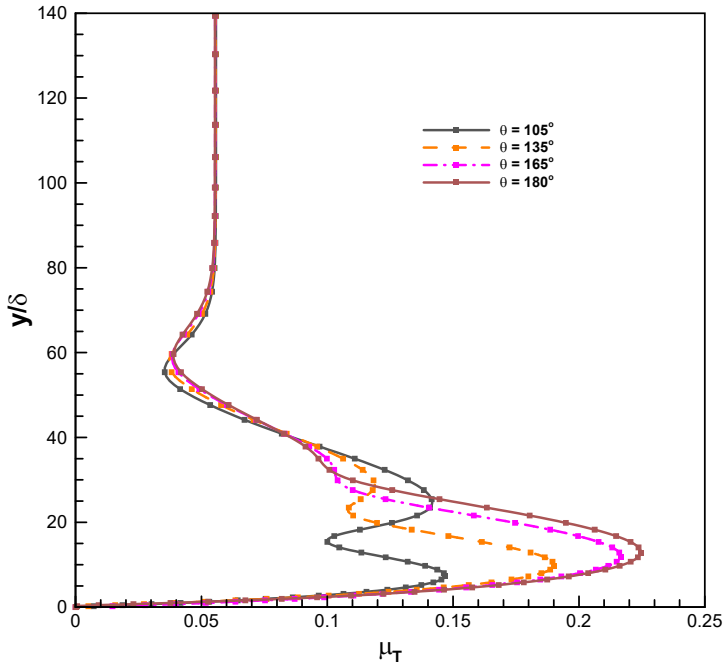

Figure 6.29: Predicted eddy viscosity profiles in deceleration phase for Re_δ 3464

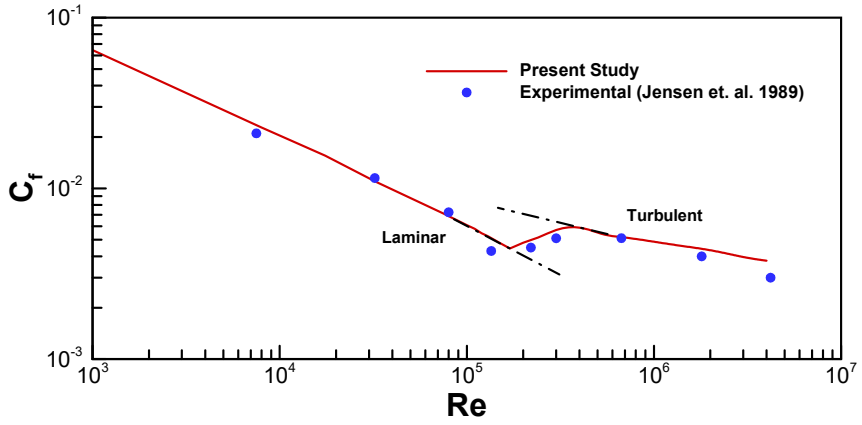

Figure 6.30: Predicted friction coefficient and its comparison with experimental results Jensen et al. (1989)

7 Undulatory Self-Propulsor Simulations

7.1 Overview

A three-dimensional slender body theory was developed by Lighthill (1960) to study hydrodynamics on a lamprey and applied ideal flow theory with vortex shedding along with skin friction correction to account for viscosity. For a relatively high Reynolds number, a thin boundary layer flow exists (Lighthill 1971). Vorus (2005) used the same assumptions and proposed a conceptual model of an ideal swimming motion for thin oscillating strip, in which vortex wake was absent. Vorus and Taravella (2011) extended this model to 3D slender body object.

The oscillatory displacement function for the thin strip advancing with speed U_o and frequency ω, as given by Vorus (2005).

$$h(x,t) = \mathrm{Re}\left[H(x)\exp^{-i\omega t}\right] \tag{7.1}$$

Further extension to 3D requires the sectional force coefficient to be integrated along the length to find total thrust coefficient, C_T Vorus and Taravella (2011). Then the non-dimensional complex amplitude $\bar{H}(\overline{x})$ becomes:

$$\bar{H}(\overline{x}) = \mathrm{i}\Gamma\left[\exp^{2\pi\mathrm{i}\overline{x}} - \exp^{\frac{2\pi\mathrm{i}\overline{x}}{U}}\right] \tag{7.2}$$

$$\text{where} \quad \Gamma = \sqrt{\frac{C_T}{4\pi^3 r_o^2(1-U)(1-\cos 2\pi/U)}} \tag{7.3}$$

where the advance ratio is U= U_o/V , V is speed of backward traveling wave. This also becomes the reference velocity for non-dimensionalization of thrust and power coefficients. The frequency of oscillation is defined as $\omega = 2\pi\, V/L$, where L is length of the undulating cylinder. Non-dimensional time is $\bar{t} = Vt/L$, $\bar{x}$ and $\bar{h}(\bar{x},\bar{t})$ is non-dimensionalized based on length, L. Tab

Table 7.1: Displacement parameters

Length, L	1.0275 m
Forward Speed, U_{inf}	0.25 m/sec
Design Speed, U_o	0.25 m/sec
Wave Speed, V	0.357 m/sec
Advance ratio, U	0.7
Radius, r_o	0.0278 m
Gamma, Γ	0.0890

7.1 presents the parameters for the displacement equation used in simulations. U_{inf} is the speed at which anguilliform is swimming or the inflow speed, U_o is the design speed at which the anguilliform motion is expected or designed to swim. To numerically study hydrodynamic analysis of undulatory self-propulsor ANSYS Fluent is chosen to simulate the flow problem and solve the governing differential equation of mass and momentum. It is also capable of solving the Euler(inviscid) equations by ignoring the viscous terms. Due to the nature of the problem under investigation, dynamic meshing is required to solve the governing differential equation in the discretized domain for the flow around the undulating anguilliform.

The conventional form of dynamic meshing available requires the re-meshing at every time step which may cause decrease in quality of the mesh around the moving object. In this particular study, the undulations of the anguilliform have significant amplitudes and derivatives causing cells to collapse. Therefore to circumvent these obstacles the method of *Overset grid*, also known as Chimera mesh, was adopted. Overset mesh is already available in the solver used in this study (ANSYS 2020). This method allows the user to create separate meshes for each region (components and background) of the flow problem and then combine them into one computational domain. The fundamental principle of this technique is to solve the governing differential equations on background and component meshes. In the background mesh the nodes or elements corresponding to the interior of the component mesh are marked as holes and removed from the computational domain. The values at the boundary of the overset mesh are interpolated to the background mesh (Petra 2019). For dynamic cases, such as this, the background mesh is undisturbed while the component mesh around the immersed body undulates with it. The

Table 7.2: Solver Settings

Description	Settings
Solver	Pressure Based
Pressure-Velocity Coupling	Coupled
Gradient Discretization	Least Squares Cell Based
Pressure	Second Order
Momentum	Second Order Upwind
Transient Formulation	First Order Implicit
Residual Criteria	$1e^{-10}$

advantage of this method is that it eliminates the need of re-meshing and allows more control over component mesh characteristics with moving geometries (Ramakrishnan and Scheidegger 2016). The prescribed kinematics for the undulation motion is achieved using a User-Defined function (UDF), which uses the DEFINE_GRID_MOTION macro, to move the nodes of the cylindrical body as well as the mesh around it in an anguilliform like motion defined by Eqn 7.2. The settings for the solver are shown in Tab 7.2.

7.1.1 Computational Domain and Grid

Fig 7.1 shows the schematic of flow problem as well as computational domain. The computational domain consists of a background mesh which is a cuboid with length of approximately 5.5L, width of 1L and height of 3L and a cylindrical mesh of radius $2.5r_o$ surrounding the cylinder, where L is length of cylinder in its straight position and r_o is the radius of cylinder. The head of the 3D flexible cylinder is placed $20r_o$ from the inlet plane. Both background mesh and component mesh are structured. The component mesh surrounding the body is stretched from the cylinder walls to its own outer edge to resolve for the boundary and has a total of 200,000 nodes. The background mesh has about 1.3 million nodes. After the hole cutting process the whole domain is left with approximately 1.15 million nodes.

Fig 7.2 and Fig 7.3 shows the mesh at the center plane of the domain. The axial flow is in x-direction with undulations performed in y-direction and z-axis is taken as the radial axis. As shown in Fig 7.1, the immersed flexible cylinder has no-slip wall boundary condition. The outer boundaries have following boundary conditions: uniform inlet flow at the inlet plane, slip wall

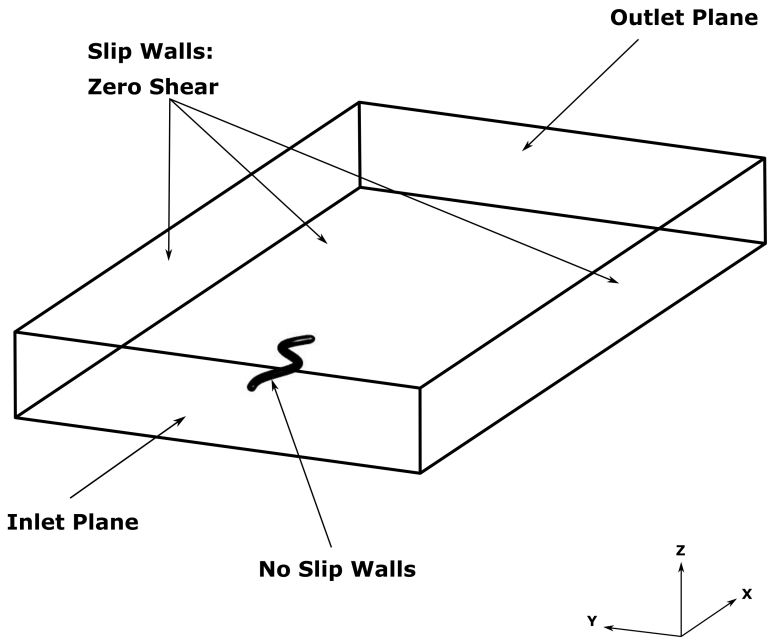

Figure 7.1: Schematic diagram of flow problem

condition on the lateral boundaries and pressure-outlet at the outlet plane. The time period of undulation motion was divided into 120 steps, $\Delta t = T/120$. The calculation was performed for 10 oscillation cycles for every simulation to ensure the elimination of initial transient effects from the final set of results. Each time step had 180 iterations to drive the velocity and divergence residuals are set below 10^{-10} for tight convergence. To assess the grid independence of the

Table 7.3: Grid Independence Study

Nodes	$\bar{C}_F$	$\bar{C}_T$	$\bar{C}_P$
600,000	-3.21×10^{-5}	1.45×10^{-3}	8.17×10^{-4}
1.15 million	-6.35×10^{-5}	2.738×10^{-3}	1.789×10^{-3}
2.01 million	-6.42×10^{-5}	2.756×10^{-3}	1.792×10^{-3}

results, three meshes were taken into consideration; coarse grid with 600,000 nodes, fine grid with 1.15 million and finer grid with 2.01 million nodes total after hole cutting process. The mean net force ($\bar{C}_F$), mean thrust ($\bar{C}_T$) and mean power ($\bar{C}_P$) were compared for Re=183796.

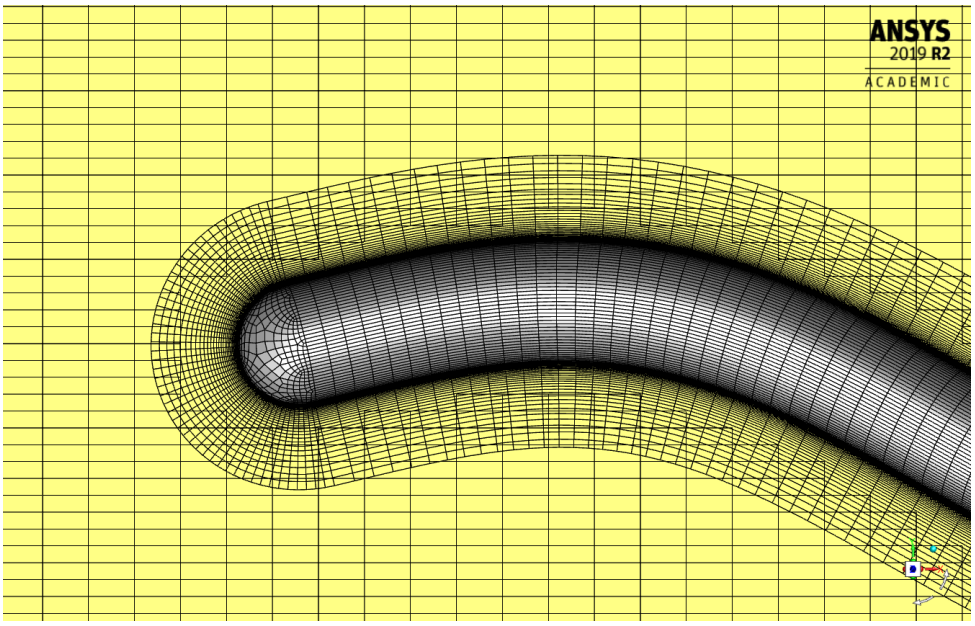

Figure 7.2: Side view of mesh and geometry near to head at center plane

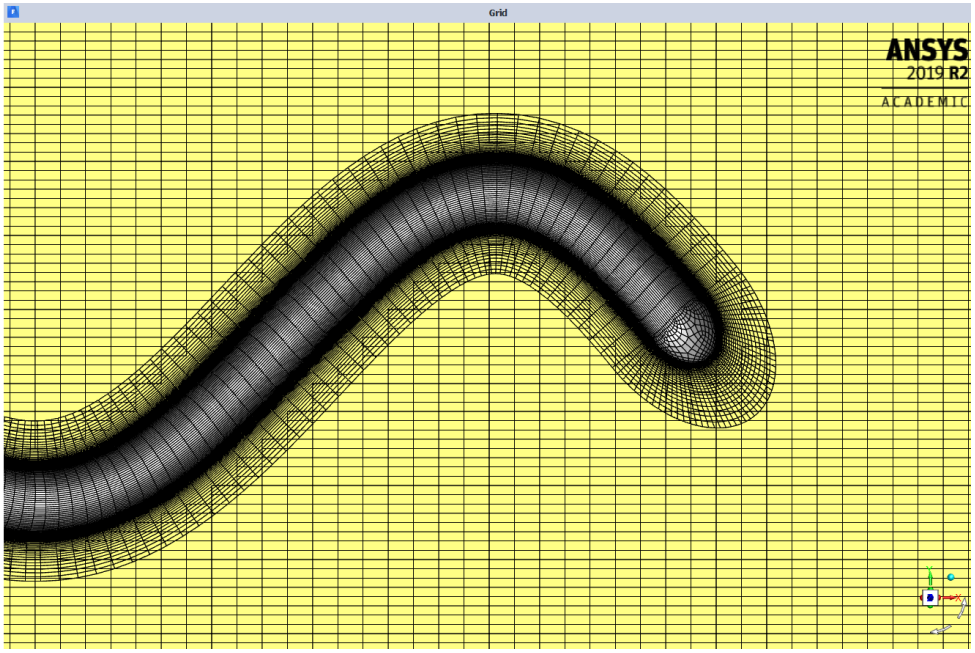

Figure 7.3: Side view of mesh and geometry near to tail at center plane

It can be observed from Tab 7.3, that $\bar{C}_F$ deviated by 1.1 %, $\bar{C}_T$ deviated by 0.657 % and $\bar{C}_P$ by 0.16 % from fine to finer grid which seems to be within acceptable range. In addition reducing time step size by a factor of 2 ($\Delta t = T/240$) for the fine grid solution did not result in much change in general characteristics of net mean force, thrust and power loss.

7.2 Force Decomposition & Efficiency

In the case of marine propulsion systems, it is easy to define efficiencies for the hull and propeller as the thrust produced is solely by the propeller while the drag is produced by ship's hull. However, this is not the case with anguilliform like propulsors as the body producing thrust is the same body producing drag also. Shultz and Webb (2002) explained that for such combined system of propeller and body, Froude efficiency is zero for steady speeds when axial thrust force is balanced by hydrodynamic drag.

Theories such as Lighthill's elongated body theory (EBT),(Lighthill 1970), and motion under consideration, (Vorus and Taravella 2011), defined Froude efficiency, thrust and lateral power losses using mathematical models. Lighthill (1970) defines efficiency in a very simple and elegant way by taking ratio of the thrust power produced to overcome viscous drag to the power spent by flexural movements to overcome drag. The Froude efficiency defined by EBT for steady inline swimming is:

$$\eta_{EBT-1} = \frac{1}{2}\left(1 + \frac{U}{V}\right) \tag{7.4}$$

where U is the swimming speed and V is the backward traveling wave speed. Vorus and Taravella (2011) defined efficiency as output power or thrust power over input power for ideal swimming motion:

$$\eta_{ideal} = \frac{UC_T}{VC_P} \tag{7.5}$$

Here C_T is the thrust coefficient and C_P is power coefficient. For the case of ideal swimming, independent of viscous effects, the ideal efficiency (η_{ideal}) is 100%. These mathematical models will be used in this research for comparison with numerical simulations (viscous and inviscid flows). Tytell and Lauder (2004) and Borazjani and Sotiropoulos (2009) defined the Froude efficiency for steady speed inline swimming in more physically accurate manner:

$$\eta = \bar{T}U \big/ \left(\bar{T}U + \bar{P}_L\right) \tag{7.6}$$

where $\bar{T}$ is average thrust over the swimming cycle and $\bar{P}$ is average power loss during lateral undulation over a swimming cycle. The challenge lies in measuring the thrust power, $\bar{T}$, ex-

perimentally, (Borazjani and Sotiropoulos 2009) and (Tytell and Lauder 2004). This obstacle is circumvented when using numerical techniques to find solution to the flow problem. The thrust and drag forces required to calculate efficiency using Eqn 7.6, can be calculated directly from computation. The approach adopted to separate drag and thrust from net force, calculated by solver, for this study is similar to one adopted by Borazjani and Sotiropoulos (2009). The anguilliform undulatory propulsor swims in negative x-direction (x_1) with undulations in y-direction (x_2). The instantaneous hydrodynamic forces produced in flow direction (x_1) will be the pressure and viscous forces. The net force acting on the body at any instant will be given by:

$$F(t) = \int_A p n_1 \mathrm{d}A + \int_A \tau_{1j} n_j \mathrm{d}A \tag{7.7}$$

where p is the pressure acting on the surface, n_1 is the unit normal vector acting in x_1 direction on area $\mathrm{d}A$ and τ_{ij} is the viscous stress tensor. Now the thrust force can be decomposed due to thrust produced by pressure (T_p) and viscosity (T_v). Similarly drag force can also be decomposed due to drag produced by pressure (D_p) and viscosity (D_v). The net thrust force can be written as:

$$T(t) = T_p + T_v = \frac{1}{2}\left(\int_A p n_1 \mathrm{d}A - \left|\int_A p n_1 \mathrm{d}A\right|\right) + \frac{1}{2}\left(\int_A \tau_{1j} n_j \mathrm{d}A - \left|\int_A \tau_{1j} n_j \mathrm{d}A\right|\right) \tag{7.8}$$

and the net drag can be written as:

$$D(t) = D_p + D_v = \frac{1}{2}\left(\int_A p n_1 \mathrm{d}A + \left|\int_A p n_1 \mathrm{d}A\right|\right) + \frac{1}{2}\left(\int_A \tau_{1j} n_j \mathrm{d}A + \left|\int_A \tau_{1j} n_j \mathrm{d}A\right|\right) \tag{7.9}$$

Since the swimming direction is the negative x-direction; the net instantaneous force becomes:

$$F(t) = D(t) - T(t) \tag{7.10}$$

So if at any instant the net force $F(t)$ is negative it contributes to the thrust force $T(t)$ and if positive it contributes to the drag force $D(t)$. The calculated net force F(t) is also compared with one calculated by the solver with its own built-in function to calculate the axial force.

Similarly the power losses due to lateral undulation are calculated by:

$$P_L = \int_A p n_2 \dot{h} \mathrm{d}A + \int_A \tau_{2j} n_j \dot{h} \mathrm{d}A \tag{7.11}$$

where $\dot{h}$ is the time derivative of the swimming function h which is lateral displacement in the x_2 direction.

7.3 Results and Discussion

Viscous flow simulations were carried out for the swimming speed, U_{inf}, of 0.25 m/s corresponding to a Reynolds number of 241844 with design speed, U_o, of 0.25 m/s. This will be referred to as the design speed case. Another simulation keeping the design speed same and the swimming speed, U_{inf} of 0.19 m/s corresponding to Reynolds number of 183796 was carried out and will be referred to as off-design speed case. The time history of the instantaneous hydrodynamic forces, thrust force and drag force are compared to the ideal slender body theory (Vorus and Taravella 2011) and inviscid flow simulation, carried out at design speed and swimming speed of 0.25 m/sec. Further comparison of the decomposed forces (thrust and drag) due to effects of pressure and viscosity are presented in this study.

7.3.1 Ideal Flow vs Inviscid vs Viscous

Fig 7.4 shows the time variation of instantaneous hydrodynamic axial force coefficients C_F for ideal slender body theory (mean force coefficient), inviscid flow (carried out at design speed of 0.25 m/s) and viscous flow simulations (carried at design speed of 0.25 m/s and off-design speed

of 0.19 m/s). Considering the sign convention for this study, $C_F > 0$, which means drag force (D) from Eq 7.9 is higher than thrust force (T) from Eq 7.8 at that instant and the net force becomes of drag type. Similarly, when $C_F < 0$, T becomes greater than D and net force becomes thrust type. It can be observed for all simulations, C_F in each cycle has two peaks corresponding to tail strokes due to undulation motion (Müller et al. 2001). The net instantaneous force is

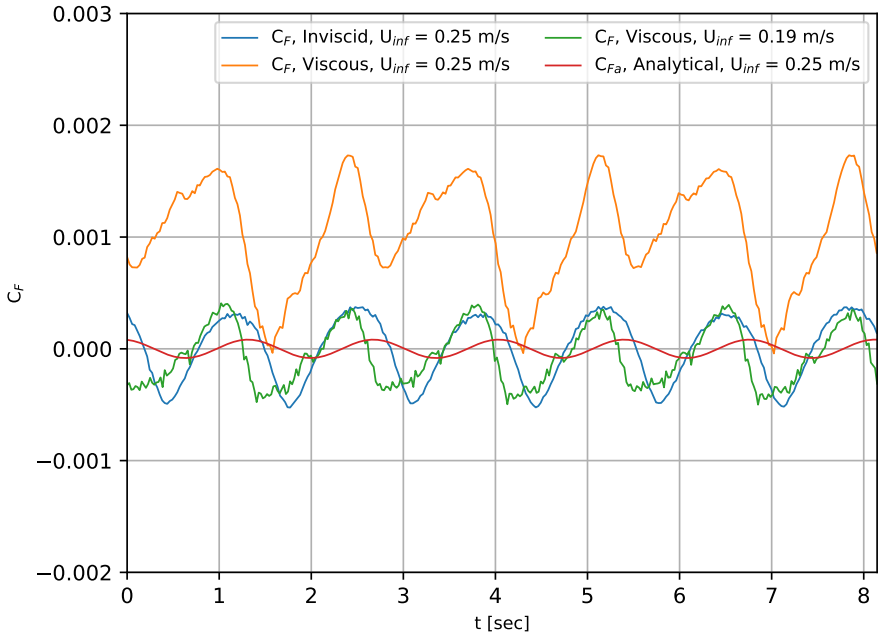

Figure 7.4: Time history of axial force coefficients (C_F) for Viscous, Inviscid and analytical solution at design and off-design speeds

Table 7.4: Mean Force coefficients for Inviscid and Viscous cases at design and off-design speed

Forces	Inviscid	Viscous-design	Viscous-off-design
$\bar{C}_F$	1.53×10^{-6}	1.03×10^{-3}	-6.35×10^{-5}
$\bar{C}_{Fpressure}$	1.53×10^{-6}	3.76×10^{-4}	-6.57×10^{-4}
$\bar{C}_{Fviscous}$	0	6.51×10^{-4}	5.94×10^{-4}

decomposed into its thrust (T(t)) and drag (D(t)) components using Eq 7.8 and 7.9. Fig 7.6 shows the thrust and drag force for inviscid simulation and analytical thrust calculated by slender body theory. The mean net force coefficient ($\bar{C}_F$) for the inviscid flow simulation is approximately

0 (as also shown in Tab 7.4). This can also be observed in Fig 7.6 where thrust forces almost balances drag forces in time and gives an inline constant swimming speed case at design speed of 0.25 m/s. Tab 7.5 also shows mean thrust coefficient ($\bar{C}_T$) approximately equal to the mean drag coefficient ($\bar{C}_D$). The analytical drag force (not shown here) is assumed to be equal and opposite of the analytical thrust force shown in Fig 7.6 (Vorus and Taravella 2011). It can be observed that the magnitude of thrust and drag forces are higher than the analytical thrust and drag. This can be attributed to the assumption of potential flow on which the analytical solution is developed. The boundary layer thickness is assumed to be thin for high Reynolds number and ideal flow theory is applied (Vorus and Taravella 2011). The equation of motion derived gives rise to vortex free wake and absence of wake-induced drag. The forces calculated are due to pressure field derived using Bernoulli equation which is different from inviscid flow simulation which uses Euler equations to solve for the flow field. The difference in the magnitude of the net instantaneous force coefficients as shown in Fig 7.4 is due to the ends of the anguilliform geometry which is not accounted by theory. At the aft end of the anguilliform, a high pressure region is observed at the tip, with a low pressure region around it, as show in Fig 7.5. This causes flow to change direction, resulting in higher thrust. Similarly, a stagnation point is observed on the fore end of the anguilliform causing drag. Due to the nature of the tail and head movement, the time on which aft pressure is higher than forward pressure, the net instantaneous force becomes of thrust type and when forward pressure is higher than aft pressure the net force becomes drag type.

Fig 7.4 also shows force coefficients of the viscous flow simulation at design speed. It was clearly observed that the net instantaneous force is always of drag type. This is also evident from Fig 7.7 where the drag force is higher than the thrust generated at that speed and also higher than the drag force observed/calculated in the inviscid flow simulation. Tab 7.4 shows that the mean coefficient of viscous force ($\bar{C}_{Fv}$) is almost twice of mean coefficient of pressure force ($\bar{C}_{Fp}$). Tab 7.5 also shows that the C_D is about 32% higher than C_T. This due to the fact that the viscous forces are important, which were modelled empirically in the analytical solution (Vorus and Taravella 2011). As show in Fig 7.8, the viscous forces are evident and are of drag producing/type in nature. The thrust force and drag force produced by pressure is very close

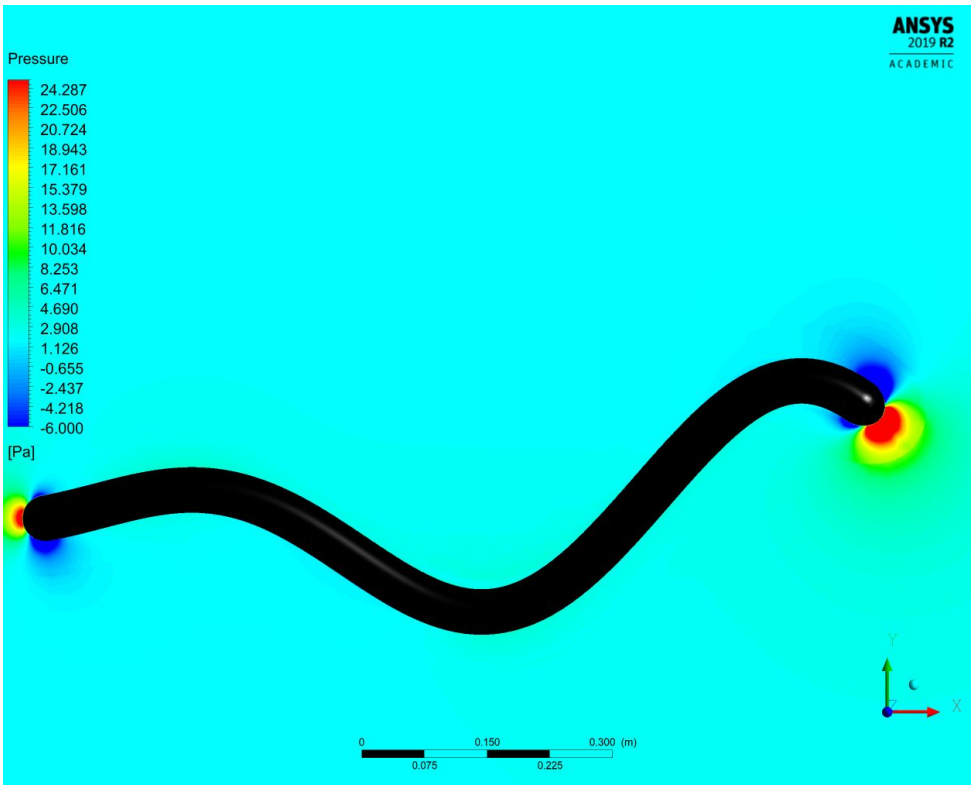

Figure 7.5: Pressure Contour plot for Inviscid flow

to one produced for inviscid flow simulation as shown in Fig 7.8. The components of thrust and drag produced, as shown in Fig 7.8, are calculated using Eqs 7.8 and 7.9. An important observation can be made here that, the anguilliform designed for this speed will experience a net drag force and constant inline swimming speed case will be difficult to achieve. In other words, it either accelerates or decelerates and the swimming velocity U_{inf} will not be constant. The definition of efficiency will be inconsequential. Now there are many parameters like frequency, tail amplitude or advance ratio, that can be calibrated to achieve the desired case of net zero force. For the purpose of this study we reduced the swimming speed U_{inf} keeping the advance ratio same. The speed was reduced systematically to observe the value at which the anguilliform motion achieves net zero force. The desired case was observed at swimming speed of U_{inf} of 0.19 m/s. This case from hence forth will be referred to as the off-design case.

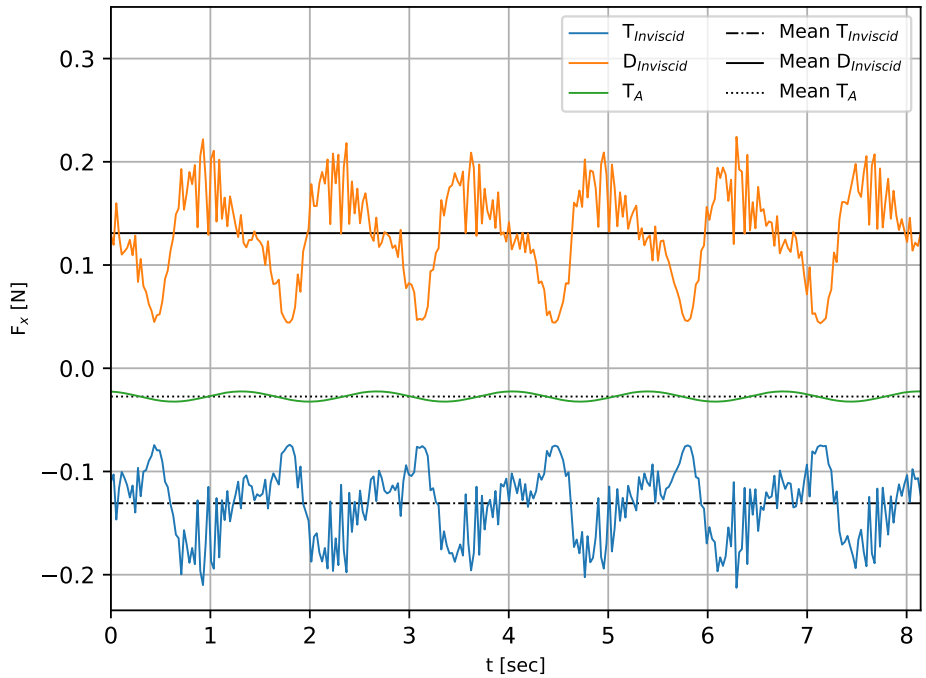

Figure 7.6: Thrust and drag forces as predicted by inviscid flow simulation and thrust force calculated by the analytical solution(Vorus and Taravella 2011)

Table 7.5: Mean power, thrust and drag coefficients for inline swimming speed of U_{inf} of 0.25m/s (design speed)

Case	$\bar{C}_p$	$\bar{C}_T$	$\bar{C}_D$
Analytical	1.348×10^{-5}	1.9257×10^{-5}	1.9257×10^{-5}
Inviscid	2.751×10^{-4}	2.1770×10^{-3}	2.1772×10^{-3}
Viscous	1.094×10^{-3}	1.9223×10^{-3}	2.850×10^{-3}

7.3.2 Off-Design Reynolds Number for Efficiency

Fig 7.4 shows the net force coefficient C_F for the off-design case which is very similar to one predicted by inviscid flow simulation. The $\bar{C}_F$ approximately 0 as from Tab 7.4. The drag force is almost balanced by thrust force produced. The $\bar{C}_D$ is just slightly lower by 0.4% than $\bar{C}_T$ as show in Tab 7.6. Fig 7.9 shows thrust and drag forces experienced by anguilliform for off-design case. It also shows the analytical thrust calculated at the off-design speed. There is a clear evidence of the reduction of drag force and increase of thrust force. The thrust force is increased by 42.4% from viscous design speed case while drag only reduced by 4.2%. The mean pressure

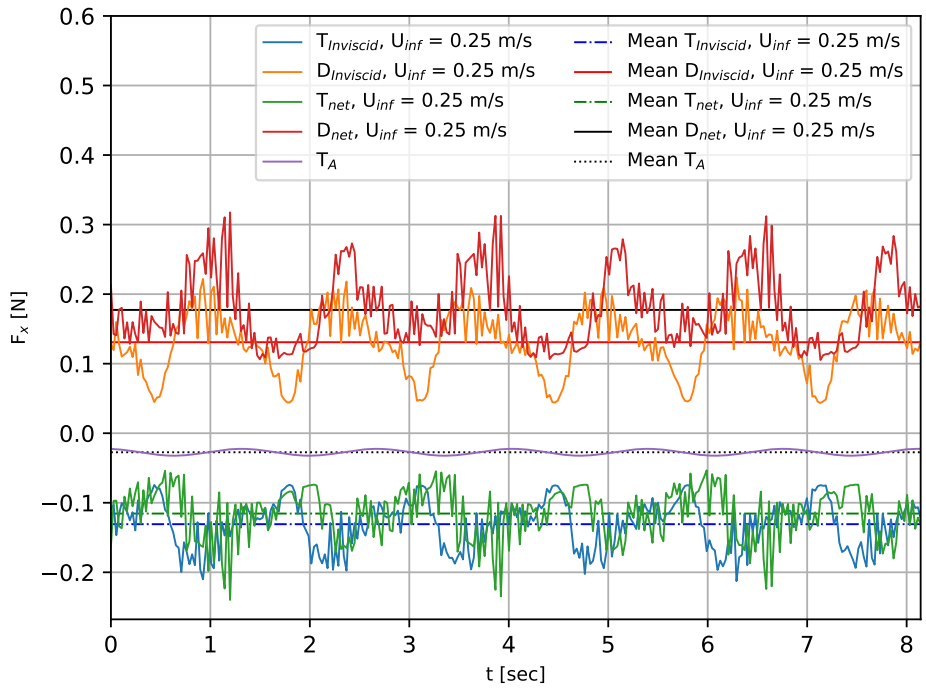

Figure 7.7: Thrust and drag forces as predicted by inviscid flow simulation, Thrust force calculated by analytical solution(Vorus and Taravella 2011) and thrust and drag forces predicted by the viscous flow simulation

Table 7.6: Power, thrust and drag coefficients for inline swimming speed of U_{inf} of 0.19m/s (Off-design speed)

Case	$\bar{C}_p$	$\bar{C}_T$	$\bar{C}_D$
Analytical	2.421×10^{-5}	3.8265×10^{-5}	3.8265×10^{-5}
Inviscid	2.751×10^{-4}	2.1770×10^{-3}	2.1772×10^{-3}
Viscous	1.789×10^{-3}	2.738×10^{-3}	2.728×10^{-3}

force is of thrust type which balances drag type mean viscous force as shown in Tab 7.4. Fig 7.10 shows components of thrust and drag produced by pressure and viscosity. Comparing Figs 7.8 and 7.10; it can be observed that due to reduction in swimming speed, eventually reducing inertial forces, thrust produced due to pressure increases by 42.4% with reduction of form drag by 4% while the drag due to viscosity is only reduced by 0.2%. This observation is in agreement with the findings of Borazjani and Sotiropoulos (2009) that the viscous drag is fairly constant at high Reynolds number.

Tab 7.5 and 7.6 also shows coefficient of lateral power for undulation for analytical, inviscid

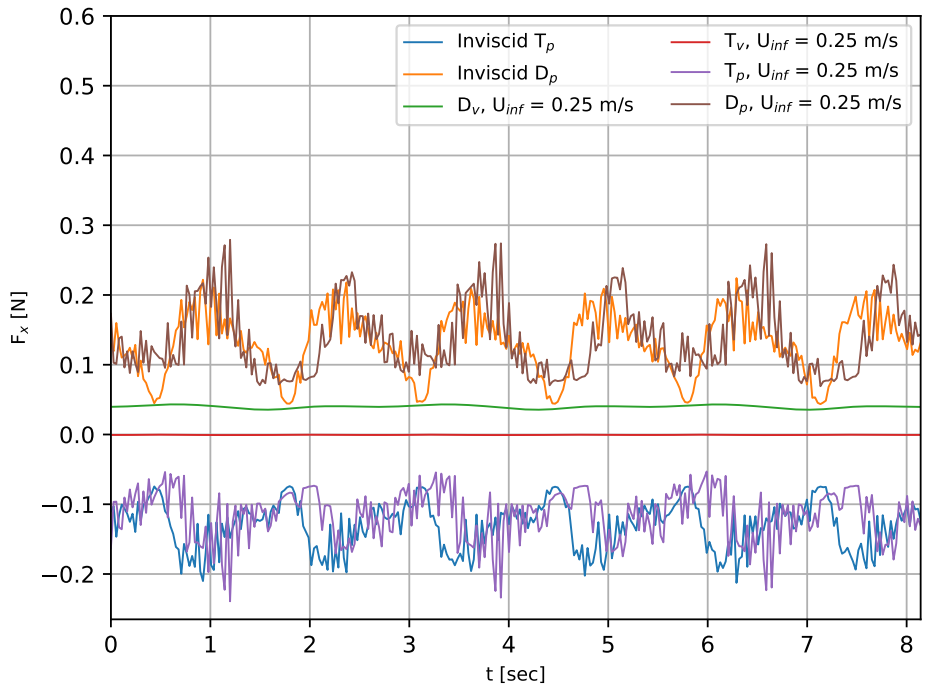

Figure 7.8: Components of thrust and drag forces due to pressure and viscous effects predicted by viscous and inviscid simulation

and viscous flow simulation at design and off-design speeds. For constant steady swimming speed, mean axial power is zero since mean axial force is zero; therefore, the total power requirement is only the lateral power calculated by Eq 7.11. The total power is non-dimensionalized by a factor of $1/2\rho V^3 L^2$. It is to be noted that analytical lateral power calculated is almost two orders of magnitude less than viscous power, this is again due to fact the assumption of potential flow and absence of viscous effects. It is to be noted that power required for anguilliform motion decreases when swimming speed, i.e. Reynolds number, is increased. The same was observed by Tytell and Lauder (2004) and Borazjani and Sotiropoulos (2009) who a reported decrease of lateral swimming power as the Reynolds number is decreased for inline constant swimming speed case. A concrete conclusion is yet to be drawn for the motion function used in this study as to whether at even higher and lower Reynolds number the power requirement would decrease or increase. More simulations are being carried out for various Reynolds numbers to answer this question and will be communicated in future work. It is worthwhile to mention that the power coefficient for inviscid flow simulation does agree very well with the findings of Borazjani

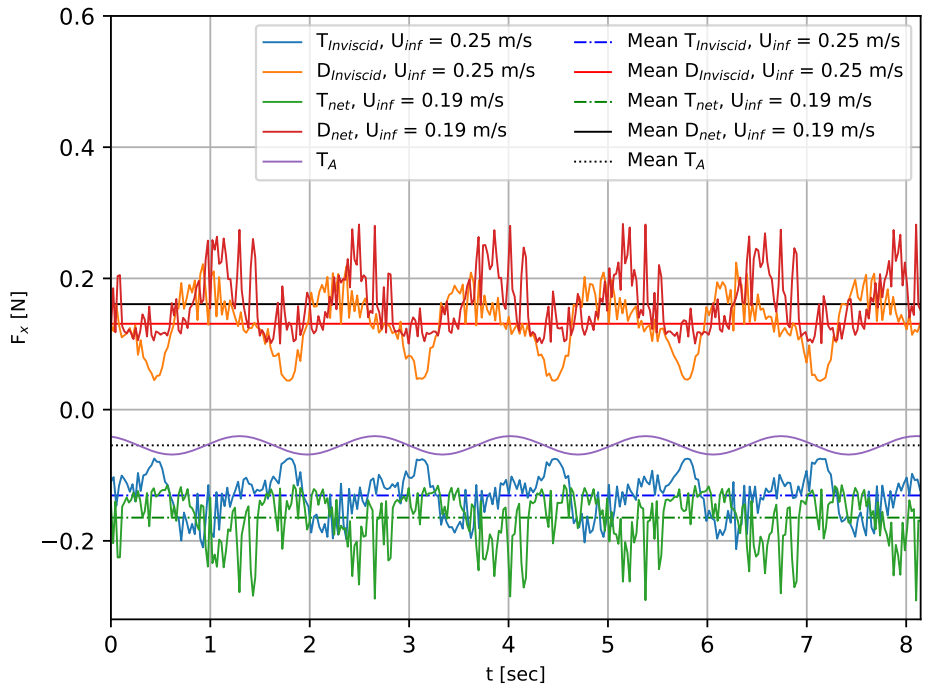

Figure 7.9: Thrust and drag forces as predicted by inviscid flow simulation, thrust force calculated by analytical solution(Vorus and Taravella 2011) and thrust and drag forces predicted by viscous flow simulation for non-ideal flow case

and Sotiropoulos (2009). The power requirement for the current study is $1.789\times10e^{-3}$ for off-design viscous simulation at Reynolds number 183,796, while for Borazjani and Sotiropoulos at Reynolds number 4,000 was $4.726\times10e^{-3}$. Since the the order of magnitude is the same, this may give an idea that at higher Reynolds number the power requirements may decrease but at a very slow rate; however, the authors do not claim this as a definite conclusion and more studies are underway. Tab 7.7 gives the Froude efficiencies for analytical and inviscid flow simulations at

Table 7.7: Froude Efficiencies

Case	η
$\text{Analytical}_{\text{design speed}}$	100%
$\text{Analytical}_{\text{off-design speed}}$	84.13%
$\text{Inviscid}_{\text{design speed}}$	84.71%
$\text{Viscous}_{\text{off-design speed}}$	45.03%
EBT	75%

design speed and viscous, analytical and elongated-body theory at off-design speed. Vorus and

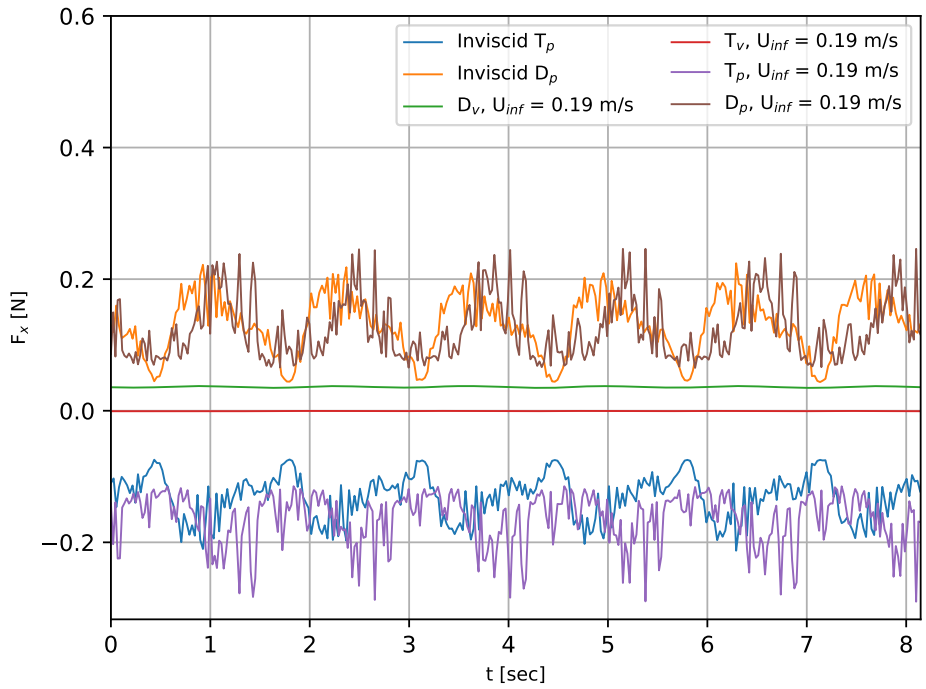

Figure 7.10: Components of thrust and drag forces due to pressure and viscous effects predicted by viscous and inviscid simulation for non-ideal flow case

Taravella (2011) calculated the ideal efficiency for the anguilliform motion to be 100% at design speed. As discussed before, this theoretical efficiency is based on assumptions of a potential flow model. The definition of analytical efficiency does not include the power to overcome the drag produced in axial direction as seen in Eq 7.5 (Vorus and Taravella 2011). Considering inviscid flow, where there is absence of viscous effects, the efficiency for inline swimming case at design speed is about 84% due to the fact as discussed earlier, that there are effects due to the ends of the anguilliform which are not accounted in the ideal theory.

7.3.3 Comparison to experimental results

A qualitative comparison of experimentally observed velocities (Eastridge 2020) and numerically predicted velocities at two different cross section locations, L/2 and 3L/4, for design speed case are presented below. Figure 7.11 and 7.12 shows cross section contours plots for axial velocity at half length for design speed case. Figure 7.13 and 7.14 shows cross section contours plots for axial velocity at three-quarters of the length for the design speed case. Comparison between

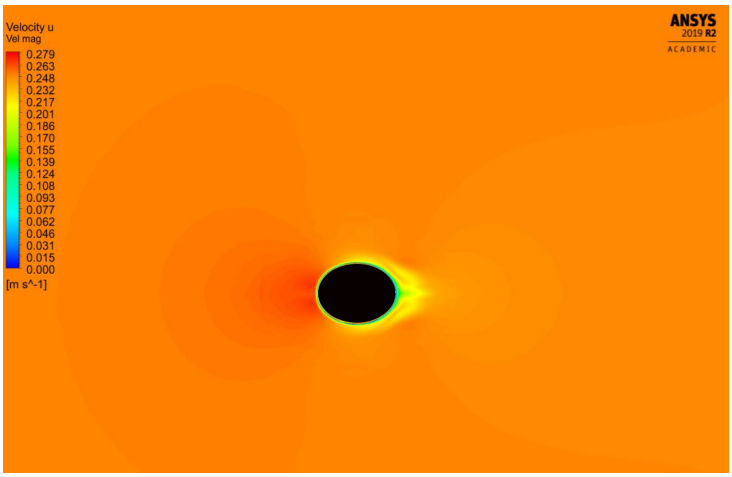

Figure 7.11: Numerically predicted axial velocity plots for cross-section at L/2 for swimming speed of 0.25 m/s

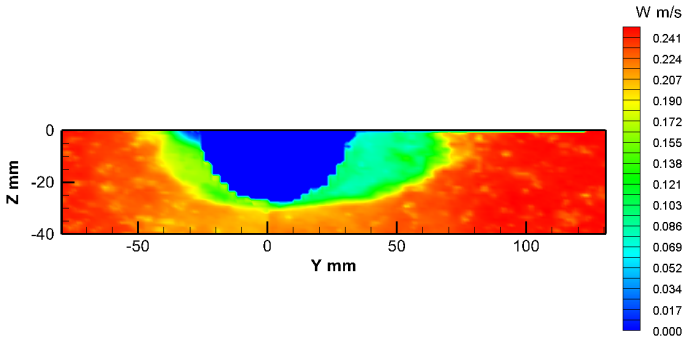

Figure 7.12: Experimentally observed axial velocity plots for cross-section at L/2 for swimming speed of 0.25 m/s

Figs 7.11 and 7.12 are made when the cross section crosses the centerline to be consistent with the experimentally acquired data. It can be observed that the numerically predicted boundary layer is very thin around the anguilliform which is in consistent with assumptions made by Vorus (2005). The comparison with experimental data indicates that there is not boundary layer separation at that time step also as observed by Eastridge (2020). However, some effects

of reflection while obtaining the experimental data, as discussed by Eastridge (2020), can be observed in downstream of Fig 7.12. A similar comparison is made at the axial location of

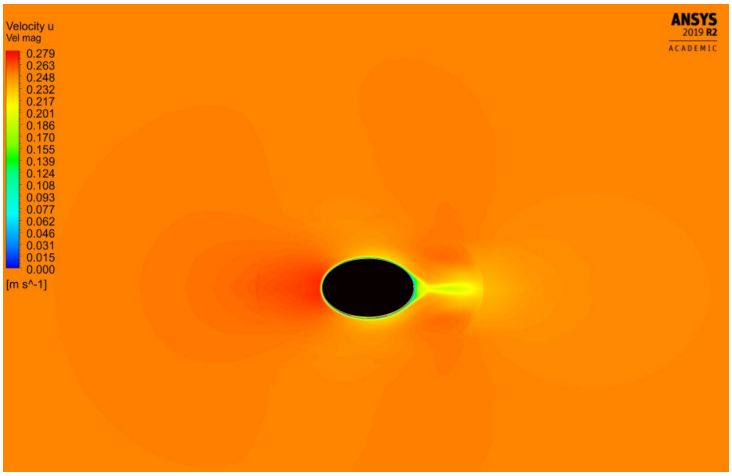

Figure 7.13: Numerically predicted axial velocity plots for cross-section at 3L/4 for swimming speed of 0.25 m/s

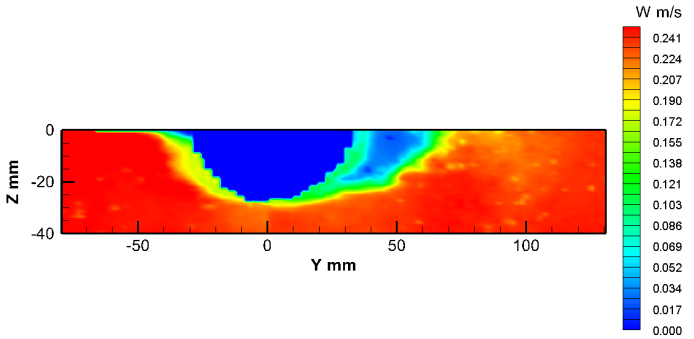

Figure 7.14: Experimentally observed axial velocity plots for cross-section at 3L/4 for swimming speed of 0.25 m/s

three-quarters of length in Fig 7.13 and 7.14. It can be observed that boundary layer is very thin and starts to separate in the downstream. The lower shear stress observed and reported by Eastridge (2020) in the down stream can be attributed to the separation. The increase in

shear stress as observed by Eastridge (2020) at top of the cross section (angle of 90^o) can be attributed to thinning of boundary layer. This can also indicate transitional behavior during the acceleration phase. Fig 7.15 shows the numerically predicted velocity in deceleration phase of a

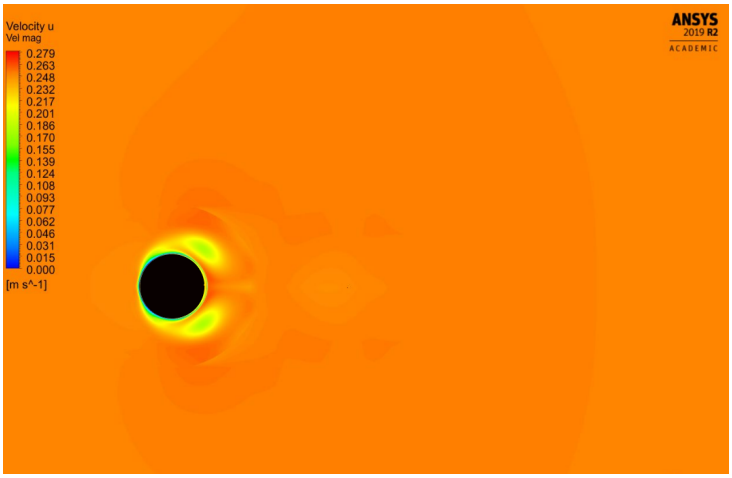

Figure 7.15: Numerically predicted axial velocity plots for cross-section at 3L/4 for swimming speed of 0.25 m/s

cross section at three quarters of length. It can be observed that the boundary layer thickens and starts to separate with formation of two vortex like structure. This is also seen in Fig 7.16 which shows the vortex shedding in the wake which is consistent with observation made by Potts (2015) however, strength of these vortex sheet is observed to be less. This supports the above argument made regarding the transitional behavior of boundary layer. However, turbulence study is needed to conclusively determine the behavior of boundary layer.

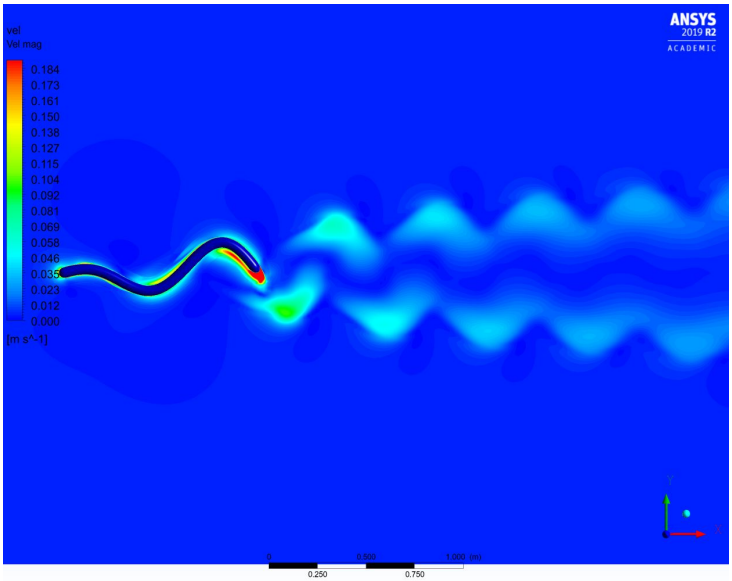

Figure 7.16: Velocity contour plots for off-design case with vortex shedding

8 Concluding Remarks

8.1 Conclusions

A CFD numerical solver based on pseudo-compressibility technique was developed to solve governing differential equation for laminar (NS) and intermittently turbulent (RANS) for flow over a flat plate and oscillating flow over a flat plate. The code is validated for flow over a flat plate by comparing to experimental data obtained using PIV techniques. The stream wise velocities predicted by the code are within 2% range of experimentally observed velocities. The code is verified for discretization accuracy using GCI method. It was observed that the discretization error was found to be 1.7% with global order of accuracy of 5.7% which is again within acceptable range. After the code is used to solve RANS equations along with two equation turbulence model by Chien's (k–ϵ) model. The velocity profiles predicted by RANS equations were compared to ones predicted by NS equations for lower and higher ranges of intermittently turbulent regime. The results indicated that the model does well in intermittently turbulent regime.

The developed CFD code was ultimately applied to to study the boundary layer characteristic in oscillating flow over a flat plate in intermittently turbulent regime. To validate the code, the predicted velocity profile in laminar regime were compared to analytical solution. The predictions and analytical solution were in good agreement. To study oscillating flow in intermittently and fully turbulent regime, an intermittency bypass transition model, k–ϵ–γ , is proposed which is simpler than those published and without data correlation. It depends only on local variables. One single intermittency equation is developed and coupled with Jones and Launder's k–ϵ RANS model. The model is only proposed for oscillating flows and for bypass transition, where turbulent intensity greater than 1%. The phenomenon of bypass transition a characteristic os oscillating boundary layer flows in high Reynolds number. Transition is initiated by diffusion of turbulence into the boundary layer and the source term carries it to turbulence. The intermittency model

was successfully able to forestall the onset of turbulence.

Numerical study was performed for Reynolds number (based on stokes thickness) ranging from laminar to intermittently to fully turbulent flows. The predicted velocity profiles and wall shear stress were compared to experimental data and DNS data. The prediction were in good agreement with data. The deviations observed were within the acceptable ranges of 2% for intermittently turbulent regime and 8% for fully turbulent regimes. The onset of transition was observed by a sharp increase in shear stress profile. In intermittently turbulent regime, during acceleration phase, burst of kinetic energy were observed in mid part of acceleration phase causing transition and were sustained through late part of deceleration phases. The peak of kinetic energy were observed to be much closer to wall as Reynolds number was increased as well as the bursts were observed in early phases of cycle and sustained through the whole cycle in fully turbulent regimes. The excellent agreement of predicted results with the published data suggests that the proposed intermittency model k–ϵ–γ coupled with RANS equations is capable of predicting boundary layer characteristic for unsteady oscillating flow over a flat plate in laminar, intermittently and fully turbulent regimes.

Numerical analysis of hydrodynamics of an anguilliform-like propulsor has been performed by applying a specific kinematics that has theoretically proven to shed no vortices in the wake. A commercial CFD software (ANSYS-FLUENT) has been used to discretize and solve full NS equations for anguilliform swimming motion prescribed by Vorus and Taravella (2011). Overset meshing method is used to simulate the eel movements as it has higher tail amplitudes. This has easily circumvented the problem of negative-cell volumes which is common with conventional dynamic meshing methods. Fluent's option for solving Euler equations was also exploited to solve inviscid flow to compare to theoretical calculation (Vorus and Taravella 2011) at design speed of the anguilliform (Re=241,844). The trust and drag were balanced at the design speed in the inviscid flow simulation and thus comparison to theory was made. It was observed that the magnitude of thrust and drag were higher than the theoretically calculated thrust and drag. This difference was attributed to the fact that the theory does not account for the ends of the anguilliform. The power losses were also higher for inviscid flow simulations leading to lower efficiency of the motion when compared to the ideal swimming theory. When the same design

speed simulation was performed with NS equations (include viscous effects) non-zero net force case was observed. It was due to viscous effects which was evident and significant. Furthermore to achieve the inline constant swimming speed case, the swimming speed was reduced (Re=183,796). This was needed to find the efficiency of the motion as the definition would only be meaningful at the constant swimming speed case. At high Reynolds number, viscous effects did not change much when swimming speed was reduced. This was also observed in previous studies. There was significant increase in thrust force produced, which balanced higher drag. The production of thrust is mostly due to pressure variation caused by undulatory motion. The proposed motion is much more efficient at higher speeds, both for inviscid and viscous flow simulations, as compared to swimming motions of live eels studied by Borazjani and Sotiropoulos (2009). This can be attributed to the proposed motion Vorus and Taravella which is designed to shed no vorticies in wake i.e. no wake-induced drag. A mathematical model which describes this motion was easier to solve if potential flow assumptions were made. This, however, will not be that trivial when considering full NS equations. However, the function does produce vortex shedding in the wake (viscous flow) but the effect of wake-induced drag is minimized, leading to higher efficiency than the actual live swimmers. This proposed motion is of high interest to engineers that design under water vehicle which propels itself. The proposed motion would provide an efficient means of propulsion as compared to conventional methods.

In the present study it is clear that at such high Reynolds number the anguilliform will have difficulties reaching its design speed with the proposed motion. However, the effect of Reynolds number on the lateral power spent is still an open-ended question even in live eel swimmers (Borazjani and Sotiropoulos 2009). The same is yet to be answered for the design speed versus swimming speed. Therefore, the current work cannot yet determine conclusively the range of efficiencies for various Reynolds number. Further simulations are underway in which it is being tested if at any such Reynolds number the design speed will match swimming speed and what would be its efficiency. These simulation results will be reported in future communication. Nonetheless, the findings of this study do state that the proposed motion achieves higher hydrodynamic efficiency than the one adopted by actual live anguilliform swimmers for higher Reynolds number.

8.2 Future Work

As discussed in chapter 7 that there were evidence of transitional behavior of the boundary layer on an anguilliform propulsor. To study such oscillatory behavior on the anguilliform using RANS equations, an intermittency or transitional model can be used. The proposed k–ϵ–γ model can be improved upon and used for turbulent simulation of the anguilliform. The current model proposed has the incapability of predicting transition with turbulent intensity less than 1%. It can be only applied to to predict bypass transition only. To counter the effects of re-laminarization of boundary layer, a phenomenon that exists in intermittent turbulent flows, perhaps a sink term can be introduced in the proposed γ equation.

Another issue to handle will be the effects of boundary layer separation which is evident in anguilliform at the trailing edge. This further leads to formation of vortex sheet in the wake. The proposed turbulence model can be further developed to predicted or handle boundary layer separation. For this as suggested more experimental work is required as suggested by Eastridge (2020) using volumetric PIV. The data can be used to modify the turbulence model and incorporate the effects for high pressure gradient and boundary layer separation. Finally after making modifications to the turbulence model, RANS simulations of the anguilliform propulsor can be used to perform optimization of the geometry and the motion function proposed by Vorus and Taravella (2011) to produce wakeless swimming in real fluid.

References

Akhavan, R., Kamm, R. D., and Shapiro, A. H. (1991a). "An Investigation of transition to turbulence in bounded oscillatory Stokes flows Part1. Experiments". In: *Journal of Fluid Mechanics* 225, pp. 395–422.

Akhavan, R., Kamm, R. D., and Shapiro, A. H. (1991b). "An Investigation of transition to turbulence in bounded oscillatory Stokes flows Part2. Numerical Simulations". In: *Journal of Fluid Mechanics* 225, pp. 423–444.

Akyuzlu, K. M. (Nov. 2017). "A Numerical and Experimental Study of Laminar Unsteady Lid-Driven Cavity Flows". In: *International Mechanical Engineering Congress & Exposition* (Tampa, Florida).

Akyuzlu, K. M. and Farkas, J. (Nov. 2012). "A Study of Formation Of Circulation Patterns in Laminar Unsteady Lid-driven Cavity Flows Using PIV Measurement Techniques". In: *International Mechanical Engineering Congress & Exposition* (Houston, Texas).

Alfonsi, G. (2009). "Reynolds-Averaged Navier-Stokes Equations for Turbulence Modelling". In: *Applied Mechanics Review* 62, pp. 1–20.

ANSYS (2020). *Overset Mesh*. URL: `www.ansys.com/products/fluids/ansys-fluent/overset-mesh` (visited on 05/11/2020).

Azhdarzadeh, M. and Razavi, S. (2008). "A Pseudo-Charateristic Based Method for Incompressible Flows with heat Transfer". In: *Journal of Applied Sciences 8* 18, pp. 3183–3190.

Blondeaux, P. (1987). "Turbulent boundary layer at the bottom of gravity waves". In: *J. Hydro. Res.* 25, pp. 447–464.

Borazjani, I. and Sotiropoulos, F. (2009). "Numerical investigation of the hydrodynamics of anguilliform swimming in the transitional and inertial flow regimes". In: *The Journal of Experimental Biology* 212, pp. 576–592.

Breuer, M. and Hänel, D. (1993). "A dual Time-stepping method for 3-D Viscous, Incompressible Vortex Flows". In: *Computers Fluid* 22, pp. 467–484.

Buchholz, J. H. J. and Smiths, A. J. (2008). "The wake structure and thrust performance of a rigid low-aspect-ratio pitching panel". In: *Journal of Fluid Mechanics* 603, pp. 331–365.

Carling, J., Williams, T. L., and Bowtell, G. (1998). "Self-Propelled Anguilliform Swimming: Simultaneous Solutions of The Two-Dimensional Navier-Stokes Equations and Newton's Laws of Motion". In: *Journal of Experimental Biology* 201, pp. 3143–3166.

Celik, I. B., Ghia, U., Roache, P. J., Feritas, C. J., Coleman, H., and Raad, P. E. (2008). "Procedure for Estimation and Reporting of Uncertainty Due to Discretization in CFD Application". In: *ASME Journal of Fluids Engineering* 130, pp. 1–4.

Chang, J., Kwak, D., Dao, S., and Rosen, R. (1985). "A Three-Dimensional Incompressible Flow Simulation and its Application to Space Shuttle Main Engine, Part 1-Laminar Flow". In: *AIAA* 83-0175.

Chang, J. and Kwak, D. (1984). "On the Method of Pseudo-Compressibility for Numerically Solving Incompressible Flows". In: *AIAA* 22^{nd} *Aerospace Science meeting* 84-0252.

Chen, K.-H. (1990). "A primitive variable, strongly implicit calculation procedure for two and three dimensional unsteady viscous flows: application to compressible and incompressible flows including flows with free surface". Ph.D Dissertation. Iowa State University.

Chen, K.-H. and Pletcher, R. (1993). "Simulation of Three-Dimensional Liquid Sloshing Flows Using a Strongly Implicit Calculation Procedure". In: *American Institute of Aeronautics and Astronautics* 31, pp. 901–910.

Cheng, J. Y. and Blickhan, R. (1994). "Note on the calculation of propeller efficiency using elongated body theory". In: *Journal of Experimental Biology* 208, pp. 3519–3532.

Chien, K. (1982). "Predictions of Channel and Boundary-Layer Flows with a Low-Reynolds-Number Turbulence Model". In: *AIAA* 20, pp. 33–38.

Chorin, A. (1967). "A Numerical Method for Solving Incompressible Viscous Flow Problems". In: *Journal of Computational Physics* 2, pp. 12–26.

Costamagna, P., Vittori, G., and Blondeaux, P. (2003). "Coherent Structures in oscillatory boundary layer flows". In: *J. Fluid Mech.* 474, pp. 1–33.

Dabri, J. O. (2005). "On the estimation of swimming and flying forces from wake measurements". In: *Journal of Experimental Biology* 185, pp. 179–193.

Dippold, V. (Jan. 2005). "Investigation of Wall Function and turbulence Model Performance within the Wind Code". In: *43rd AIAA Aerospace Science Meeting and Exhibit* (Reno, Nevada).

Durbin, P. (2012). "An intermittency model for bypass transition". In: *International Journal of Heat and Fluid Flow* 36, pp. 1–6.

Eastridge, J. R. (2020). "Experimental Investigation into the Boundary Layer of a Robotic Anguilliform Propulsor". PhD thesis. University of New Orleans.

Eckelmann, H. (1974). "The structure of the viscous sublayer and the adjacent wall region in the turbulent channel flow". In: *J. Fluid Mech.* 65, pp. 439–459.

Fan, S., Lakshminarayana, B., and Barnett, M. (1993). "Low-Reynolds-Number k-ϵ Model for Unsteady Turbulent Boundary-Layer Flows". In: *AIAA Journal* 31, pp. 1777–1784.

Feritas, C. J. (1993). "Journal of Fluids Engineering Editorial Policy Statement on Control of Numerical Accuracy". In: *ASME Journal of Fluids Engineering* 115, pp. 399–340.

Gray, J. (1933). "Studies in animal locomotion. I. The movement of fish with special reference to the eel". In: *Journal of Experimental Biology* 10, pp. 88–104.

Hanjalic, K. and Launder, B. (1972). "A Reynolds stress model of turbulence and its application to thin shear flows". In: *J. Fluid Mech.* 52, pp. 609–638.

Hino, M., Kashiwayanagi, M., Nakayama, A., and Hara, T. (1983). "Experiments on the turbulence statistics and the structure of reciprocating oscillatory flow". In: *Journal of Fluid Mechanics* 131, pp. 363–400.

Hsu, C., Lu, X., and Kwan, M. (2000). "LES and RANS Studies of Oscillating Flows Over Flat Plate". In: *Journal Of Engineering Mechanics* 126, pp. 186–183.

Hultmark, H., Leftwich, M., and Smits, A. (2007). "Flowfield measurements in the wake of robotic lamprey". In: *Experiments in Fluids* 43, p. 683.

Hunt, J. C. R., Wray, A. A., and Monin, P. (1988). "Eddies, streams and convergence zones in turbulent flows". In: *Studying Turbulence Using Numerical Simulation databases, 2.* Stanford, CA: Summer Program.

Issa, R. (1983). "Numerical Methods for two- and three-dimensional recirculating flows". In: *Comp. Methods for Turbulent, Transonic, and Viscous Flows*. Ed. by J.-A. Essers. Hemisphere/Springer, p. 183.

Jensen, B., Summer, B., and Fredsøe, J. (1989). "Turbulent Oscillatory Boundary Layer at High Reynolds Number". In: *Journal Of Fluid Mechanics* 206, pp. 265–297.

Jones, W. and Launder, B. (1972). "The Prediction of Laminarization With A Two-Equation Model Of Turbulence". In: *Int. J. Heat Mass Transfer* 15, pp. 301–314.

Justesen, P. and Spalart, P. R. (1990). "Two-Equation Turbulence Modeling Of Oscillatory Boundary Layers". In: *28th Aerospace Sciences Meeting*. Reno,NV,USA.

Kaul, U. K. (July 2010). "Effect of Inflow Boundary Conditions on the Solution of Transport Equations for Internal Flows". In: *40th Fluid Dynamics Conference and Exhibit* (Chicago,Illinois).

Kern, S. and Koumoutsakos, P. (2006). "Simulations of optimized anguilliform swimming". In: *The Journal of Experimental Biology* 209, pp. 4841–4857.

Kreplin, H. and Eckelmann, H. (1979). "Behavior of the three fluctuating velocity components in the wall region of a turbulent channel flow". In: *Physics of Fluids* 22, pp. 1958–1988.

Kwak, D. and Chakarvarthy, S. (1986). "A Three-Dimensional Incompressible Navier-Stokes Flow Solver Using Primitive Variables". In: *American Institute of Aeronautics and Astronautics* 24, pp. 390–396.

Lamas, M. I. and Rodriguez, C. G. (2020). "Hydrodynamics of Biomimetic Marine Propulsion and Trends in Computational Simulations". In: *Journal of Marine Science and Engineering* 8, p. 479.

Launder, B. and Spalding, D. (1974). "The Numerical Computation of Turbulent Flows". In: *Computer Methods in Applied Mechanics and Engineering 3*, pp. 269–289.

Lighthill, M. J. (1960). "Note on swimming of slender fish". In: *Journal of Fluid Mechanics* 9, pp. 305–317.

Lighthill, M. J. (1970). "Aquatic animal propulsion of high hydromechanical efficiency". In: *Journal of Fluid Mechanics* 44, pp. 265–301.

Lighthill, M. J. (1971). "Large amplitude elongated-body theory for fish locomotion". In: *Proceedings of the Royal Society of London* B 179, pp. 125–138.

Lodefier, K., Merci, B., Langhe, C. D., and Dick, E. (2004). "Transition modeling with k-ω turbulence model and an intermittency transport equation". In: *Journal of Thermal Sciences* 13, pp. 220–225.

Madsen, P. and Schäffer, H. (2006). "A discussion of Artificial Compressibility". In: *Coastal Engineering* 53, pp. 93–98.

Merkle, C. and Athavle, M. (1987). "Time Accurate Unsteady Incompressible Flow Algorithms Based on Artificial Compressibility". In: *American Institute of Aeronautics and Astronautics*, pp. 397–407.

Miloh, T. and Galper, A. (1993). "The Self-propulsion of a deformable shapes in a perfect fluid". In: *Proceedings of the Royal Society of London* A 442, pp. 273–299.

Müller, U. K., Smith, J., Stamhuis, E. J., and Videler, J. J. (2001). "How body contributes to the wake in undulatory fish swimming: flow fields of a swimming eel (Anguilla anguilla)". In: *Journal of Experimental Biology* 204, pp. 2751–2762.

Özişik, M. N. (1994). *Fnite Difference Methods in Heat Transfer*. 1st ed. CRC Press.

Patel, V., Rodi, W., and Scheuerer, G. (1985). "Turbulence Models for Near-Wall and Low Reynolds Number Flows: A Review". In: *AIAA Journal* 23, pp. 1308–1319.

Petra, T. (2019). "Description of the overset mesh approach in ESI version of the OpenFOAM". In: *CFD with OpenSource Software*. Ed. by H. Nilsson.

Pope, S. B. (2000). *Turbulent Flows*. 1st ed. Cambridge University Press.

Potts, J. B. (2015). "Developing and Testing an Anguilliform Robot Swimming with Theoretically High Hydrodynamic Efficiency". PhD thesis. University of New Orleans.

Qian, Y.-. and Arakawa, C. (1993). "Turbulent flow simulation around aerofoil with pseudo-compressibility". In: *Engineering Turbulence Modelling and Experiments 2: Proceedings of the Second International Symposium on Engineering Turbulence Modelling and Measure*, pp. 701–710.

Radhakrishnan, S. and Piomelli, U. (2008). "Large-Eddy simulation of oscillating boundary layers: Model comparison and validation". In: *Journal Of geophysical Research* 113, pp. 1–14.

Rahman, M. and Sükonen, T. (2001). "An Artificial Compressibility Method for Incompressible Flows". In: *Numerical Heat Transfer, Part B* 40, pp. 391–409.

Ramakrishnan, S. and Scheidegger, T. (Oct. 2016). "Overset Meshing in ANSYS Fluent". In: *13th Symposium on Overset Composite Grids and Solution Technology* (Future of Flight Aviation Center, Oct. 17–20, 2016). Mukilteo, Washington.

Rogers, S., Kwak, D., and Kiris, C. (1987). "On the accuracy of the pseudocompressibility method in solving the incompressible Navier-Stokes equations". In: *Appl. Math. Modelling* 11, pp. 35–44.

Rogers, S., Kwak, D., and Kiris, C. (Dec. 1989). "Numerical solution of the incompressible Navier-Stokes equations for steady-state and time-dependent problems". In: *10th Australasian Fluid Mechanics Conference* (University of Melbourne), pp. 17–20.

Saffman, P. G. (1967). "The Self-propulsion of a deformable body in a perfect fluid". In: *Journal of Fluid Mechanics* 28, pp. 285–289.

Salon, S., Armenio, V., and Crise, A. (2007). "A Numerical Investigation Of Stokes Boundary Layer in Turbulent Regime". In: *Journal Of Fluid Mechanics* 570, pp. 253–296.

Sarpkaya, T. (1993). "Coherent structure in oscillatory boundary layer flows". In: *Journal of Fluid Mechanics* 253, pp. 105–140.

Schlichting, H. and Gersten, K. (2017). *Boundary-Layer Theory*. Trans. by K. Mayes. 9th ed. Springer-Verlag Berlin Heidelberg.

Shome, B. (2013). "Numerical Study of oscillating boundary layer flow over flat plate using k-k$_l$-ω turbulence model". In: *International Journal of Heat and Fluid Flow* 42, pp. 131–138.

Shultz, W. W. and Webb, P. W. (2002). "Power Requirement of Swimming: Do New Methods Resolve Old Question?" In: *Integrative and Comparative Biology* 42, pp. 1018–1025.

Soh, W. and Goodrich, J. (1988). "Unsteady-Solution of Incompressible Navier-Stokes Equations". In: *Journal of Computational Physics* 79, pp. 113–134.

Spalart, P. R. and Baldwin, B. S. (1989). "Direct Simulation of a Turbulent Oscillating Boundary Layer". In: *Turbulent Shear Flows 6*. Ed. by J. Andre. Ed. by J. Cousteix. Ed. by F. Durst. Berlin, Heidelberg: Springer.

Srivastava, S., Eastridge, J. R., Taravella, B. M., and Akyuzlu, K. M. (May 2019). "A Numerical Study of Laminar and Intermittently Turbulent Flow Over a Flat Plate Using

Pseudo-Compressibility Model". In: *ASME Verification and Validation Symposium* (Las Vegas, Nevada).

Stokes, G. G. (1850). "On the effect of internal friction of fluids on the motion of pendulums". In: *Trans. Cambridge Philos. Soc.* 9, pp. 8–43.

Tannehill, J. C., Anderson, D. A., and Pletcher, R. H. (1997). *Computational Fluid Mechanics and Heat Transfer*. 2nd ed. Taylor & Francis.

Taravella, B. M. and Rogers, C. T. (2017). "A Computational Fluid Dynamics Analysis of an Ideal Anguilliform Swimming Motion". In: *Marine Technology Society Journal* 51, pp. 21–32.

Triantafyllou, M. S. and Triantafyllou, G. S. (1995). "An Efficient Swimming Machine". In: *Scientific American* 272, pp. 64–70.

TSI (2006). *Phase Doppler Particle Analyzer/Laser Doppler Velocimeter(LDV). Operations Manual*. Version E. TSI.

Tytell, E. D. (2007). "Do trout swim better than eels? Challenges for estimating performance based on the wake of a self-propelled bodies". In: *Experiments in Fluids* 43, pp. 701–712.

Tytell, E. D. and Lauder, G. V. (2004). "The hydrodynamics of eel swimming". In: *The Journal of Experimental Biology* 207, pp. 1825–1841.

Vittori, G. and Verizzco, R. (1998). "Direct Simulation of Transition in an Oscillatory Boundary Layer". In: *Journal Of Fluid Mechanics* 371, pp. 207–232.

Vorus, W. S. (2005). "Swimming of the semi-infinite strip revisited". In: *Journal of Engineering Mathematics* 51, pp. 35–55.

Vorus, W. S. and Taravella, B. M. (2011). "Anguilliform Fish Propulsion of Highest Hydrodynamic Efficiency". In: *Journal of Marine Science Application* 10, pp. 163–174.

Walter, D. K. and Cokljat, D. (2008). "Three-equation eddy viscosity model for Reynolds Averaged Navier-Stokes simulations of transitional flow". In: *Journal of Fluids Engineering* 130, pp. 1–14.

Wu, T. Y. (1961). "Swimming of a waving plate". In: *Journal of Fluid Mechanics* 10, pp. 321–344.

ZhanSen, Q., JingBai, Z., and ChunXuan, L. (2010). "Preconditioned pseudo-compressibility methods for incompressible Navier-Stokes equations". In: *Science China Physics, Mechanics & Astronomy* 53, pp. 2090–2102.

Vita

Shivank Srivastava was born in Lucknow, India in 1991 and is eldest son to Dr. Rajnish Bharti and Mrs. Kshipra Bharti. He completed his bachelors in Marine Engineering from Birla Institute of Sciences and Technology, Pilani in 2014. He then served in capacity of Marine Engineer on various merchant ships. In 2016 he moved to New Orleans, USA to study Naval Architecture and Marine Engineering and completed his masters in 2018. He enjoys studying computational fluid dynamics and imparting knowledge to students in their incipient years of education. He also enjoys outdoor activities, exercising and practice Muay Thai. Currently he and his wife Dr. Manika Bhondeley are living in New Orleans and looking forward for new adventures in life.